

University of Louisville

ThinkIR: The University of Louisville's Institutional Repository

Electronic Theses and Dissertations

12-2016

Experimental observation of the relationship between the pressure drop and flow rate of radial flow through porous media.

Matthew William Okruch
University of Louisville

Follow this and additional works at: <https://ir.library.louisville.edu/etd>



Part of the [Mechanical Engineering Commons](#)

Recommended Citation

Okruch, Matthew William, "Experimental observation of the relationship between the pressure drop and flow rate of radial flow through porous media." (2016). *Electronic Theses and Dissertations*. Paper 2596.
<https://doi.org/10.18297/etd/2596>

This Master's Thesis is brought to you for free and open access by ThinkIR: The University of Louisville's Institutional Repository. It has been accepted for inclusion in Electronic Theses and Dissertations by an authorized administrator of ThinkIR: The University of Louisville's Institutional Repository. This title appears here courtesy of the author, who has retained all other copyrights. For more information, please contact thinkir@louisville.edu.

EXPERIMENTAL OBSERVATION OF THE RELATIONSHIP BETWEEN THE PRESSURE
DROP AND FLOW RATE OF RADIAL FLOW THROUGH POROUS MEDIA

By
Matthew William Okruch
B.S., University of Kentucky, 2013

A Thesis
Submitted to the Faculty of the
J.B. Speed School of Engineering at the University of Louisville
in Partial Fulfillment of the Requirements
for the Degree of

Master of Science
in Mechanical Engineering

Department of Mechanical Engineering
University of Louisville
Louisville, Kentucky

December 2016

EXPERIMENTAL OBSERVATION OF THE RELATIONSHIP BETWEEN THE PRESSURE
DROP AND FLOW RATE OF RADIAL FLOW THROUGH POROUS MEDIA

By

Matthew William Okruch
B.S., University of Kentucky, 2013

A Thesis Approved on

November 29, 2016

by the following Thesis Committee:

Dr. Stuart Williams

Dr. Andrea Kelecy

Dr. Eric Berson

ACKNOWLEDGMENTS

I would like to thank all of the people who helped me through this project. My advisors, Dr. Williams and Dr. Kelecy, provided me with valuable advice and ensured that I kept the project heading in the right direction. Dr. Berson was very generous volunteering to serve on the committee on short notice. Valerie Anderson, Greg Chernov, Bryce Hann, Matt Moore, Bart Nuss, and Nick Okruch all lent me their time and expertise in specific areas, including water filtration, software development, equipment operation, and plastic part production methods. Without them, this project would not have been possible.

Finally, I would like to thank my wife, Jill, who helped keep me motivated and focused even when I didn't think there was an end in sight. I couldn't have made it without her love, patience, and encouragement.

ABSTRACT

EXPERIMENTAL OBSERVATION OF THE RELATIONSHIP BETWEEN THE PRESSURE DROP AND FLOW RATE OF RADIAL FLOW THROUGH POROUS MEDIA

Matthew W. Okruch

November 29, 2016

This research experimentally observed the relationship between pressure drop and flow rate for high velocity, radial flow through porous media. The criterion for what represents high velocity is a function of the Reynold's number of the flow. Pressure drop – flow rate curves were developed by flowing air and water through the porous carbon block samples. Each sample's permeability was calculated from on the air test results. Each sample's porosity was determined through digital microscope image analysis. Darcy's Law, the Forchheimer equation, and the Ergun equation were converted to the radial flow domain and compared to the experimental data. The modified Forchheimer equation appeared to be the most accurate predictor of a component of the physical results, although further geometric analysis is necessary to determine the form drag coefficient and end effects. Obtaining these values will allow for a full pressure drop – flow rate relationship prediction.

TABLE OF CONTENTS

ACKNOWLEDGMENTS.....	iii
ABSTRACT.....	iv
LIST OF TABLES.....	vii
LIST OF FIGURES.....	viii
1. INTRODUCTION.....	1
a. Water Filtration Background.....	1
b. Existing Porous Media Equations.....	5
c. Activated Carbon.....	9
d. Past Research.....	12
e. Planned Work.....	14
2. METHODS AND MATERIALS.....	15
a. Materials.....	15
b. Block Manufacturing Methods.....	16
c. Porosity Measurement.....	21
d. Carbon Block Finishing.....	25
e. Air Test Method.....	26
f. Water Test Method.....	26
3. RESULTS AND DISCUSSION.....	28
a. Particle Size Distribution.....	28
b. Density Calculations.....	30
c. Porosity Analysis.....	32
d. Air Test.....	36

e. Permeability Calculations.....	38
f. Water Test.....	42
4. SUMMARY AND CONCLUSIONS.....	55
REFERENCES.....	57
APPENDIX.....	59
LIST OF SYMBOLS AND ABBREVIATIONS.....	104
CURRICULUM VITA.....	105

LIST OF TABLES

1. Dimensions of the extruder dies and screws used to produce samples.....	18
2. Settings for tiling feature when imaging 1.9” OD samples.....	22
3. Material designations and average particle sizes.....	28
4. Batch numbers and the corresponding cross-section and material configurations.....	30
5. Average nominal density for each batch of extruded samples.....	32
6. Calculated porosity values from analysis of Batch 9 images.....	33
7. Threshold values used to analyze Batch 9 images.....	33
8. Average porosity for each batch of extruded samples.....	35
9. Raw data collected from air test for Batch 1.....	37
10. Calculated permeability values for each sample and air flow rate in Batch 1.....	39
11. Experimental data collected from water test on Batch 6, Block 7.....	43
12. Modified Ergun pressure drop prediction and comparison to experimental data for Batch 1, Blocks 1 & 2.....	51
13. Raw particle size data from sieve analysis for each material.....	63
14. Raw height and weight data used to calculate density of each sample.....	64-66
15. Calculated porosity values from analysis of images of each sample.....	70-72
16. Raw data collected from the air test for each batch of extruded samples.....	76-78
17. Calculated permeability values for each sample and air flow rate. Highlighted cells indicate values that were not considered in block average due to pressure gauge error.....	82-85
18. Experimental pressure drop and flow rate data from water testing of all extruded samples.....	86-98

LIST OF FIGURES

1. Particle size distribution of common contaminants and associated filtration technology.....	3
2. Illustration demonstrating the impact increasing pore size has on the relationship between flow rate and pressure drop.....	5
3. 2-D cross-section views of radial and longitudinal flow paths.....	7
4. Illustration of the pressure vs. flow curve of a Harmsco WB 5x170FL filter housing with a 20 micron filter cartridge.....	8
5. Artist’s conception of molecular discrimination effects of carbon pores.....	10
6. Carbon and binder mixture before and after blending, left and right respectively.....	16
7. Layout of carbon block extruder components.....	17
8. Examples of a fully-formed carbon block, left, and a block that was not sufficiently heated and formed, right.....	18
9. Cross-section view of compression mold used to produce carbon block samples.....	20
10. Image of the surface of a carbon block taken with a digital microscope at 200X zoom. This image is serialized 01-02-004.....	21
11. Graphical summary of “ImageAnalysis_Oct10” after analyzing image 01-02-004, also shown in Figure 10.....	24
12. Graphical summary of “ImageAnalysis_Oct10_ManualThresh” after analyzing image 01-11-007 with a user-given threshold limit.....	25
13. Layout of carbon block sample assembled with end caps and manifold for water test. Arrows signify direction of water flow.....	27
14. Particle size distribution for each material as determined by sieve analysis.....	29

15. Calculated density of each sample extruded in Batch 1, with error bars included.....	31
16. Calculated density of each sample extruded in Batch 2, with error bars included.....	32
17. Calculated porosity of each sample extruded in Batch 9.....	34
18. Calculated porosity of each sample extruded in Batch 5.....	34
19. Comparison of calculated porosity between the three cross-sections extruded with each material.....	36
20. Graphical summary of Batch 1 air test data, also shown in Table 9.....	37
21. R^2 values for linear trendline between flow rate and pressure drop for air test results.....	38
22. Permeability values for each block calculated from the results of the air test.....	40
23. Permeability values for each block compared to the corresponding porosity values.....	41
24. Permeability values for each block compared to the nominal particle size of the extruded material and cross-section.....	42
25. Experimental pressure vs. flow curve obtained from Batch 6, Block 7.....	43
26. Experimental pressure vs. flow curve obtained from Batch 5, Block 7.....	44
27. Difference of the linear and quadratic R^2 values, relative to the sample permeability.....	44
28. Experimental pressure vs. flow curves for all samples in Batch 1.....	45
29. Experimental pressure vs. flow curves for all samples in Batch 2.....	46
30. Relationship between experimental C_2 values and inverse sample permeabilities.....	48
31. Experimental error between theoretical and experimental values for Forchheimer linear coefficient compared to the sample permeability.....	49
32. Experimental error between theoretical and experimental values for Forchheimer linear coefficient compared to the sample length.....	50
33. Error between experimental pressure drop data and modified Ergun pressure drop prediction.....	52
34. Linear coefficient of modified Ergun equation for each block in Batch 1.....	53
35. Linear coefficient of modified Ergun equation for all samples tested.....	54

36. MATLAB code “ImageAnalysis-Oct10” used to analyze digital microscope images for porosity.....	59-60
37. Arduino code “matt_arduino_rev_1” used to capture and record flow rate and pressure data in the water flow test.....	61-63
38. Calculated density graphs for each batch of extruded samples.....	67-69
39. Calculated porosity graphs for each batch of extruded samples.....	73-75
40. Graphical summaries of air test data for each batch of extruded samples.....	79-81
41. Experimental pressure vs. flow curves from the water test for all batches of samples.....	99-103

INTRODUCTION

Water Filtration Background

Water filtration is an industry that has a significant economic presence beyond the United States. The global market for water treatment and supplies, which includes everything from large commercial process water treatment to single home filtration systems, was worth nearly \$50 billion in 2012. This market is projected to continue to grow as the world's population increases and becomes more urbanized. The United States exported \$1.8 billion worth of water filtration and purification parts and equipment in 2011, generating \$548 million in surplus (David, 2012). The scale of this business is such that any significant steps forward in understanding the physics behind the filters' performance will have a major impact around the world.

Water filters are commonly used to treat water in a variety of applications, ranging from municipal wastewater to household drinking water. Water contaminants that are typically targeted by water filters include particulate matter, micro-organisms, volatile organic compounds (VOC's), heavy metals, and pharmaceuticals. Removing these contaminants often improve the taste and odor of the water, which are two key factors when treating potable water. These contaminants are all different sizes and can require various sizes of water filters.

Water contamination can occur anywhere from the water source to the municipal treatment plant to the pipes in someone's home. Flint, Michigan, a city with a population of 98,310 in 2015, experienced one of the largest epidemics of water contamination on record in 2015 (U.S. Census Bureau, 2015). The Flint water crisis occurred when the city changed water supplies from Lake Huron to the Flint River. The Flint River is over 19 times more corrosive than Lake Huron. During this transition, the high corrosiveness of the water caused lead from the

aging city pipes to leach into the water supply. Tests from citizens' homes indicated lead levels were 880 times above the EPA's allowable limits for drinking water, or more than twice the limit for what is considered "hazardous waste" (CNN, 2016).

While this is an extreme case of contamination, a similar phenomenon can happen on a much smaller scale in someone's home without their knowledge. The EPA does not require homeowners to disclose if they have lead pipes to potential buyers or renters (Reagor, 2016). A household water filter is the last line of defense before human consumption.

A household water filter must balance the ability to allow water to flow through it at a flow rate that is sufficient for the given application, and to filter out contaminants present in the water at that same rate. Particulate contaminants are suspended in the water and are removed mechanically by the filter. Simply, if the particle is larger than the pore size of the filter, the particle cannot flow through and is filtered from the water. Figure 1 illustrates the relative scale of various contaminants and filtration technologies (EPA, 2003). Some of the most harmful contaminants - cysts, bacteria, and viruses - are also some of the smallest particulates that challenge a cartridge-style water filter. As filter pore sizes are reduced in an effort to remove these contaminants, the filter's flow rate is also reduced at the same pressure. The opposite is also true. As filter pore sizes are increased in an effort to increase flow rate, the amount of small particles allowed to pass through the filter increases. The filter designer must work with these two competing factors to come to a design that satisfies both needs.

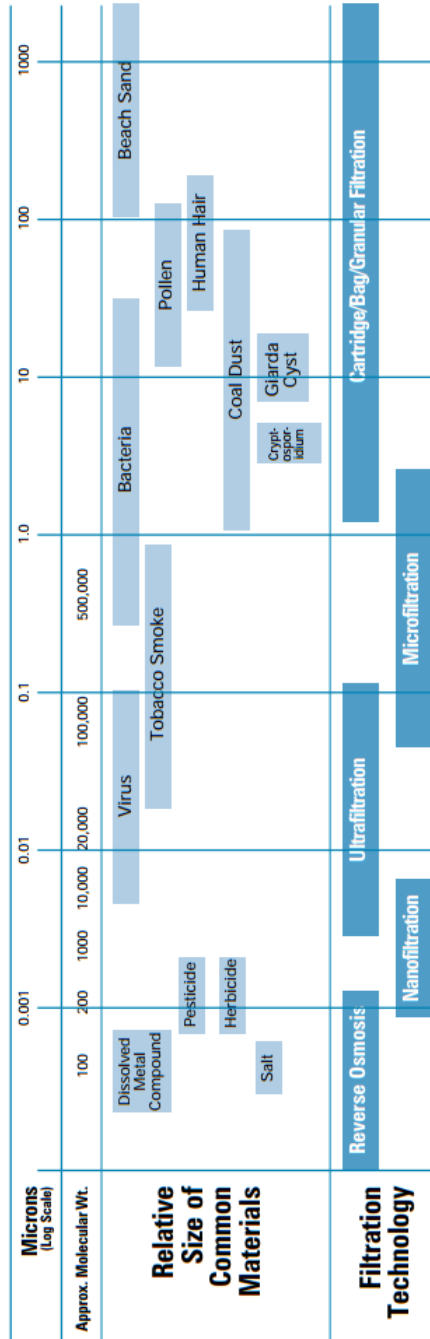


Figure 1 – Particle size distribution of common contaminants and associated filtration technology (EPA, 2003)

Chemical adsorption and catalytic reactions also play an important role in household water filtration, particularly when the targeted contaminant is smaller than the pore size of the filter or is dissolved in the water. One of the best materials that support these reactions is activated carbon. Many filters, including those to be analyzed in this research, are composed of activated carbon powder held together with a binder resin. As the powder particle size decreases, the block's pore size decreases and available surface area of carbon increases for a given overall volume of filter. This increases the filter's ability to remove VOC's and other contaminants from the water. Similar to particulate filtration, as pore size is reduced, filtration performance increases.

While performance increases as the pore size of a water filter decreases, it also requires more back pressure to achieve the same flow rate through the filter. This effect is shown in Figure 2 (Sutherland, 2008). For homes with low water pressure or in other low pressure applications, a filter with too large of a pressure drop will result in drastically reduced flow rates. When the operating environment of a filter only supplies a certain amount of pressure, the ability to predict the pressure drop through a given geometry of filter becomes an important design consideration. Numerous relations already exist to predict pressure drop through pipes, valves and other water system components. There also exist numerous relations to predict pressure drop through porous media with various flow conditions, which will be discussed in the next section. The pressure drop across a porous media filter in radial flow conditions at a high flow rate is not one of these readily available relations (Harrison, 2004).

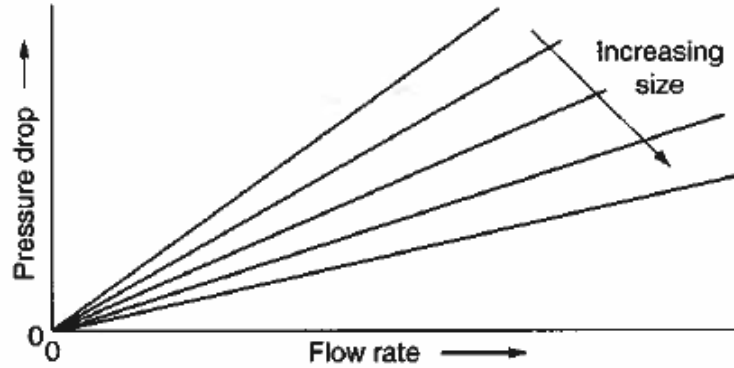


Figure 2 – Illustration demonstrating the impact increasing pore size has on the relationship between flow rate and pressure drop (Sutherland, 2008).

Existing Porous Media Equations

There are multiple existing relationships that describe pressure drop across porous media as a function of flow rate. The first is Darcy's Law, seen in Equation 1. Darcy's Law is a linear relationship between the fluid flow rate and the pressure drop across the porous media. Darcy's Law is valid for small pressure differentials (Scheidegger, 1974).

$$Q = \frac{\kappa A(P_1 - P_2)}{\mu L} ; \Delta P = \frac{Q\mu L}{\kappa A} \quad (1)$$

In Darcy's Law, ΔP is the pressure drop of a fluid with viscosity, μ , flowing at a volumetric flow rate, Q , over a bed of porous media of a given length, L , cross-sectional area, A , and permeability, κ . The high-side and low-side pressures are represented by P_1 and P_2 , respectively.

At high velocities, Darcy's law becomes invalid for both gas and liquid flows. The definition of the cutoff point for flow that deviates from Darcy's Law has been debated and discussed in the past. One view has been to characterize this critical value as a Reynold's number, defined in Equation 2. Reynold's number, Re , is defined as of fluid density, ρ , particle diameter, D_p , and fluid velocity, V , to the fluid viscosity, μ .

$$Re = \frac{\rho D_p V}{\mu} \quad (2)$$

The opposing view has been to characterize the critical value as Forchheimer number, Fo , as defined in Equation 3. The Forchheimer number is defined as a ratio of the permeability, κ , non-Darcy coefficient, β , fluid density, and fluid velocity to the fluid viscosity.

$$Fo = \frac{\kappa\beta\rho V}{\mu} \quad (3)$$

The range of critical values for non-Darcy flow using Reynold's number is much wider and more contested than the range of Forchheimer numbers. Cutoff values using Reynold's number have been measured anywhere from 0.4-1000. As described by Zeng, the critical limit of Forchheimer number for non-Darcy flow is dependent on the amount of deviation from Darcy's Law that is required before the flow is termed "non-Darcy." The other challenge of using Forchheimer number is that the values of permeability and non-Darcy coefficient must be experimentally determined (Zeng, 2006). This experiment will be looking at experimental data rather than attempting to predict the critical point for which flow becomes non-Darcy. For this reason, we do not need to settle on a criteria and predict the non-Darcy behavior prior to performing the experiment.

Regardless of the defined cutoff criteria, past research has validated that as fluid velocity increases, it deviates from Darcy's Law and can be described by other equations (Sedghi-Asl, 2014).

One of these, an extension of the Darcy equation, is the Forchheimer equation, or Hazen-Dupuit-Darcy equation, seen in Equation 4. The Forchheimer equation further describes the flow as the increasing fluid velocity causes the flow to deviate from Darcy's Law. The fluid velocity could also be represented by a ratio of the flow rate, Q , to the cross sectional area of the flow path.

$$\Delta P = \frac{\mu}{\kappa}V + \rho CV^2 \quad (4)$$

Another equation that could be useful in describing this flow is the Ergun equation, which is seen in Equation 5. This equation is built upon the Forchheimer equation by defining the form drag coefficient, C , and permeability as terms of the porous media geometry.

Similar to Darcy's Law and the Forchheimer equation, the Ergun equation was developed for flow through a packed media bed, assuming the bed is made up of spherical particles with diameter of D_p . The porosity of the bed is represented by ϵ .

$$\Delta P = \frac{150\mu L (1 - \epsilon)^2}{D_p^2 \epsilon^3} V + \frac{1.75 L \rho (1 - \epsilon)}{D_p \epsilon^3} V^2 \quad (5)$$

The packed beds analyzed by Darcy's Law, the Forchheimer equation, and the Ergun equation all assume longitudinal flow paths, while many existing household water filters, including those of this research, utilize radial flow paths. It is understood that flow in different domains (longitudinal and radial) will result in different pressure drops for a given flow rate. Longitudinal and radial flow paths are pictured in Figure 3 (McGowan, 2000).

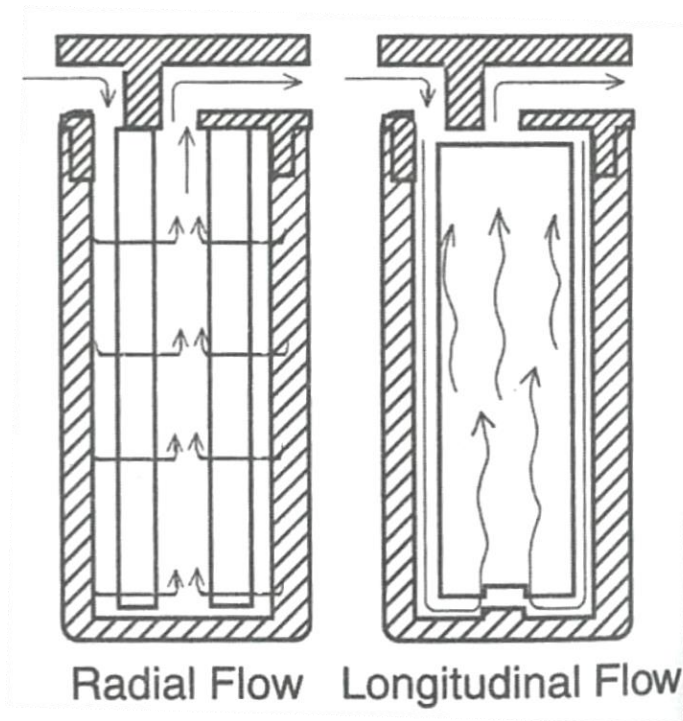


Figure 3 – 2-D cross-section views of radial and longitudinal flow paths (McGowan, 2000).

Darcy’s Law has been extensively studied in radial flow in the petroleum industry. The flow of oil into wells is modeled as a radial flow condition (Engler, 2010). Darcy’s Law in radial flow describes the pressure drop of flow through a cylinder with height, h , outer radius, r_o , and inner radius, r_i . This relationship is shown in Equation 6.

$$\Delta P = \frac{Q\mu}{2\pi kh} \ln\left(\frac{r_o}{r_i}\right) \quad (6)$$

Existing data from testing of water filters show that the relationship between pressure drop and liquid flow rate is quadratic, rather than linear. Figure 4 depicts the pressure drop of a Harmsco WB 5x170FL filter housing with a 20 micron filter cartridge (Harmsco). This indicates that the Forchheimer and Ergun equations are a better starting point when trying to develop a relationship between flow and pressure drop across radial flow porous media.

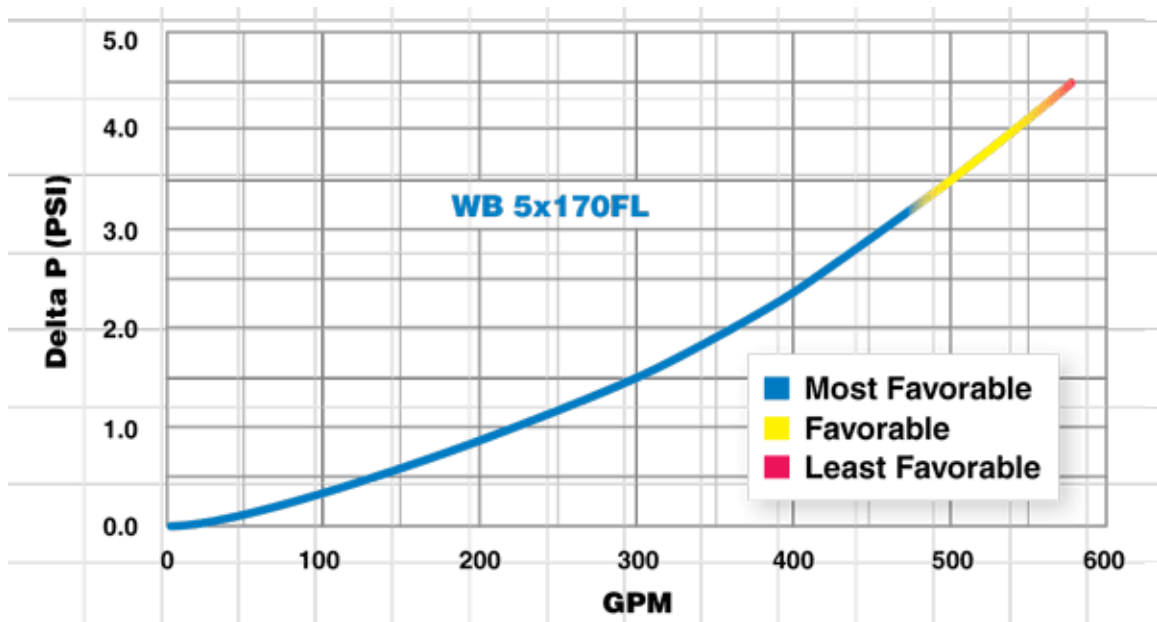


Figure 4 – Illustration of the pressure vs. flow curve of a Harmsco WB 5x170FL filter housing with a 20 micron filter cartridge (Harmsco)

Darcy’s Law, the Forchheimer equation, and the Ergun equation all assume identical spherical particles make up the porous media. If this assumption holds true, the theoretical porosity can fall between 25.95-47.64%. As more sizes of spheres are added, the theoretical

porosity can reach as low as 3.9% (White, 1937). The application of interest of this research consists of activated carbon (AC) particles held together with a binder resin. Activated carbon particles are not spherical. The true shape of these particles has an unknown impact on the accuracy of the Darcy, Forchheimer, and Ergun equations. Particle shape also affects the possible porosity values. As the shape of the particle moves from a sphere to an ellipse to a cube, the porosity of the densest packing configuration moves to 0% (Torquato, 2012).

Whether or not the binder resin affects the pressure drop over an identical radial bed of carbon also remains to be seen. Prior studies have shown that when considering fibrous air filters, the binder needs to be included in any CFD models if it is present in that filter (Zhou, 2009). It is possible that the hydrophobicity of the binder used could contribute to a pressure drop that deviates from that of a binder-less block with otherwise identical properties. The amount of binder that must be present for this effect to become significant is still unknown.

Activated Carbon

While AC is used at the forefront of filtration technology, it is not a new material. The use of charcoal as a purification agent dates back to 1550 B.C. when it was utilized in ancient Egyptian medicine. Its adsorptive properties were first scientifically recognized in 1773 when Scheele experimented with gas purification. A few years later, in 1785, Lowitz discovered its ability to act as a decolorizing agent. This then led to its use in sugar purification during the 1800s. In the mid-1800's, charcoal began to be used in the fields that activated carbon is most prevalent today – air and water purification (Hassler, 1974).

Activated carbon is a commonly used material in water filters. It has an extremely high surface area per unit mass, $500\text{-}2500\text{ m}^2/\text{g}$, giving it extraordinary adsorptive capabilities. This surface area is a product of the high porosity of AC. Anotoine-Alexandre-Brutus Bussy, a French chemist, is credited as the first to scientifically suggest that porosity was the driving force behind AC's adsorptive powers. (Achaw, 2012). These pores are classified as either macropores, those which are greater than 1000\AA , or micropores, those which are $10\text{-}1000\text{\AA}$. Smaller micropores are

able to adsorb smaller adsorbate molecules than the larger macropores. Depending on the size of the chemical contaminants in the water, some areas of porosity may not be available to provide adsorption. Figure 5 illustrates this effect (Cheremisinoff, 1978).

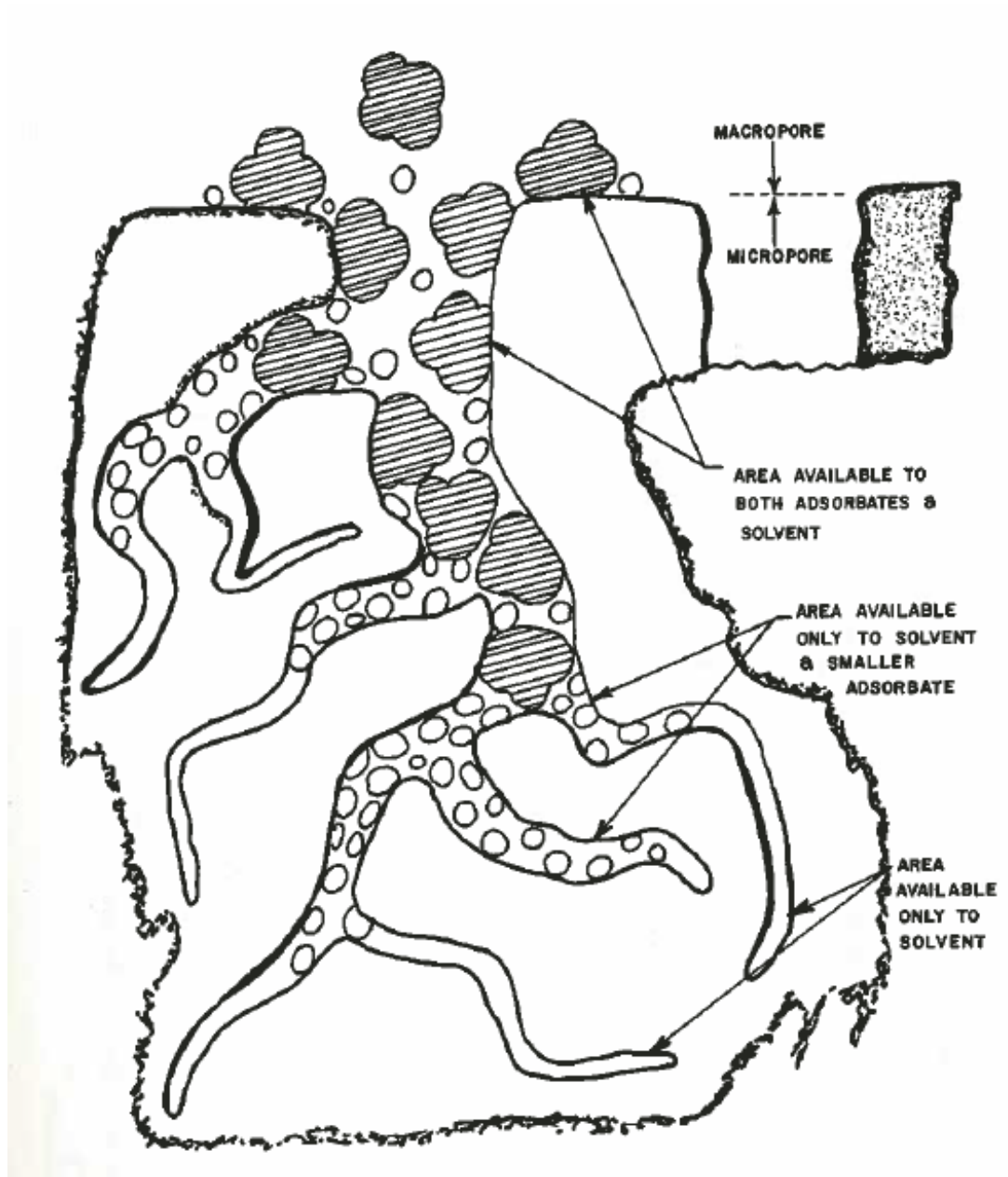


*Figure 5 – Artist’s conception of molecular discrimination effects of carbon pores
(Cheremisinoff, 1978).*

The production of activated carbon has been extensively studied in the past. The following background of the process is a summary of the information presented in Hassler's 1974 work, *Purification with Activated Carbon*.

Activated carbon can be manufactured from any carbon-based material, the most common of which are coal, coconut shell, and sawdust. Activated carbon is produced in two steps, carbonization and activation. Carbonization can be performed physically or chemically. In this step, the base material, in absence of air, is heated to temperatures ranging from 400-900C, depending on the method being used. Chemical carbonization uses a chemical, typically a strong acid, base, or salt, as a catalyst to reduce the process time and allow a lower process temperature .

After the material undergoes carbonization, it must be activated. Activation re-introduces an oxidative agent to the material while it is still at high temperature. Examples of oxidation agents include air, steam, or carbon dioxide. It is during this step that the material gains its porosity, high specific surface area, and adsorptive capabilities.

After it is activated, one batch of AC consisting of base material A cannot be chemically distinguished from another batch of AC consisting of base material B. The differentiation points between batches are their adsorptive and catalytic properties.

Today, the determination of these differentiating properties can be done in multiple different ways. If the target contaminant is known, developing adsorption isotherms for this specific contaminant is the most direct method to differentiate between carbons. This is a labor intensive test procedure that involves exposing a varying amount of carbon to a known level of contaminant and measuring the residual contaminant level after a specified amount of time (Hassler, 1974).

A quicker test method for differentiating between carbons is described by Nowicki as an AC tester. In this test method, given amounts of AC and mineral oil are mixed together. The resulting reaction between the two is an exothermic reaction. A thermometer is used to measure the heat-of-immersion (HOI) temperature rise resulting from this exothermic reaction. A larger

HOI temperature rise indicates that a sample of AC has a larger surface area available for adsorption than a different AC with a lower HOI temperature rise (Nowicki 2009). This method does not require any specialized equipment to measure chemical concentrations, greatly reducing the complexity of the test. The result of this test is more general than a specific adsorption isotherm, making this procedure favorable for generic comparisons, or comparing one batch to itself over its useful life.

Past Research

Numerous experiments have been conducted in the past that can provide guidance for this research. While not all are directly related to activated carbon blocks or porous media with high-velocity radial flow, the applicable topics are described in this section.

Past research has been completed to determine the effect of a sample's length on porous-flow parameters. For very thin samples of porous media, the drag coefficient and permeability of the porous material are measured to be a function of the thickness of the sample. These permeability and drag coefficient values are important parts of the Darcy and Forchheimer equations. Hence, pressure drop will also be a function of sample thickness in these ranges. Entrance and exit effects are negligible if the sample's length is equal to or greater than one hundred times the pore size of the media (Dukhan, 2011). Assuming this same value can be applied to radial flow, only samples that fit this thickness requirement will be studied in this research.

Characterizing the geometry of the samples to be measured presents a challenge. While overall geometry of the block, such as outer diameter, inner diameter, and length, are easy to measure, measuring porosity can be difficult. Mercury porosimetry is the standard defined by ASTM to take this measurement, but it requires specialized equipment and a lab capable of handling mercury (ASTM D4404-10). Past experiments have used a scanning electron microscope (SEM) or a digital microscope to image small sections of the sample (Wang 2008). These images can be analyzed to determine the local porosity of that cross-section.

A 2007 study found that the technique used to capture the image, the user analyzing the images, and the thresholding technique used all played a significant role in the final determination of porosity value. They determined that SEM images produce the most contrast and, therefore, produce the most accurate porosity values when analyzed. When microscopes take images, they rely on the diffusion of light, creating less contrast than SEM images. This causes pores to appear smaller in the image than they are in the physical sample. This effect is most pronounced when very small pores are being investigated. The differences are minimized when the pores of interest are all very large (Marcelino, 2007). This effect emphasizes the importance of choosing the correct magnification level before capturing the pictures to be analyzed.

When SEM is not practical, a resin can be injected into the material to fill the vacant space of the pores. This produces increased contrast, a critical item when analyzing images taken with a digital camera or microscope. This technique is commonly used when studying fibrous air filters (Jaganathan, 2008). The major drawback of this technique is its destructive nature. After the resin is injected into the filter, it is not possible to evaluate pressure drop or other performance characteristics of the sample.

Depending on the porosity distribution within the sample, this local porosity may or may not be able to represent the overall porosity of the sample. This will need further study in this research. Past research has indicated that inhomogeneity of the filter structure general results in lower pressure drops than a homogeneous models suggest (Straub, 2009). Considering this fact, consistency within the samples to be examined becomes paramount. Evaluating this consistency is one of the first steps that will need to take place during sample preparation.

Extremely detailed porosity measurements of fibrous air filters have been taken in three dimensions using MRI technology (Hoferer, 2006). This method provides very high resolution measurements of porosity and filter structure, is a non-invasive procedure, and provides full detail of all inconsistencies within the sample, but it is very expensive. This method is considered to be too costly for the scope of this project.

Another challenge is determining the particle diameter, D_p , of the samples in the study. Past research has used digital image analysis of pictures taken with a DSLR camera to determine particle diameter (Pathapati, 2009). While suitable for applications which study nominal sizes of 2 to 5 mm, a DSLR camera will not be suitable for studying powdered AC which can be smaller than .04 mm. It is possible that analysis of the SEM or microscope images taken for porosity analysis will also be useful in determining particle diameter. It is also possible that the dimensions of the powder can be determined prior to being formed into the test samples using sieve analysis.

Planned Work

The goal of this research is to experimentally observe the relationship between pressure drop and flow rate for high velocity radial flow through porous media. The ideal outcome would be to derive an Ergun-type equation that uses geometric properties of the media to describe this relationship. This experiment will be conducted using carbon block water filter cartridges as the porous media of interest.

Test samples of carbon blocks will be made with the two most commonly used production methods – compression molding and extrusion. Each carbon block will be evaluated for porosity using image analysis software to evaluate images captured with a digital microscope.

The produced carbon block samples will be tested to determine their relationships between pressure drop and flow rate. The scope of this project will be limited to the pressure drop across the entire block. No evaluation of the pressure differentials within the block will be performed.

The goal of this work is to determine an equation that can be used during the early design stages of new water filter designs to predict the flow rate or pressure drop of a given block. This equation will allow future engineers to more quickly come to a design that will work within the constraints of their application.

MATERIALS AND METHODS

Materials

The carbon blocks used in this experiment are made of a mixture of carbon powder, binder powder, and a process aide. The process aid is critical to ensuring the mixture is homogeneous. If the mixture is not homogeneous the finished product will not be consistent.

Three different carbons were used in this experiment. The carbons, all manufactured with the same method using the coconut shell as the base material, are different size particles. The material batches are designated by their nominal mesh sizes. MC20X50 is a batch that has particles that should fall between the ASTM mesh sizes 20 and 50. These meshes correspond to 841 and 297 μm , respectively. MC40X200 is a batch that has particles between ASTM mesh sizes 40 and 200, or 425 and 75 μm , respectively. MC80X325 is a batch that has particles between ASTM mesh sizes 80 and 325, or 180 and 45 μm , respectively.

The particle sizes of each material batch were determined using a Verder AS200 sieve shaker. The sieve stack included sieves with mesh sizes 40, 60, 80, 100, 140, 200, 270, 325, and 400. The mesh sizes correspond to 425, 250, 180, 150, 106, 75, 53, 45, and 38 μm , respectively. A 150 gram sample of each material batch was loaded into the 40 sieve. The shaker ran for 10 minutes with 20 second intervals and a 0.60 mm amplitude. After passing through the sieves, the amount of powder that remains between each sieve pair is weighed and recorded to determine a particle size distribution. A weighted average of this data can estimate the average particle size for each material.

The binder material used for these blocks is Microthene FN51000 low-density polyethylene. This material conglomerates with its own particles very well. This is less than

ideal when attempting to mix powders into a homogenous blend. To get around this issue, a small amount of M5 fumed silica is added to the mix to disperse these particles.

When preparing to produce a carbon block sample, the first step is to mix the powders together. For this experiment, each material batch was prepared with 1400 grams of the carbon of interest, 340 grams of binder, and 15 grams of M5 fumed silica. After measuring and combining these ingredients, the mixture is run through a Waring 1 gallon blender for 1 minute. Blending is another factor that affects the homogeneity of the material to ensure a consistent product. The high shear force from the blender blades completely disperses the binder and process aid within the carbon. Images of the material before and after blending are shown in Figure 6. After blending, the material is ready to be processed into carbon block.



Figure 6 - Carbon and binder mixture before and after blending, left and right, respectively.

Block Manufacturing Methods

The samples for this research were prepared using the two most common carbon block manufacturing methods – compression molding and extrusion. Both methods utilize a mixture of carbon and binder powder, as discussed in the previous section.

Extrusion is a much faster method of production for carbon blocks. This research used a pilot carbon block extruder purchased from KT Corporation to create the test samples. This

extruder consists of a material hopper, screw, barrel, die, heater, and cooling jacket. All of these components are shown and labeled in Figure 7.

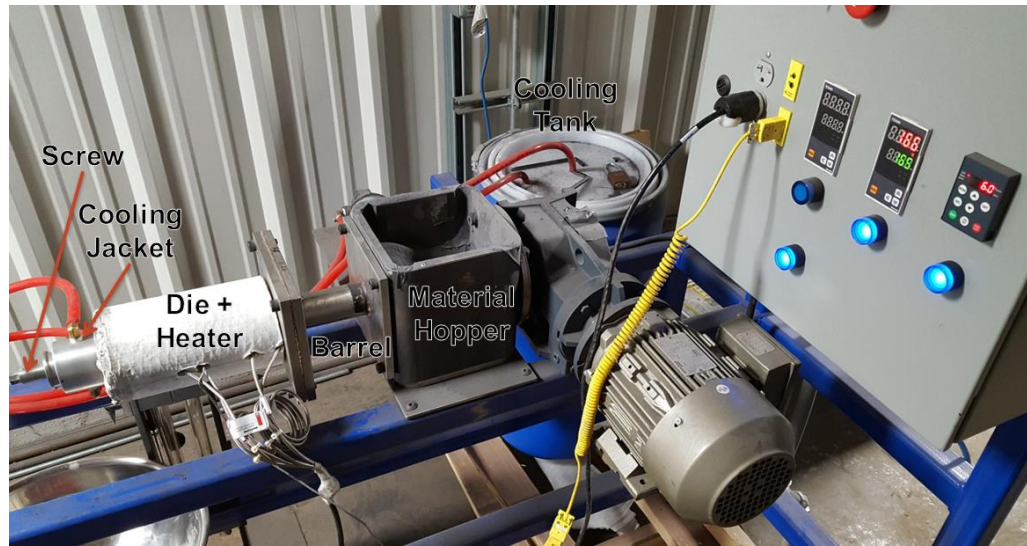


Figure 7 - Layout of carbon block extruder components.

The material to be extruded is fed into the material hopper. From there, the screw gathers the material and carries it through the barrel. The screw is controlled by a variable speed motor. Adjusting the speed of this motor will affect the rate of extrusion and the porosity of the blocks. For this experiment, all samples were extruded with the motor set to run at 6 Hz. The diameter of the base of the screw also serves to control the ID of the extrusion.

After the material works through the barrel, it enters the die. The size of the die controls the OD of the extrusion. The die is heated by the heater. This heat allows the binder in the powder mixture to solidify and form a carbon matrix. The heat from the heater must be sufficient to bring the binder at the screw surface to a temperature that can hold the material in a solid block. If the die is not hot enough, the block will not have a solid surface at the inner diameter. This will result in a non-uniform cross section, not suitable for this research. Figure 8 shows an example of both a good and bad product from the extruder. In this experiment, the temperature is set to 165°C or 175°C, depending on the OD of the extrusion. The thicker OD extrusion requires a higher temperature to fully set throughout the entire block's thickness.



Figure 8 - Examples of a fully-formed carbon block, left, and a block that was not sufficiently heated and formed, right.

After leaving the die, the block travels through the cooling jacket. This jacket is water-cooled using a 20 gallon tank of water. It is important that the block spends enough time in this jacket to solidify, or else the matrix will fall apart as it leaves the tool. This limits the extrusion rate. Any attempts to increase the extrusion rate above this limit would require a larger cooling jacket.

This experiment used three different die and screw combinations to produce three different OD and ID combinations. These values are listed in Table 1.

Cross-Section	OD (in)	ID (in)
M	1.200	0.375
R	1.200	0.825
K	1.900	0.750

Table 1 - Dimensions of the extruder dies and screws used to produce samples.

After the extrusion process is complete, the long rod is cut off of the extruder using a hacksaw. This long rod is then cut to their final length using a Stanley Adjustable Angle Clamping Mitre Box Saw. The sample lengths to be used in this experiment are 1.5", 2.25", 3"

and 5". Three samples of each length were cut out of each batch of extrusion, along the full length of each batch.

Compression molding is similar to injection molding. There are two mold halves and an insert to create the hollow block. The insert is placed between the two mold halves and the halves are bolted together. The carbon mixture is dispensed into the mold cavity, the top is put onto the mold and compression is applied. This assembled mold is then placed in a high temperature environment, which allows the powder mixture to form into a hard matrix block.

Figure 9 illustrates a simple mold design. This design was milled from aluminum during the initial stages of this experiment. The cycle time to produce one sample with this mold was around 4 hours. Due to this high cycle time, and the cost associated with milling multiple molds, this production technique was not investigated further during this research.

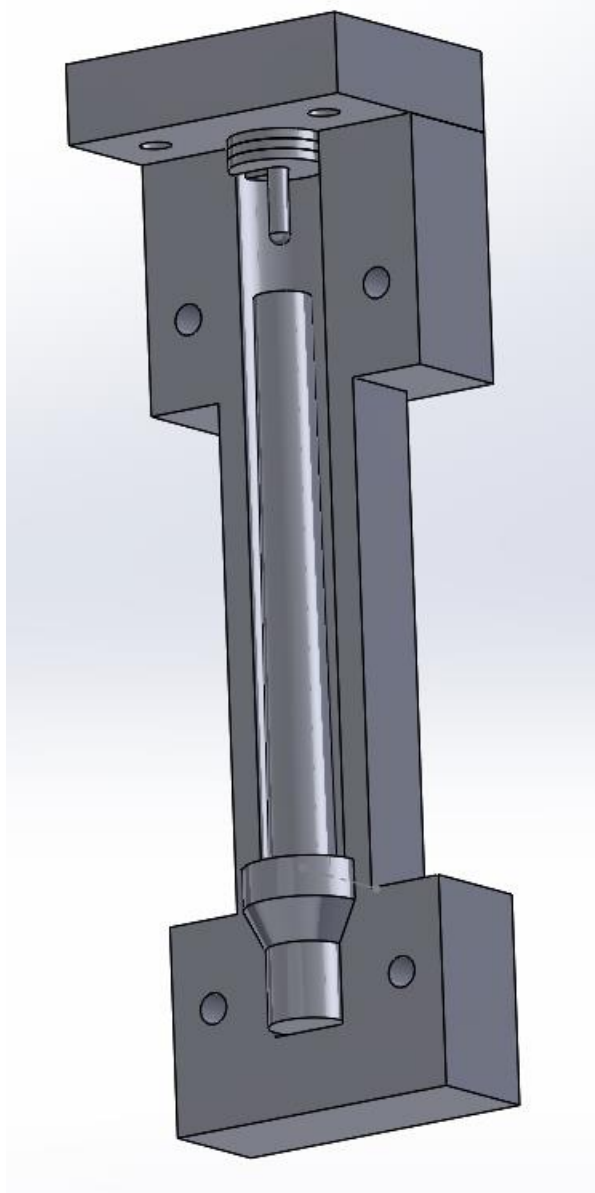



Figure 9 - Cross-section view of compression mold used to produce carbon block samples.

Porosity Measurement

The porosity of each of the samples was calculated by analyzing 2-D images of the sample surface taken with a Hirox KH-8700 digital microscope. This microscope was equipped with a MXG-5040RZ mount and a AD-5040SS lens. All images were taken with the shade on the lens extended fully down. The light control on the microscope mount was set to the middle level, . The brightness level of the microscope was set to 128. Each image was captured in a JPG-1 format with the “Standard Size (1200 x 1600 pixels)” option selected. An example of an image is shown in Figure 10.

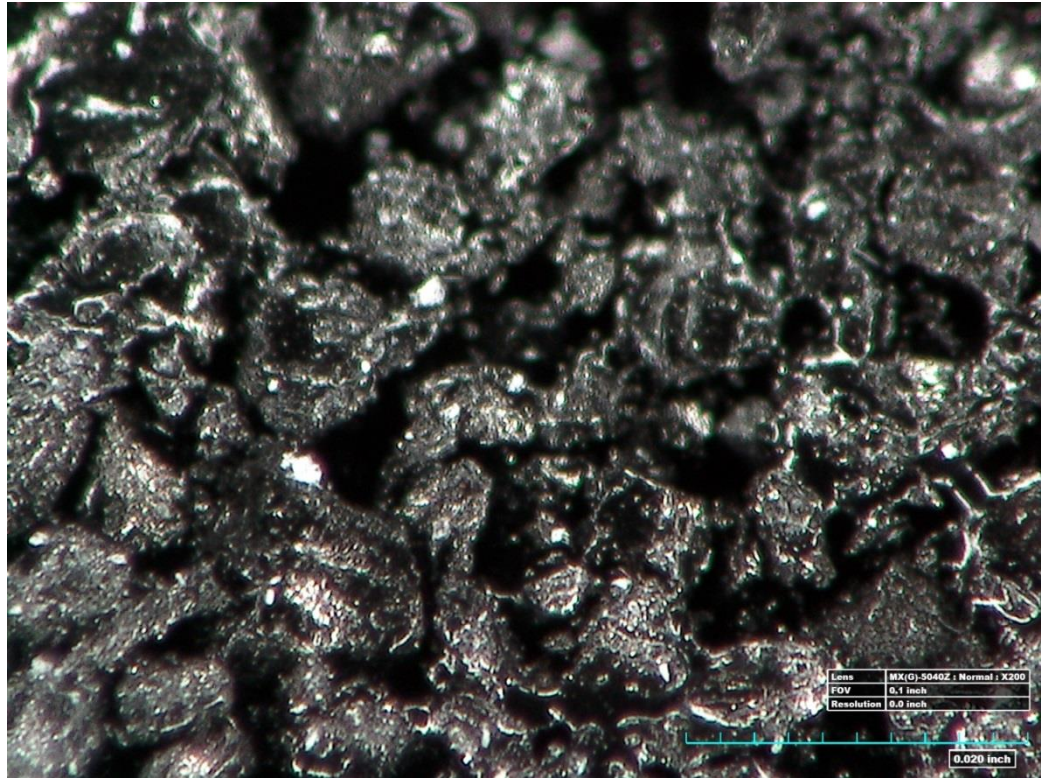


Figure 10 - Image of the surface of a carbon block taken with a digital microscope at 200X zoom. This image is serialized 01-02-004.

The samples produced with the MC40X200 carbon and the MC80X325 carbons were imaged with a 200X magnification. The samples produced with the MC20X50 carbon were imaged with a 100X magnification. If the MC20X50 samples were imaged at 200X magnification, the field of view was so limited that it could be filled with one or two pores or

particles. This would produce a porosity measurement that is not representative of the sample as a whole.

The samples that had a 1.2” outer diameter were imaged with one single image per test point. The samples that had a 1.9” outer diameter were too large to fit in the sample holder beneath the microscope. Due to this, they had to be hand-aligned underneath the lens. To remove as much user error from the alignment and focus procedure as possible, these samples were imaged using the microscope’s tiling feature. An upper and lower limit on the lens height was given to the filter, above and below the focus point, respectively. The microscope would step through this range of lens heights, taking pictures at each step. At the end of the range, the microscope would tile these images together to create a single in-focus image. The inputs used for each of these values are listed in Table 2.

Zoom	Upper Lens Height (µm)	Lower Lens Height (µm)	Lens Height Range (µm)	# of Steps	ΔHeight per Step (µm)
100X	5880	4121	1759	8	219.875
200X	5467	4704	763	8	95.375

Table 2 - Settings for tiling feature when imaging 1.9” OD samples

Each image was analyzed in MATLAB using tools from the Image Processing Toolbox in a custom function. The function, named “*ImageAnalysis_Oct10*”, is written in full in Figure 36 in the Appendix.

After receiving input from the user, this code reads the image, converts it to black and white and removes the scale from the bottom of the image. The images collected with the tiling process do not include a scale, so line 8 is removed when analyzing these files. Next, the program generates a histogram of all of the pixel’s brightness values. This histogram is the key to determining the difference between a pore and a particle.

Thresholding converts grayscale images to black and white images by comparing each pixel’s intensity value to a threshold limit. Any value below the limit is converted to a 0. Any value above the limit is converted to a 1. The result is a binary image that represents two distinct items, particles and pores in this case. This threshold limit is set by examining the shape of the

image histogram. Bimodal distributions, or distributions with two distinct peaks, are easiest to analyze because the threshold limit is at the minimum value between these two peaks.

Lines 16-50 in the code perform the task of setting the threshold limit by locating the peaks and valleys in the histogram, determining the location of the 2nd large peak, and finding the local minimum, or valley, between the start and the 2nd peak.

Note, on line 43, the location of the 2nd peak is determined by finding the first peak taller than at least 20 pixel values to the left and 20 pixel values to the right. This value was determined after running through multiple images of the carbon blocks. Some image histograms did not have this distinct of a peak, and this value was reduced until a peak was located.

After the image is converted to a binary image, lines 53-55 remove some of the noise in the image, or “pores” that are smaller than 3 pixels. Given the zoom levels at which the images were captured, any binary values smaller than 3 pixels are lighting anomalies and not true pores.

To calculate the porosity, the code counts the number of black pixels and white pixels in the thresholded image. The black pixels represent the pores and the white pixels represent the particles. A ratio of the black pixel count to the total pixel count gives a porosity value. It is important to note that this calculation assumes that the porosity is isotropic with respect to the radial position within the block. Any anisotropic effects are not considered in this analysis.

After this analysis is complete, the code outputs three items – a porosity value, a thresholding limit, and a graphical summary of the analysis. The graphical summary of the analysis, as shown in Figure 11, displays the original image, the grayscale image with the scale removed (if necessary), the histogram of the grayscale image, and the black and white image that represents pores and particles.

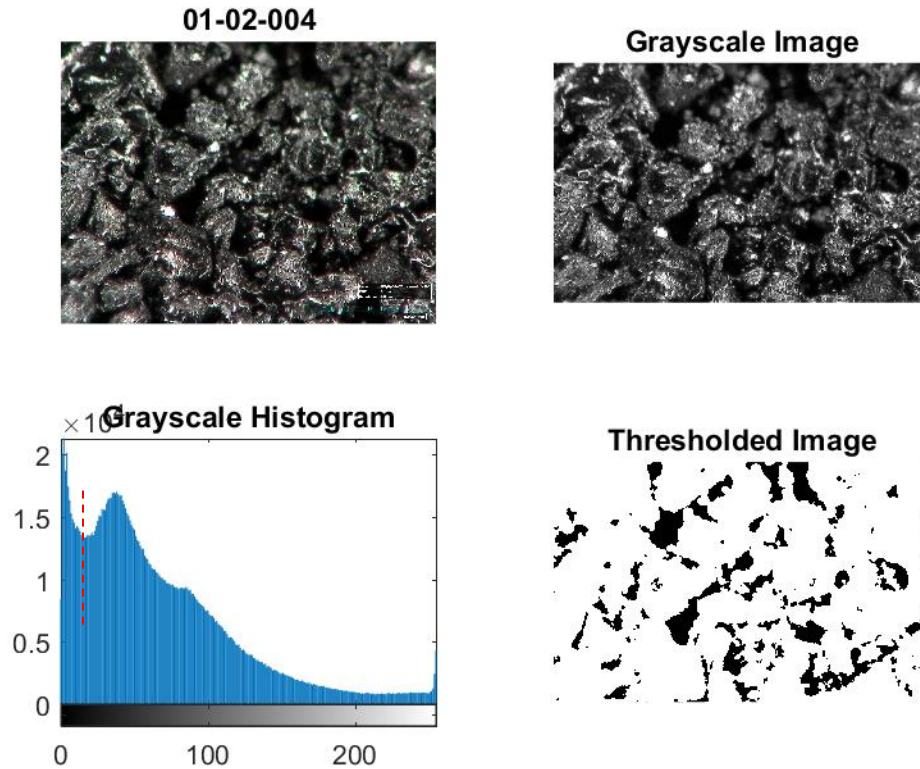


Figure 11 - Graphical summary output of “ImageAnalysis_Oct10” after analyzing image 01-02-004, also shown in Figure 10.

Each graphical summary was examined to determine the validity of the analysis. A number of the summaries displayed histograms that were not bimodal. They only displayed one peak, making it difficult to set a threshold limit. The porosity values for these images were not considered in this analysis. Any further calculations performed using porosity values instead utilized block or batch averages.

There were also some samples that had more than two peaks that were relatively close in intensity. An example of such a situation is shown in Figure 12. In these cases, another code was written that prompted the user to set a custom threshold input. This input value was determined by examining the original analysis and finding the first minimum between the peaks.

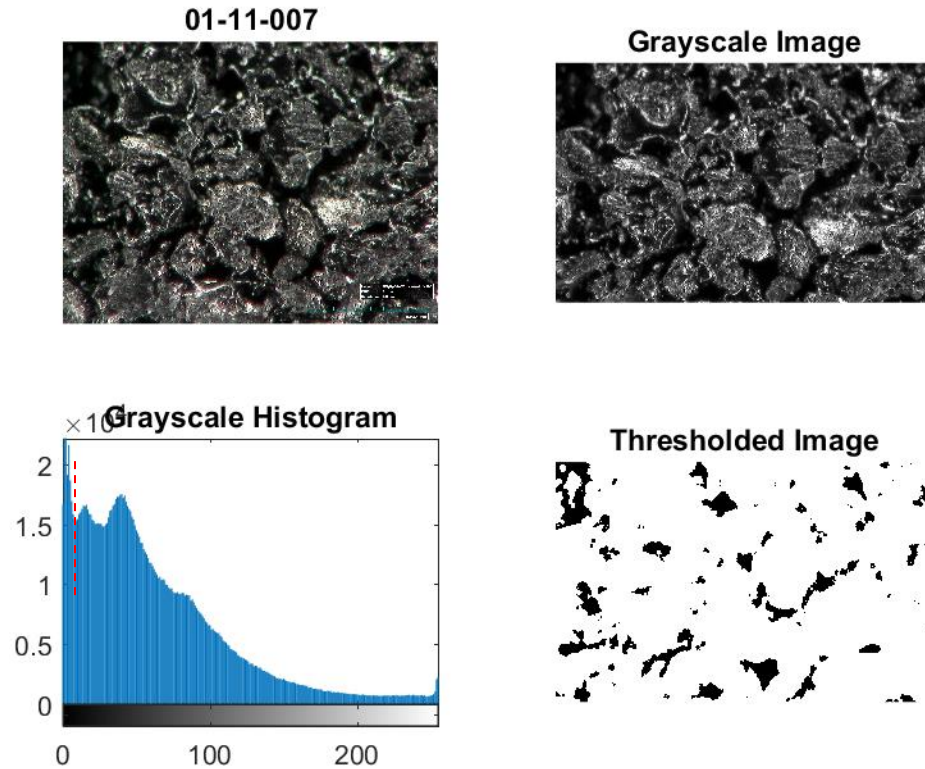


Figure 12 - Graphical summary output of “ImageAnalysis_Oct10_ManualThresh” after analyzing image 01-11-007 with a user-given threshold limit.

Carbon Block Finishing

After each block is produced and evaluated for porosity, it is finished in three steps. First, its height is measured with a pair of Mitutoyo digital calipers and recorded. Next, its weight is measured with a Weigh-Tronix digital scale. These values are used to calculate each block’s density. This density should provide good information about the consistency of the production process within each batch of extrusion.

Finally, each block receives two end caps. Both end caps serve to prevent the fluid from flowing around the block and force radial flow. The top end cap mates with a manifold. The top end cap also has a hollow center that allows fluid at the interior of the carbon block to flow out of the manifold. Each end cap is held onto the carbon block using Loctite Hysol 232 hot melt

adhesive. The end caps were produced out of ABS using 3D-printed prototype injection molding tools and a Morgan Press.

Air Test Method

The first test performed on the finished blocks is an air test. In this test, a vacuum pump pulls air out of the center of the carbon block. A diagram of this flow path is shown in Figure 13. The air flow is adjusted using a small control valve. The air flow rate is measured and displayed with an Aalborg GFM17 flowmeter. The pressure drop is measured by an Omega PX277-30D5V digital pressure transmitter. The pressure transmitter, which has field selectable ranges, was programmed to output 0-10V, which corresponds to 0-1875 Pa. An Agilent DAQ program monitors the output of the pressure transmitter.

During this test, each sample is installed onto the manifold and subjected to 0.2, 0.4, 0.6, 0.8, and 1.0 L/min airflow. The pressure drop at each point is recorded by the user in an Excel spreadsheet for future analysis.

Water Test Method

After undergoing the air test, the samples are put through a water test. The concept is similar to the air test – each sample is subjected to various flow rates of the fluid and the pressure drop at each point is observed. There are a number of small differences between each test, however.

The first difference is the physical method by which the pressure differential is created. In the air test, the vacuum pump pulls air from the OD of the block to the ID. In the water test, the pressure line is plumbed to the OD of the block and the ID is exposed to atmospheric pressure. While the fluid still flows in the same direction, OD to ID, this difference should be noted. A diagram of the water flow path is shown in Figure 13. This figure also shows the geometry of the end caps and manifold used to hold the block in place. Note, the o-rings between the end cap and the manifold are not shown.

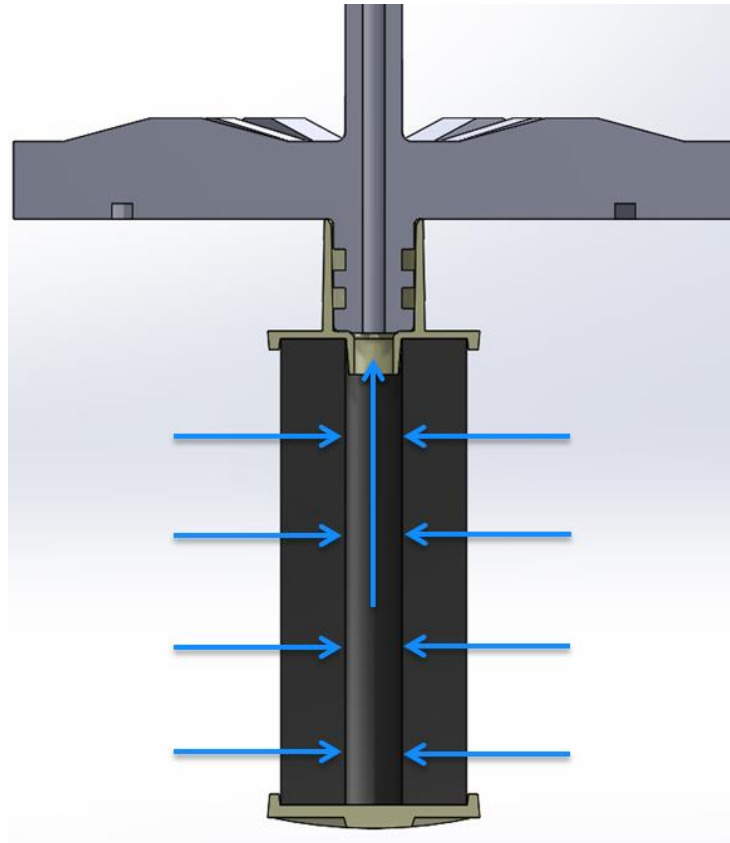


Figure 13 - Layout of carbon block sample assembled with end caps and manifold for water test. Arrows signify direction of water flow.

The equipment used to measure the flow and pressure is also different between the two tests. Rather than recording data by hand, a Prosense SPT-10-10-0300A pressure transmitter is used in this test. The flow rate is controlled by a King Instruments adjustable flowmeter. This flow rate is measured digitally by a Digimesa S38-7556/03 flowmeter.

The flowmeter and pressure transducer outputs are measured with an Arduino Nano. This Arduino monitors the data, outputs it to an LCD screen, and records the data to Excel when the user pushes a button on the breadboard. A copy of the Arduino code is included in the Appendix in Figure 37.

RESULTS AND DISCUSSION

Particle Size Distribution

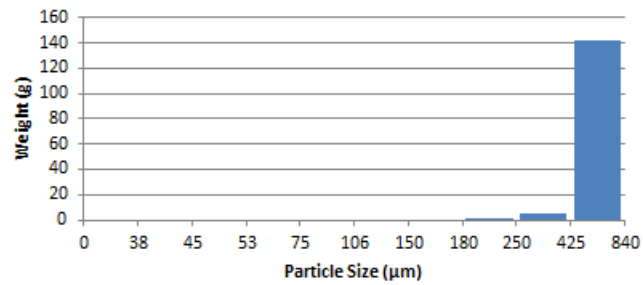
Before any material was extruded, a sieve analysis was performed on each size of carbon powder. The results from this analysis are shown in Figure 14. Using a weighted average, the average particle size for each material can be determined. The results of these calculations are shown in Table 3. The raw data from the sieve analysis can be found in the Appendix in Table 13.

From this data it is clear that there are three distinct particle sizes in the different materials. Note that the distribution of the MC20X50 carbon, referred to as Material 1, is not as normal as the other two. This is due to the fact that the sieves used in this analysis only go up to mesh size 40. Everything that falls between mesh sizes 20 and 40 fell into the same sieve.

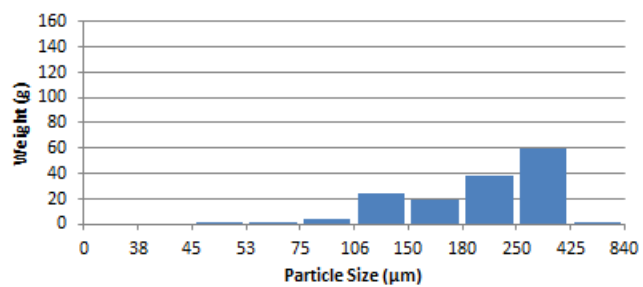
Material	Material Designation	Average Particle Size D_p (μm)
MC20X50	1	623
MC40X200	2	241
MC80X325	3	101

Table 3 - Material designations and average particle sizes.

MC20X50 Carbon - Particle Size Distribution



MC40X200 Carbon - Particle Size Distribution



MC80X325 Carbon - Particle Size Distribution

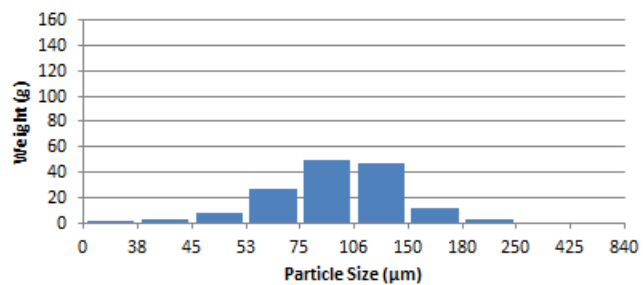


Figure 14 - Particle size distributions for each material, as determined by sieve analysis.

Each combination of Cross-Section and Material was extruded in a batch. These batches were labeled with the order in which they were extruded (Batch 1, Batch 2, etc.). These batch numbers and their corresponding characteristics are defined in Table 4. Refer back to Table 1 for cross-section dimensions.

Batch	Cross-Section	Material
1	M	2 - Medium
2	R	2 - Medium
3	K	2 - Medium
4	M	1 - Coarse
5	M	3 - Fine
6	R	3 - Fine
7	R	1 - Coarse
8	K	1 - Coarse
9	K	3 - Fine

Table 4 - Batch numbers and the corresponding cross-section and material configurations.

Each Batch consists of 12 blocks, three samples of each length (1.5", 2.25", 3", 5"), except for Batches 8 & 9. Due to the speed of extrusion, these batches only yielded enough to produce three samples of each of the three shortest lengths (1.5", 2.25", 3"), for a total of nine samples per batch.

Density Calculations

The first results obtained from each block are the density calculations based on the weight, w , and height measurements. The raw data from these measurements can be found in the Appendix in Table 14. The calculation for the density of each block is shown in Equation 7.

$$\rho_{block} = \frac{w}{\left[\pi \left(\frac{OD}{2} \right)^2 - \pi \left(\frac{ID}{2} \right)^2 \right] h} \quad (7)$$

A propagation of uncertainty calculation can be performed to determine how the uncertainties in the weight and height calculations affect the density results. This propagation is shown in Equation 8. The OD and ID dimensions are not factored into this uncertainty because they are controlled by the die/screw and were not hand measured.

$$\Delta\rho_{block} = \sqrt{\left(\frac{\delta\rho}{\delta w} \right)^2 \Delta w^2 + \left(\frac{\delta\rho}{\delta h} \right)^2 \Delta h^2} \quad (8)$$

The weights of each block, measured on a Weigh-Tronix scale in grams, had an uncertainty of +/- 2 g. The heights of each block, measured with Mitutoyo calipers, had an

uncertainty of +/- .0005". Using these error values, the propagation of uncertainty was performed. The results of this calculation were used to generate error bars on the density results graphs for each batch. The results graph of Batch 1 is shown in Figure 15.

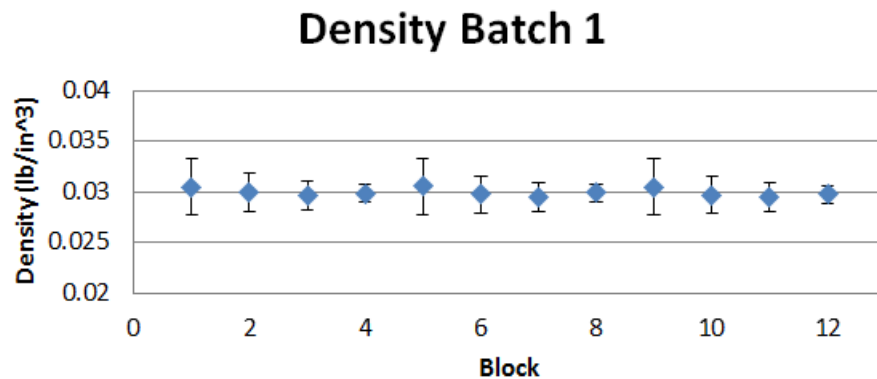


Figure 15 - Calculated density of each sample extruded in Batch 1, with error bars included.

The first item of note in this graph is that, although the nominal density has some small fluctuations from block to block, each data point is well centered within the error bars throughout the entire batch. This shows that the process was very stable when these samples were produced. Without this consistency, it would be very difficult to compare different samples with each other. The majority of the batches have very similar consistency to this example.

Batch 2 was not quite as consistent as Batch 1. These density values are shown in Figure 16. The first block has a nominal density that is lower than the rest of the batch. This typically signifies that the sample was taken too close to the front-end of the extrusion, before the back pressure fully developed in the system and a steady state extrusion process was achieved. While all of the error bars have overlap, the nominal points are not as well-centered in this data. This will need to be considered as further results are developed. Batch 9 also follows a similar pattern to this example, although it is not as large of a difference. The graphs summarizing this data for all Batches can be found in the Appendix in Figure 38.

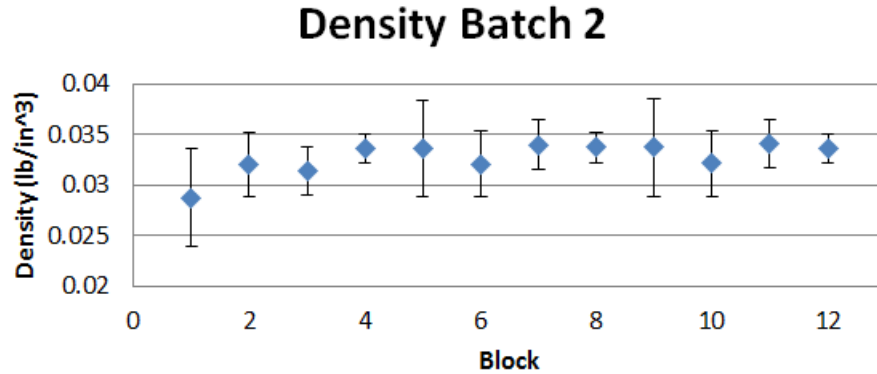


Figure 16 - Calculated density of each sample extruded in Batch 2, with error bars included.

The average nominal results for each batch are shown in Table 5. The densities for all materials are higher in the “K” cross-section. These are the cross-sections with the thinnest walls. It is likely that running the extruder at the same speed through these thin cross-sections produce more back pressure in the die, yielding a denser product. This table also shows a general density increase as the material moves from coarse to fine.

Density (lb/in ³)			
	Material		
Cross Section	1 - Coarse	2 - Medium	3 - Fine
M	0.0294	0.0295	0.0306
R	0.0280	0.0299	0.0296
K	0.0311	0.0327	0.0337

Table 5 - Average nominal density for each batch of extruded samples.

Porosity Analysis

The next step in the analysis was to determine a porosity value for each of the blocks. The first blocks were analyzed using three images per block. This did not yield a porosity that converged to one value. These blocks were re-imaged and 8-10 images were analyzed per block. The porosity values and threshold values were recorded in tables, examples of which can be seen in Tables 6 and 7. Complete porosity data can be found in the Appendix in Table 15.

		Image 1	Image 2	Image 3	Image 4	Image 5	Image 6	Image 7	Image 8	Image 9	Image 10	Average
Batch	Block#	Porosity	Porosity	Porosity	Porosity	Porosity	Porosity	Porosity	Porosity	Porosity	Porosity	Porosity
9	1	6.97%	6.43%	2.21%	2.27%	6.23%	4.36%	5.55%	3.78%	5.10%	5.59%	4.85%
9	2	3.53%	4.25%	3.53%	4.91%	3.88%	5.04%	3.64%	3.57%	3.37%	5.57%	4.13%
9	3	2.49%	1.49%	2.72%	4.21%	3.51%	3.57%	2.80%	3.00%	2.86%	4.21%	3.09%
9	4	4.61%	6.90%	2.98%	4.51%	3.88%	1.20%	2.62%	4.30%	2.93%	2.99%	3.69%
9	5	2.35%	4.53%	3.79%	5.90%	2.75%	3.58%	5.03%	2.60%	4.93%	2.12%	3.76%
9	6		3.30%	5.32%	3.92%	5.78%	4.37%	4.16%	7.08%	4.01%	6.06%	4.89%
9	7	3.16%	4.14%	5.85%	6.28%	8.65%	3.39%	6.84%	4.64%	7.29%	5.75%	5.60%
9	8	5.20%	2.52%	6.52%	4.32%	5.35%	4.23%	5.28%	3.61%	3.92%	6.46%	4.74%
9	9	7.59%	5.84%	4.84%	6.92%	3.76%	5.21%	4.66%	5.09%	4.01%	5.10%	5.30%
9	Average											4.44%

Table 6 - Calculated porosity values from analysis of Batch 9 block images.

		Image 1	Image 2	Image 3	Image 4	Image 5	Image 6	Image 7	Image 8	Image 9	Image 10
Batch	Block#	Thresh	Thresh	Thresh	Thresh	Thresh	Thresh	Thresh	Thresh	Thresh	Thresh
9	1	8	10	5	6	9	8	11	8	9	11
9	2	8	9	7	8	8	8	7	8	7	9
9	3	7	7	7	8	7	7	7	7	7	8
9	4	8	11	8	11	10	6	8	8	8	7
9	5	7	9	9	9	7	8	8	7	8	7
9	6		6	7	9	9	9	7	11	7	9
9	7	8	8	8	9	10	8	11	8	12	8
9	8	9	7	9	7	10	8	9	8	7	9
9	9	9	8	9	9	7	8	8	7	9	9

Table 7 - Threshold values used to analyze Batch 9 block images.

The colored numbers in Table 7 represent the analysis technique used when calculating the porosity values. The yellow cells used a user-input threshold value, which was obtained from manual observation and analysis of the image's histogram. The red cell did not produce a porosity value because the histogram was not bimodal and a threshold could not be determined. The orange cells were analyzed with a program that looked for smaller peaks in the histogram, but still automatically determined the location of the threshold between the two peaks with the same method as the original program..

These porosity values can be graphed similar to the density to determine consistency within the batch. The data from Table 6 is also shown in Figure 17. A similar graph for each Batch is found in Figure 37.

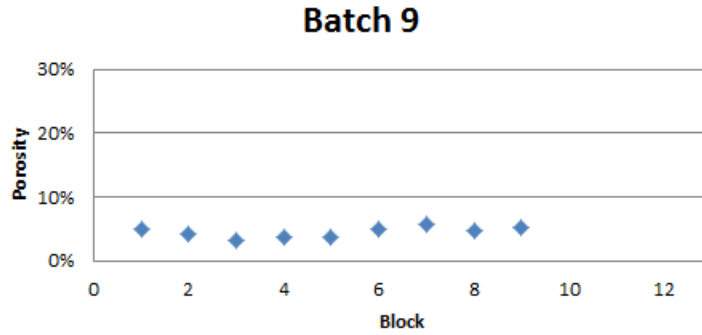


Figure 17 - Calculated porosity of each sample extruded in Batch 9.

The porosity data from Batch 9 was very consistent from sample to sample. There were a number of sets that did not exhibit this same consistency. The most extreme case of this was Batch 5. This data is shown in Figure 18. It is not known what caused this difference. The three distinct bands could signify that there was some change in the process at certain points during the extrusion, but nothing was noted at the time of production. The threshold values for these images have more variance than the rest of the images. Examining the histograms of each image does not yield any obvious errors that could cause the porosity variation. Further observation of the pressure drop data will likely indicate whether or not this is a real variation, or it is related to the image analysis process.

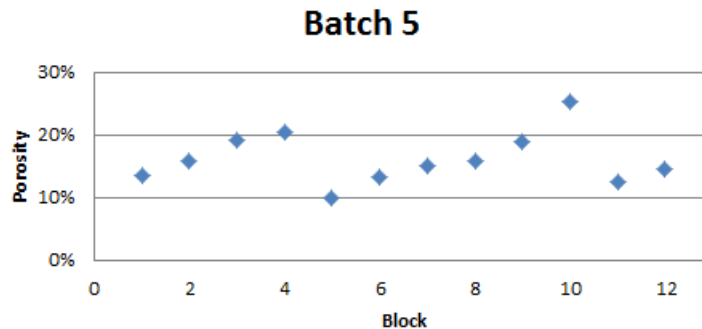


Figure 18 - Calculated porosity of each sample extruded in Batch 5.

The average porosity values for each batch are shown in Table 8. This data shows two trends. First, it is clear that as the cross-section moves from cross-section “M” to cross-section “K”, or thick-wall to thin-wall, porosity is reduced. Producing two different cross-sections with

the same material and same porosity would require a change in the extrusion settings. Second, as the powder size moves from the fine to medium powder, the porosity increases. This trend does not continue when the powder changes to coarse powder, but there is also a change in the Zoom Level of the microscope. This zoom level could be the cause for this trend change. As the zoom level changes, the diffusion of the light into the lens also changes. This could affect the location of the appearance of edges between pore and particle, also affecting the final porosity calculation.

Porosity			
	Material		
Cross-Section	1 - Coarse	2 - Medium	3 - Fine
M	13.66%	18.56%	16.02%
R	10.47%	11.80%	8.69%
K	4.44%	6.77%	4.53%
Zoom Level:	100	200	200

Table 8 - Average porosity for each batch of extruded samples.

The porosity values were compared to the density values of each block. The scatter charts of this relationship are shown in Figure 19. It is understood that as the block density increases, the block porosity decreases. Material 2 demonstrates this concept very clearly. This also holds true in the “R” and “K” cross-sections for all materials. The “M” cross-section samples were measured with the tiling feature of the digital microscope, as described in the *Materials and Methods* section. It is possible that the difference in image capture techniques caused a deviation in the porosity values. This could explain why it does not follow the same trend in Materials 1 & 3.

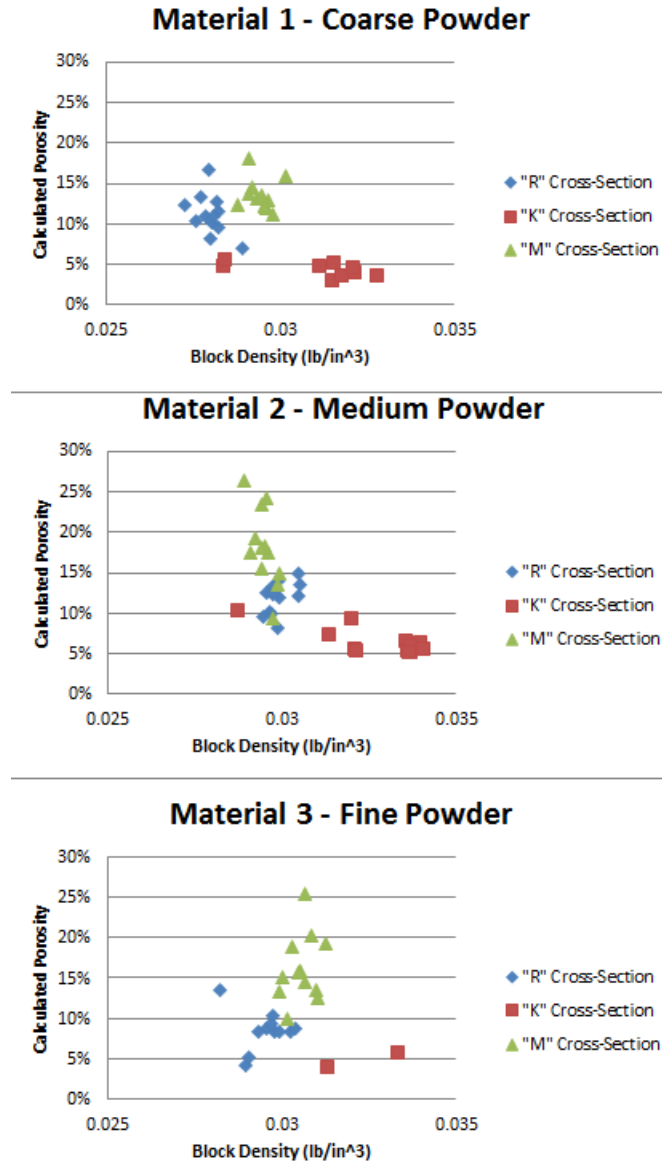


Figure 19 - Comparison of density and porosity for each material and cross-section combination.

Air Test

After the porosity evaluation is complete each sample is assembled with two end caps, preparing for the pressure drop testing. The first of these tests is the air test.

As previously stated, the goal is to collect the pressure drops across each test sample with air flow rates of 0.2, 0.4, 0.6, 0.8, and 1.0 L/min. These flow rates were selected because they fall in the normal operating range of the vacuum pump and flow meter used in the test. Some of the test samples had pressure drops that fell outside of the measurable range of the pressure sensor

used in this setup at some of these flow rates. In these cases, a pressure drop was not recorded. A minimum of two data points was collected for each filter. This required going up to 1.2 L/min for some of the higher porosity samples.

An example of the raw data compiled in this test is shown in Table 9. This data is then summarized in Figure 20. Raw data for each sample is listed in the Appendix in Table 16. The graphical summaries of this data are also in the Appendix, in Figure 38.

		Pressure (Pa)						
		Flow Rate (L/min)						
Batch	Block#	0.1	0.2	0.4	0.6	0.8	1	1.2
1	1		107	262	461	632	817	
1	2		17	116	223	320	429	
1	3		2	90	182	268	348	
1	4			7	65	123	170	
1	5		56	204	365	519	637	
1	6		41	148	270	390	504	
1	7		3	90	182	260	348	
1	8			24	90	140	197	
1	9		105	288	453	622	780	
1	10		35	163	279	388	504	
1	11			60	135	210	287	
1	12				43	90	131	

Table 9 - Raw data collected from air test for Batch 1

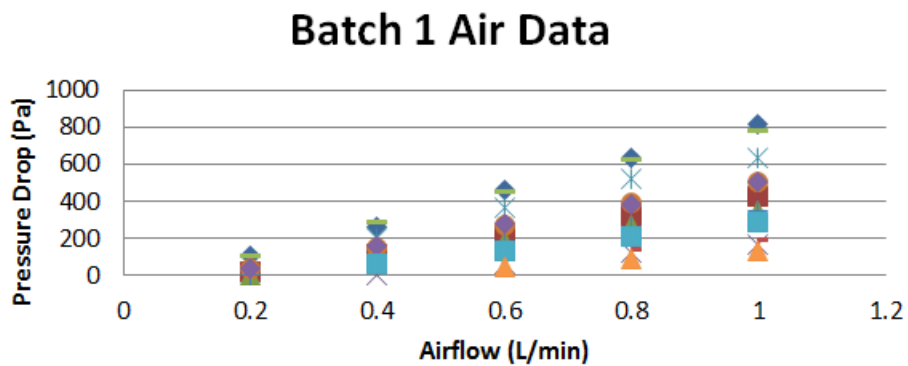


Figure 20 - Graphical summary of Batch 1 air test data, also shown in Table 9.

The air test data was very linear. Linear curve fits maintained a coefficient of determination above 0.9 for six of the nine batches. Four of the nine batches have R^2 values that remain above 0.95 for all samples. These values are shown in Figure 21.

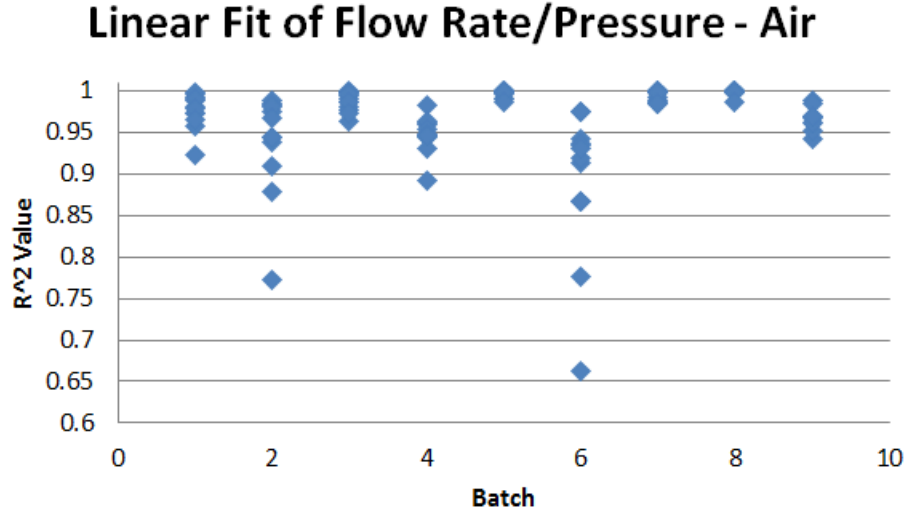


Figure 21 - R^2 values for linear trendline between flow rate and pressure drop for air test results.

Permeability Calculations

These linear results suggest that Darcy's Law is applicable in this regime. Darcy's Law in radial flow was previously described in Equation 6. This equation can be arranged to solve for the permeability of each of the samples, as shown in Equation 9. The flow rate and pressure drop are each measured in the air test. The viscosity of air at room temperature is a known value, $1.81 * 10^{-5} \frac{kg}{ms}$. The OD and ID values were set by the screw and die combination used in the extrusion process. That leaves the permeability, κ , as the only unknown in the equation.

$$\kappa = \frac{Q\mu}{2\pi\Delta Ph} \ln\left(\frac{r_o}{r_i}\right) \quad (9)$$

When solving this equation for permeability, each block has a permeability value for each air flow rate. Note, this block should be solved in Darcy units. The conversion from Darcy to square meters is shown in Equation 10. An example of these calculation results is shown in Table

10. Permeability, an intrinsic property of the geometry, should remain constant when the flow rate is varying.

$$1 \text{ Darcy} = 9.869233 * 10^{-13} \text{ m}^2 \quad (10)$$

		κ - Permeability (Darcy)						
		Flow Rate(L/min)						
Batch	Block#	0.1	0.2	0.4	0.6	0.8	1	1.2
1	1		2.6	2.2	1.8	1.8	1.7	
1	2		11.5	3.3	2.6	2.4	2.2	
1	3		94.1	3.2	2.4	2.1	2.1	
1	4			24.3	4.0	2.8	2.5	
1	5		5.1	2.8	2.3	2.2	2.2	
1	6		4.6	2.6	2.1	1.9	1.9	
1	7		42.1	3.2	2.4	2.2	2.1	
1	8			7.2	2.9	2.5	2.2	
1	9		2.7	2.0	1.9	1.8	1.8	
1	10		5.4	2.3	2.0	1.9	1.9	
1	11			4.8	3.2	2.7	2.5	
1	12				6.1	3.9	3.3	

Table 10 - Calculated permeability values for each sample and air flow rate in Batch 1.

The data shows that at the lowest pressure readings, the permeability values diverge from the relative consistency of the other values. This is due to the accuracy of the pressure gauge. The gauge has a maximum range of 0-7500 Pa. The full scale error is +/- 1%, or +/- 75 Pa. The highlighted cells in Table 10 are the permeability values that correspond to a pressure reading below this limit. When calculating the average permeability for each block, these highlighted values were not included. These averages are summarized in Figure 22.

Experimental Air Permeability

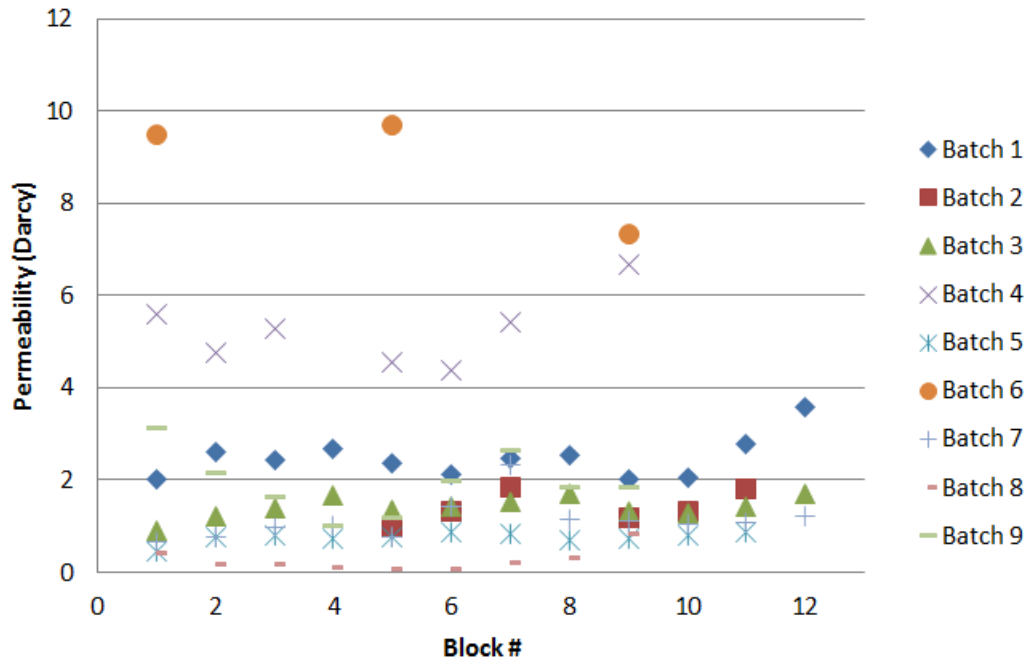


Figure 22 - Permeability values for each block calculated from results of the air test.

Batch 6 and Batch 4 have the highest permeability of the group, which suggests they will have the lowest pressure drops for a given flow rate. However, it does not appear that there is a direct correlation between the previously calculated porosity values for each block and the corresponding permeability values.

Experimental Air Permeability - Block

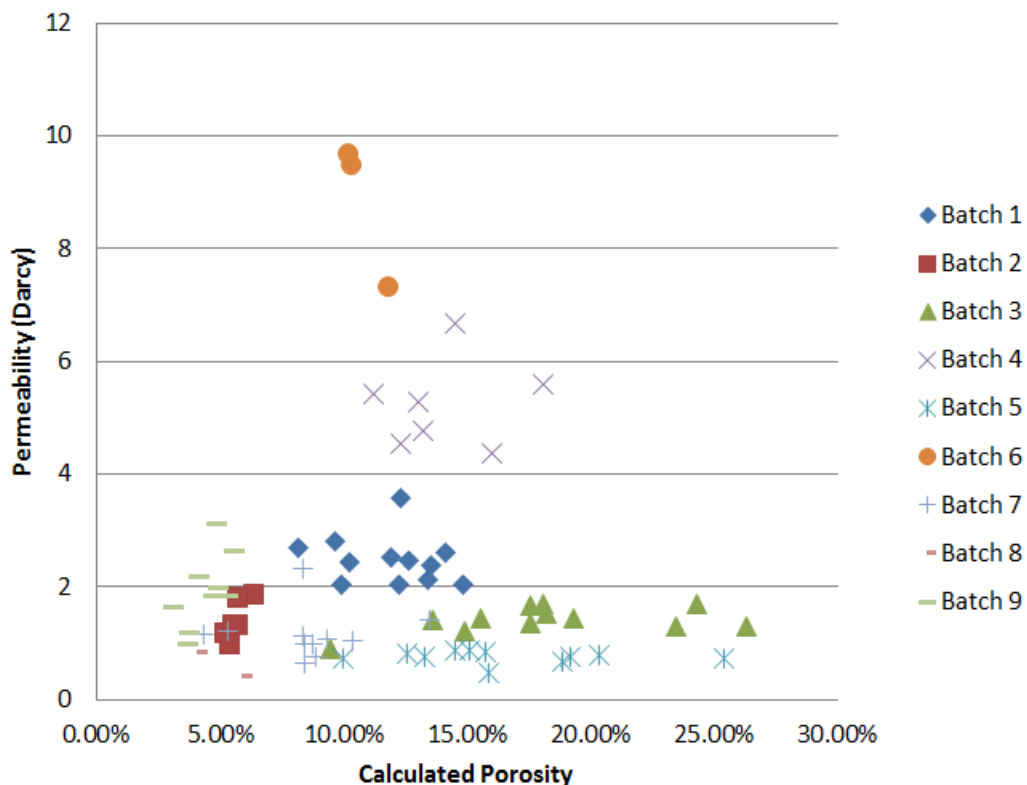


Figure 23 - Permeability values for each block compared to the corresponding porosity values.

The best way to observe trends in this data is by examining the different cross-sections made with the same material. Figure 24 shows this relationship. The “R” cross-section has the highest permeability. While “R” and “M” cross-sections had similar density and porosity values, the thinner wall of the “R” cross-section allows the permeability to increase. The “K” cross-section has the highest density and lowest porosity values of the three cross-sections. Even though it has the thinnest wall, the density and porosity differences are enough to make these samples have the lowest permeability values.

Experimental Air Permeability

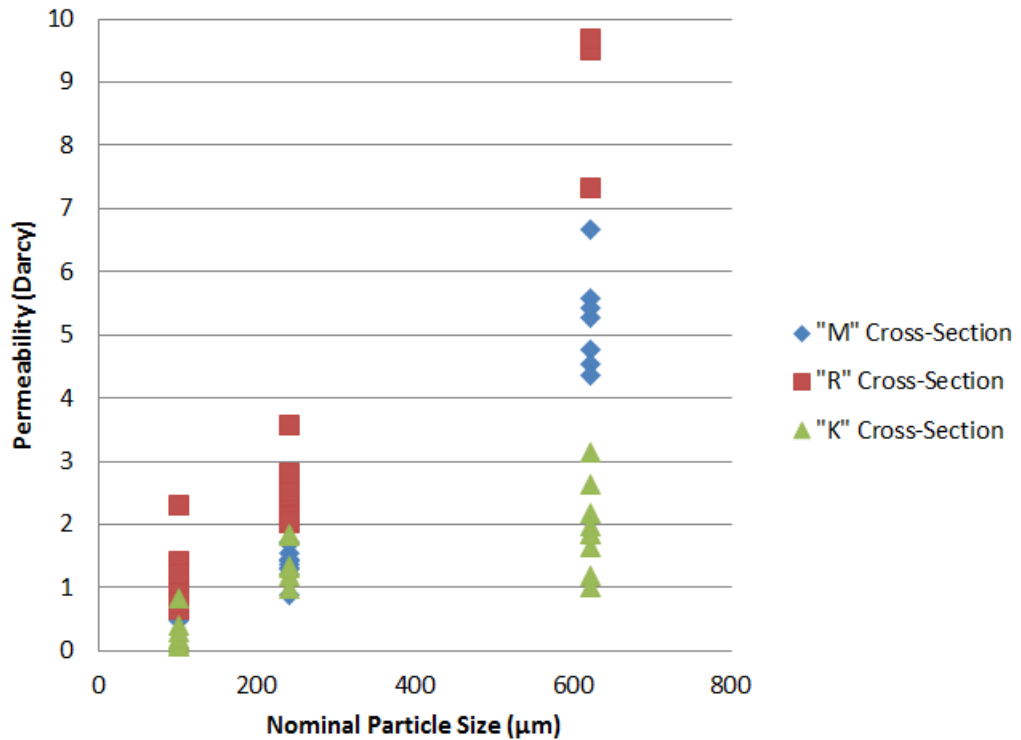


Figure 24 - Permeability values for each block compared to the corresponding material and cross-section.

Figure 24 also shows that, for a given cross-section, as the carbon powder's nominal particle size increases, the permeability will increase.

Water Test

After undergoing the air test, each sample moved to the water test. Each sample was exposed to six different flow rates, ranging from 1.3 to 0.3 GPM. The lower limit on this range, 0.3 GPM, was determined by the linearity of the flowmeter. The upper limit of this range was set by the capability of the water line that was plumbed into the test setup.

The data from each sample was collected and stored in a table, as shown in Table 11. The complete data set is in the Appendix in Table 18. This data was graphed and two trendlines were added, one linear and one quadratic. These trendlines serve to demonstrate how well the

data follows Darcy’s Law, a linear relationship, or the Forchheimer/Ergun equations, quadratic relationships. The R^2 values and coefficients of each trendline are also documented in the data table. An example of this graph is shown in Figure 25. It is important to note, after collecting the raw pressure and flow data in psi and GPM, it was converted into standard metric units for ease of analysis. This will change the values of the trendline coefficients, $C1$ and $C2$. The R^2 values for each trendline remain constant, regardless of the units used.

Batch	Sample	(GPM)	(psi)	Linear: $\Delta P = C1*Q$		Quad: $\Delta P = C1*Q^2 + C2Q$		
		Flow Rate	Pressure	R2	C1	R2	C1	C2
6	7	1.221	11.46	0.9325	8.4348	0.9977	4.0498	4.3159
6	7	1.101	9.61					
6	7	1.002	8.29					
6	7	0.809	5.92					
6	7	0.6	4.21					
6	7	0.417	2.63					

Table 11 - Experimental data collected from water test on Batch 6, Block 7.

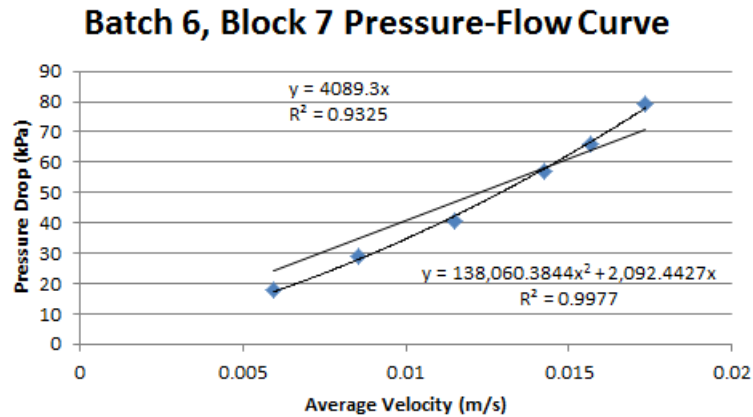


Figure 25 - Experimental pressure vs. flow curve obtained from Batch 6, Block 7.

From this data, it is clear that the data follows the quadratic trendline more closely than the linear trendline, suggesting that the flow is outside of the Darcy regime. This trend follows for all samples that were tested, although the amount of divergence varies from sample to sample. This means that some samples, such as the one shown in Figure 25, are well into non-Darcy flow and others, such as the one shown in Figure 26, are closer to the transition from Darcy to non-Darcy flow.

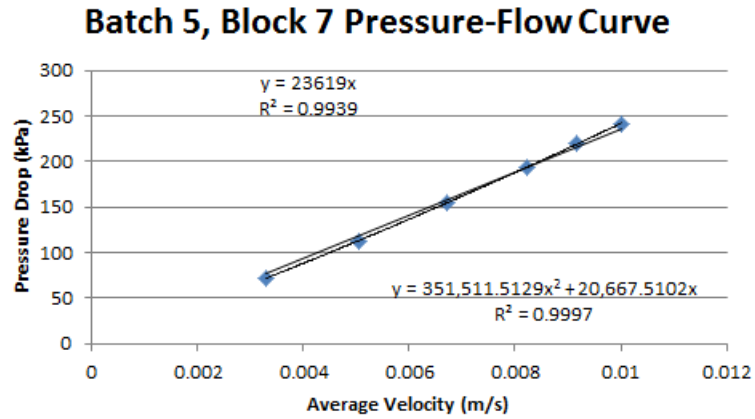


Figure 26 - Experimental pressure vs. flow curve obtained from Batch 5, Block 7.

Given that Darcy’s Law is applicable at low flow rates, it follows that there would be a strong linear correlation at the data. As the flow continues to increase and move further into the non-Darcy regime, it is expected that the difference in the trendlines to also increase. A simple way to characterize this value is by calculating the difference between the R^2 values for each trendline. A larger difference means the flow is further into the non-Darcy regime. Figure 27 compares the difference between the linear and quadratic fits with the permeability of the sample.

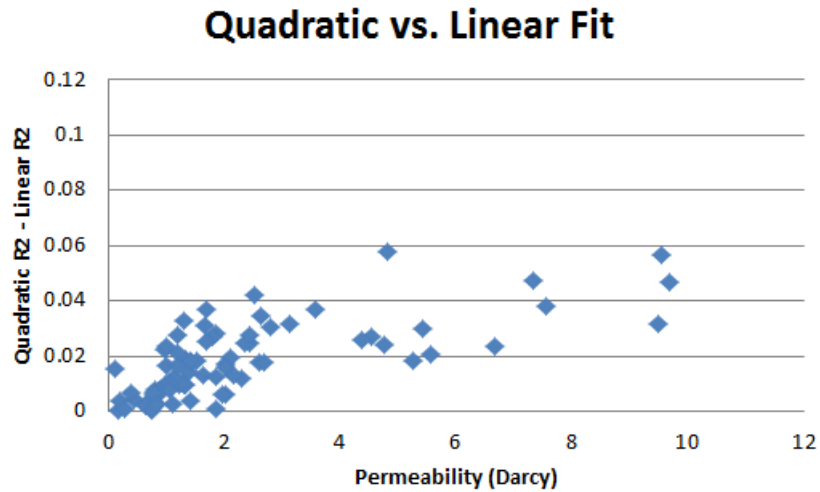


Figure 27 - Difference of the linear and quadratic trendline R^2 values, relative to the sample permeability.

At low permeability values, there is not a large difference between the quadratic and linear fits. As the permeability increases, the difference between the fit of the trendlines also increases. This suggests that the higher permeability samples enter the non-Darcy flow more easily than the low permeability samples.

Beyond simply examining the R^2 values for each trendline, the linear and quadratic constants for the trendline can also be examined. When the flow is still close to the Darcy regime, the linear coefficient, $C2$, will be much larger than the quadratic coefficient, $C1$. It is important to ensure that the data being analyzed is in the same units when evaluating $C1$ and $C2$, especially when comparing multiple data sets.

After each sample in a batch goes through the water test, the complete batch's data is graphed according to sample length. This graph is shown in Figure 28 using the data from Batch 1. This figure demonstrates the differences between the performances of samples with varying lengths. It is very clear that there is distinction between the four different lengths in the data, and the samples within these groups are relatively consistent.

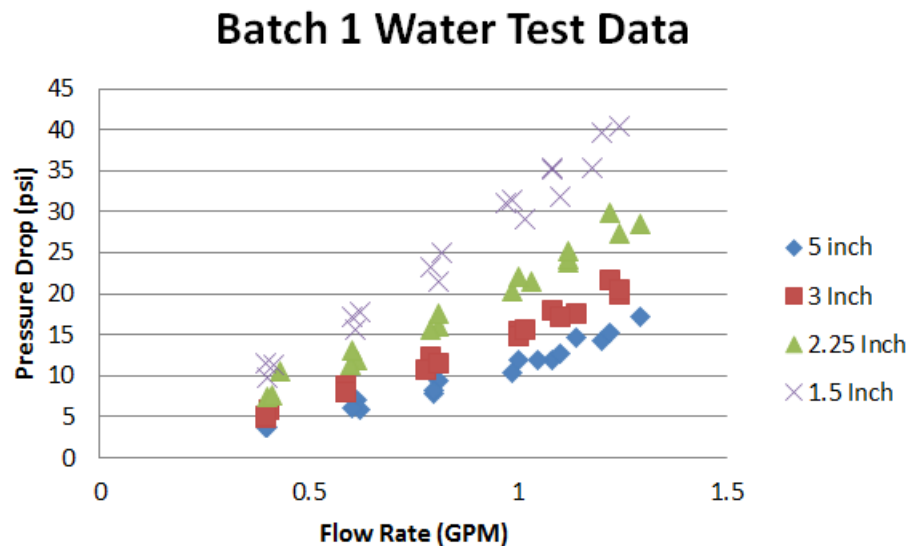


Figure 28 - Experimental pressure vs. flow curves for all samples in Batch 1.

Some of the other batches have slightly more overlap between samples of different lengths. This can generally be attributed back to the permeability values for the individual blocks. The clearest example of this is found in Batch 2. The front-end of Batch 2 demonstrated a possible difference in density and porosity and a certain increase in permeability. These physical differences produce the overlap in the pressure drop data, shown in Figure 29.

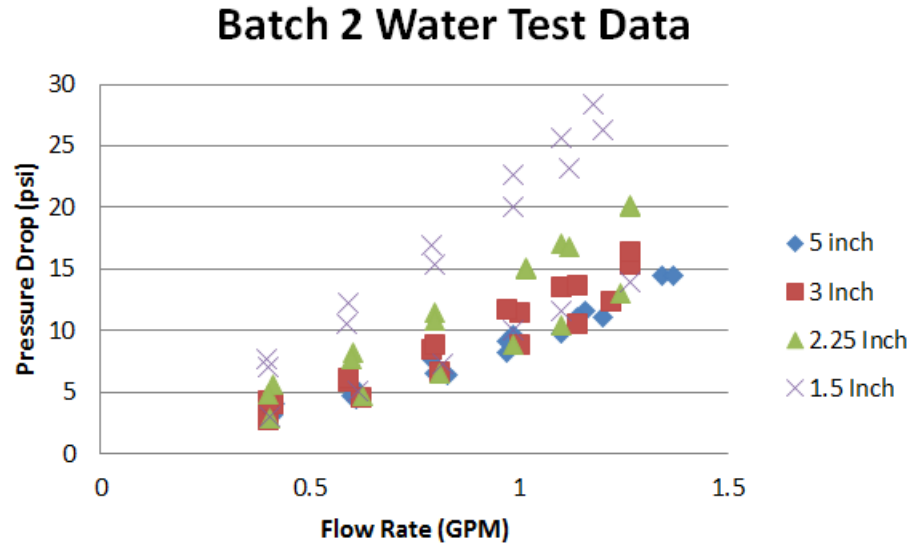


Figure 29 - Experimental pressure vs. flow curves for all samples in Batch 2.

One of the first steps in finding a correlation between flow rate and pressure drop is to attempt to fit the experimental data to the existing Forchheimer and Ergun equations. The first step to checking these equations is to change the equations from the linear domain to the radial domain. In the Forchheimer equation, the average velocity, V , is the ratio of volumetric flow rate, Q , to the cross-sectional area, A . In longitudinal flow, the volumetric flow rate and cross sectional area are constants. In radial flow, the cross-sectional area changes with the radial position, as defined in Equation 11.

$$V(r) = \frac{Q}{A} = \frac{Q}{2\pi rh} \quad (11)$$

From this relationship, the average velocity throughout the wall thickness can be found as demonstrated in Equations 12 - 14.

$$\bar{V} = \frac{1}{r_o - r_i} \int_{r_i}^{r_o} V(r) dr \quad (12)$$

$$\bar{V} = \frac{Q}{2\pi h(r_o - r_i)} \int_{r_i}^{r_o} \frac{1}{r} dr \quad (13)$$

$$\bar{V} = \frac{Q}{2\pi h(r_o - r_i)} \ln\left(\frac{r_o}{r_i}\right) \quad (14)$$

Substituting Equation 14 for the velocity term in Darcy's Law for longitudinal flow, previously shown in Equation 1, yields the same value as Darcy's Law for radial flow.

Substituting Equation 14 for the velocity term in the Forchheimer equation yields Equation 15, a quadratic equation, referred to here as the modified Forchheimer equation.

$$\Delta P = \rho C \left[\frac{Q}{2\pi h(r_o - r_i)} \ln\left(\frac{r_o}{r_i}\right) \right]^2 + \frac{\mu}{\kappa} \left[\frac{Q}{2\pi h(r_o - r_i)} \ln\left(\frac{r_o}{r_i}\right) \right] = C1 * \bar{V}^2 + C2 * \bar{V} \quad (15)$$

The modified Forchheimer equation suggests that the $C2$ term should be linear with respect to the inverse of the sample permeability. The $C2$ values from the experimental data were plotted against the inverse of sample permeability in Figure 30. While there are plenty of outliers, there is also a clear linear trend at the base of the data. The spread of this data increases as the inverse of the permeability increases. This suggests that the modified Forchheimer equation is more accurate at high permeability values.

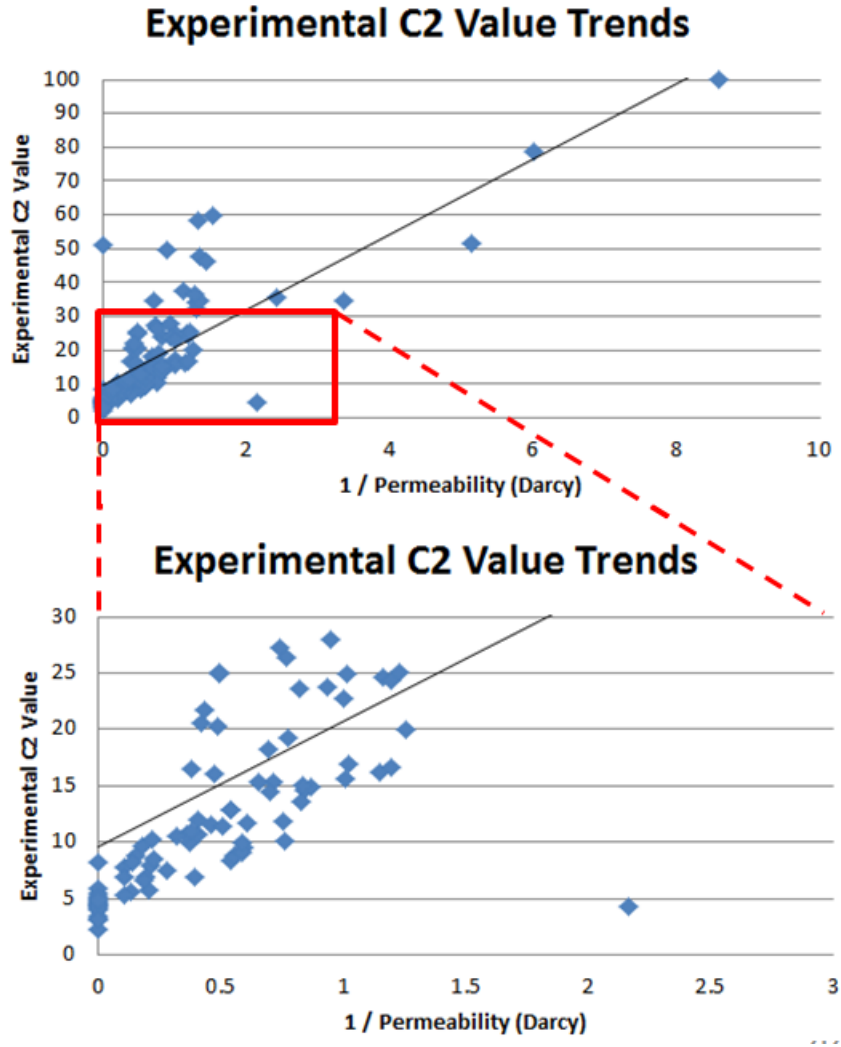


Figure 30 - Relationship between experimental C2 values and inverse sample permeabilities.

The fluid viscosity, μ , is a known value and the permeability, κ , for each block was determined from the air test results. Using these two values, it is possible to calculate the theoretical linear coefficient as defined by the Forchheimer equation. Comparing the theoretical linear coefficient with the experimental data, a percent error was calculated for each block. These errors are plotted relative to each block's permeability in Figure 31. From this chart, it is clear that at high permeability values, this formula serves to accurately predict the linear coefficient. Above 6 Darcy, the theoretical and experimental values are all within 12% error. This further

validates the observation that the modified Forchheimer equation is more accurate at higher permeability values.

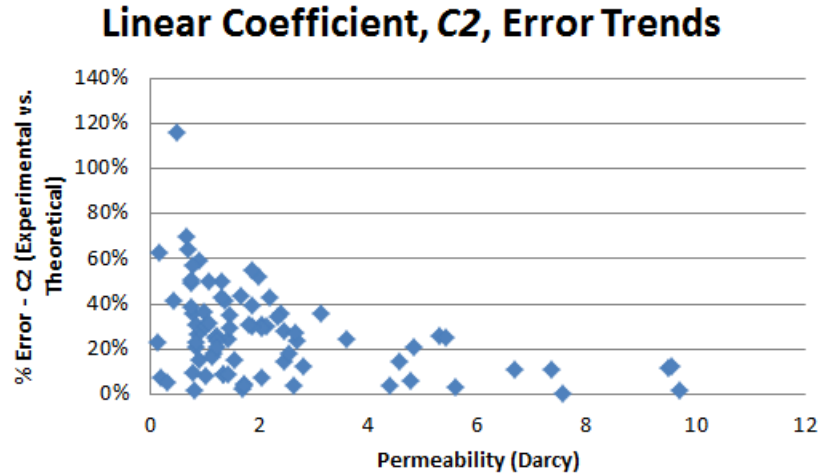


Figure 31 - Experimental error between theoretical and experimental values for Forchheimer linear coefficient compared to the sample permeability.

Figure 31 depicts what appears to be random error with the upper bound constrained by a function of the permeability. Had the error followed a singular path, linear or otherwise, a correction factor could have been determined to account for low permeability error. Instead this data suggests a lower limit for sample permeability in order to achieve a desired percent error when predicting this C_2 value. For instance, the data suggests that the linear component of the physical behavior can be predicted within 25% using the modified Forchheimer equation if the sample permeability is above 3.5 Darcy.

The other significant trend from this data is shown by charting the percent error against the sample length, shown in Figure 32. As the length of the sample increases, the amount of error decreases. This suggests that there are some end effects that are more significant at lower sample lengths. The definition of these end effects, and the critical limits of the sample geometry that produces them, should be explored in further study.

Linear Coefficient, C2, Error Trends

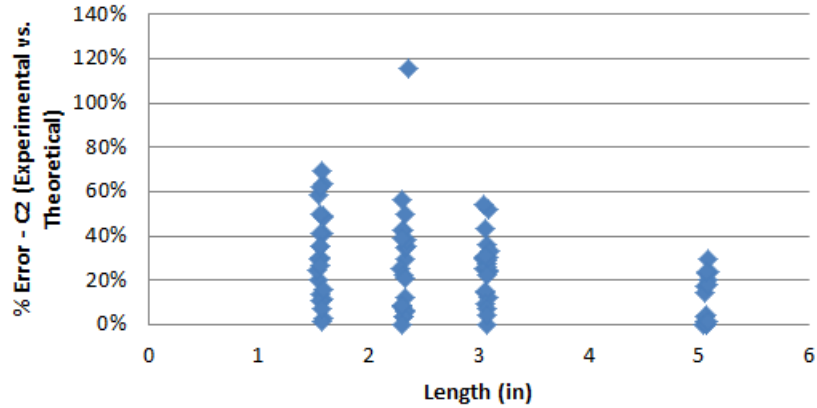


Figure 32 - Experimental error between theoretical and experimental values for Forchheimer linear coefficient compared to the sample length.

The other prediction method that can be made using the average velocity value calculated in Equation 14 is a modified Ergun prediction. Substituting this value in to Equation 5 modifies the Ergun equation for radial flow, as described in Equation 16.

$$\Delta P = \frac{150\mu(r_o - r_i)(1 - \epsilon)^2}{D_p^2} \frac{Q}{\epsilon^3} \frac{1}{2\pi h(r_o - r_i)} \ln\left(\frac{r_o}{r_i}\right) + \frac{1.75(r_o - r_i)\rho(1 - \epsilon)}{D_p} \left[\frac{Q}{2\pi h(r_o - r_i)} \ln\left(\frac{r_o}{r_i}\right)\right]^2 \quad (16)$$

Every independent variable in Equation 16 is known. Using these known values, a prediction for the pressure drop can be calculated for each block and each data point. These theoretical, modified Ergun predictions can be compared to the experimental data and a percent error can be calculated. An example of this data is shown in Table 12. Figure 33 shows the percent error when comparing the theoretical and experimental data graphed against the Reynold's number, as calculated by Ergun. This Reynold's number is described in Equation 17. In this equation, the velocity is shown as the intrinsic velocity, u , or the true velocity of the fluid inside the pores. During Ergun's experiments, he found that the flow began to become non-Darcy at a critical Reynold's number of 3-10. Zeng also describes numerous other researchers

who calculated the Reynold's number in different ways and observed critical Reynold's numbers in different ranges (Zeng 2006).

$$Re = \frac{\rho D_p u}{\mu} * \frac{1}{1 - \epsilon} \quad (17)$$

Batch	Sample	GPM	(psi)	(m3/sec)	(Pa)	(Pa)	% Difference - Modified Ergun vs. Experimental	Average % Diff - Modified Ergun vs. Experimental
		Flow Rate	Pressure	Flow Rate	Pressure	Modified Ergun Prediction		
1	1	1.244	40.45	7.85E-05	278,893	654,415.57	134.65%	146.65%
1	1	1.083	35.18	6.83E-05	242,558	564,658.49	132.79%	
1	1	0.988	31.49	6.23E-05	217,116	512,402.26	136.00%	
1	1	0.79	23.32	4.98E-05	160,786	405,173.43	152.00%	
1	1	0.622	17.78	3.92E-05	122,589	315,976.42	157.75%	
1	1	0.415	11.33	2.62E-05	78,118	208,326.43	166.68%	
1	2	1.292	28.46	8.15E-05	196,225	277,647.48	41.49%	52.15%
1	2	1.119	23.85	7.06E-05	164,440	238,853.19	45.25%	
1	2	0.988	20.42	6.23E-05	140,791	209,809.81	49.02%	
1	2	0.809	15.94	5.10E-05	109,902	170,588.10	55.22%	
1	2	0.616	11.85	3.89E-05	81,703	128,898.48	57.76%	
1	2	0.402	7.37	2.54E-05	50,814	83,400.22	64.13%	

Table 12 - Modified Ergun pressure drop prediction and comparison to experimental data for Batch 1, Blocks 1 & 2.

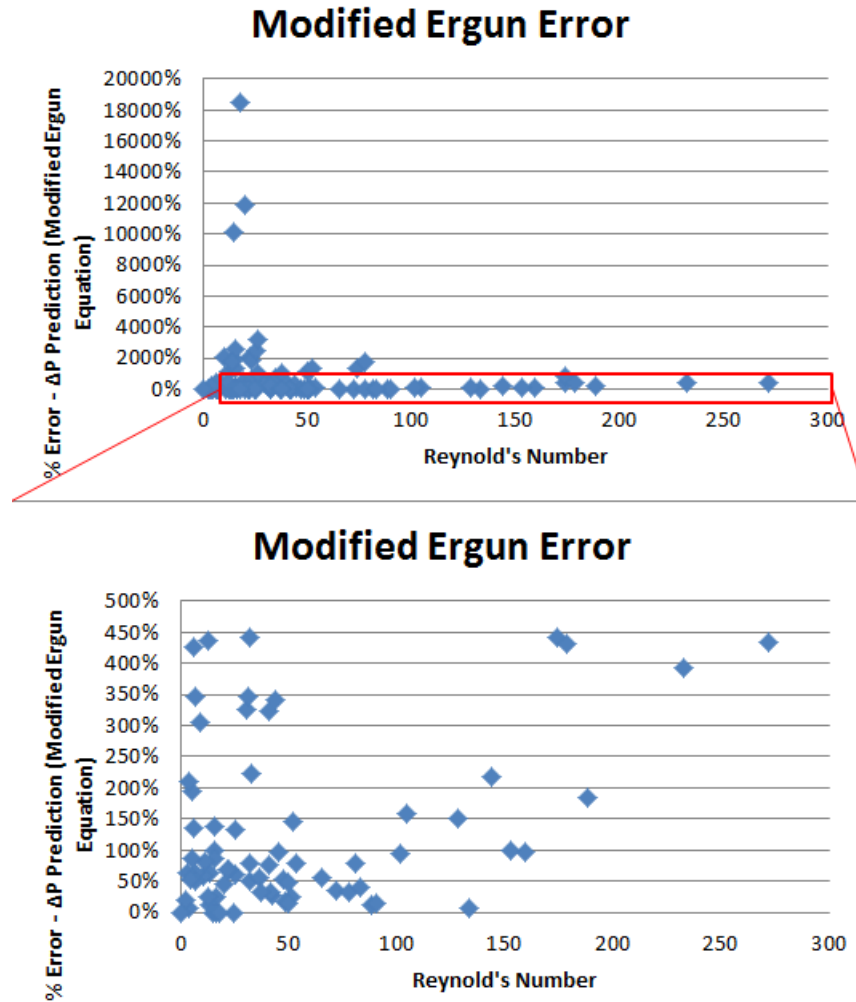


Figure 33 - Error between experimental pressure drop data and modified Ergun pressure drop prediction.

From this chart, it is clear that there is no strong correlation between the modified Ergun equation and the experimental data. The theoretical and experimental data are off by over a factor of 15 in some cases.

The lack of a clear trend provides a roadblock when attempting to modify this equation further to match the experimental data. There are a number of factors that could be supplying error to this equation, in addition those which have already been discussed for the modified Forchheimer equation. The original Ergun equation was derived from experiments with spherical particles. The carbon powder particles in this application are not spherical. It is possible that the

particle shape needs to be considered and applied in the equation as some form of correction factor.

The simplest way to determine this correction factor is to force fit the linear and quadratic coefficients to the equation. The coefficient of the linear portion of the Ergun equation (150) was experimentally derived. By rearranging the linear term of this equation the linear coefficient, X2, can be calculated for each sample and observed for trends. This calculation is shown in Equations 18 and 19. Figure 34 shows this coefficient for each block in Batch 1. All batches demonstrate this same inconsistency. When comparing the coefficients to the Reynold's number, as shown in Figure 35, there is no clear trend either. This suggests that the relationship is not valid in either low- or high-flow conditions. These observations further suggest that the modified Ergun equation needs to be further modified in order to be valid in this flow regime.

$$\Delta P = C1 * \bar{V}^2 + C2 * \bar{V} ; C2 = \frac{X2 * \mu * (r_o - r_i) (1 - \epsilon)^2}{D_p^2 \epsilon^3} \quad (18)$$

$$X2 = \frac{C2 * D_p^2 * \epsilon^3}{\mu * (r_o - r_i) * (1 - \epsilon)^2} \quad (19)$$

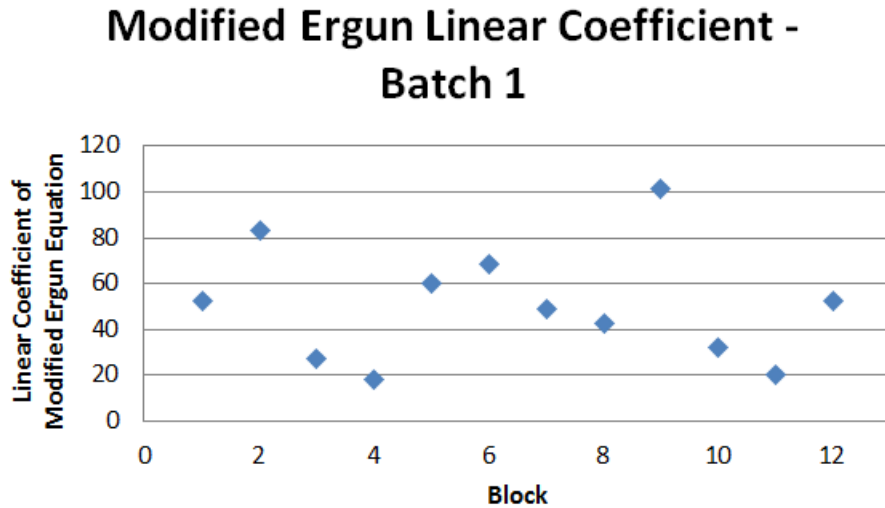


Figure 34 – Linear coefficient of modified Ergun equation for each block in Batch 1.

Modified Ergun Equation Linear Coefficient

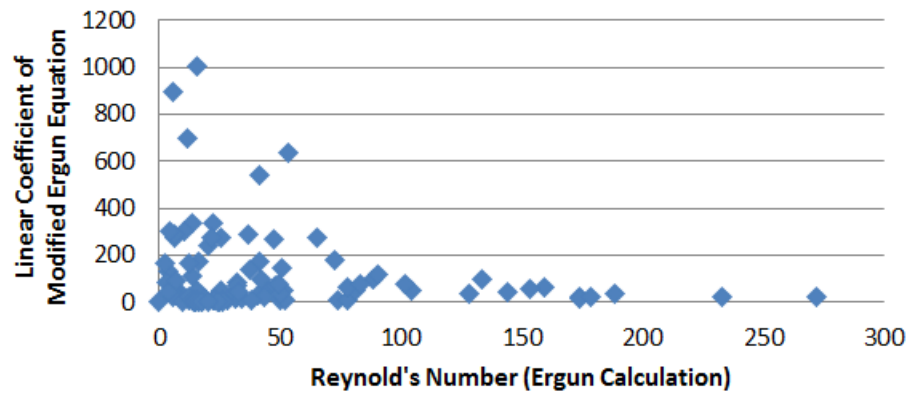


Figure 35 – Linear coefficient of modified Ergun equation for all samples tested.

The uncertainty in the porosity measurements is also a larger factor in the modified Ergun equation. The modified Forchheimer equation does not directly incorporate the porosity into the calculations. It only considers the porosity in the permeability value, which was experimentally measured. The modified Ergun equation relies on the porosity value to directly calculate the pressure drop prediction.

SUMMARY AND CONCLUSIONS

There are two main takeaways from this research. First, similar to longitudinal flow, as the flow velocity and Reynold's number increase in the radial regime, the flow behavior begins to deviate from Darcy's Law. Second, the permeability of each sample can be used to partially predict the pressure drop using the modified Forchheimer equation. This prediction is limited in accuracy by the permeability value of the sample. The modified Forchheimer equation should continue to be developed, as it demonstrated the most promise for the ability to fully predict flow behavior in this regime.

While these valuable observations were made as a result of this research, there are still a number of areas to investigate before a single relationship can be drawn between pressure drop and flow rate in this flow regime. Future work can build upon this research by focusing on some of its shortcomings.

One aspect of this experiment that could be easily improved is the pressure range at which the samples are tested. It is clear from the data presented in this paper that the samples were not exposed to extreme non-Darcy flow conditions. Being limited to the transitional regime between Darcy and non-Darcy flow may have masked additional observations that could be made from the same tests at higher Reynold's numbers. Making this improvement is as simple as obtaining more powerful pumps and sensors capable of producing and sensing larger pressure gradients.

The linear coefficient of the modified Forchheimer equation began to converge to the theoretical value as the length of the sample increased and as the permeability increased. At low permeabilities and short sample lengths, there was greater error. Future researchers should take

care to ensure that they consider any end effects or low permeability effects when they are in these areas. It would also be beneficial to produce samples that exceed the length and permeability of those in this study to determine if the observed trends continue.

One of the next steps in building off the work is to find a method of predicting the form drag coefficient for a sample. More detailed evaluation of the powder particle geometry and extruded block geometry will be necessary to characterize these values. However, once complete, this will allow a full theoretical prediction of pressure drop in radial flow using the modified Forchheimer equation.

One of the clearest items of uncertainty in this work is the determination of porosity within each of the samples. Future researchers would do well to attempt to experimentally validate their porosity values by using calibration samples that undergo both visual inspection and mercury porosimetry, or other direct porosity measurements. Perhaps as more accurate porosity numbers are obtained, the structure and coefficients of the modified Ergun coefficient could be optimized to obtain a relationship capable of accurate pressure drop predictions.

The modified Forchheimer and Ergun equations, along with the data found in this paper, can be used as foundations as future researchers continue to attempt to find a singular, direct relationship between pressure drop and flow rate in this flow regime.

REFERENCES

- Achaw, O., "A Study of the Porosity of Activated Carbons Using the Scanning Electron Microscope." *Scanning Electron Microscopy*. (2012).
- ASTM Standard D4404.
- Cheremisinoff, P., Ellerbusch, F. (1978). Carbon Adsorption Handbook. Ann Arbor, MI, Ann Arbor Science Publishers, Inc.
- David, A., Torsekar, M. "U.S. Exports of Water Filtration and Purification Equipment Show Significant Growth." *USITC Executive Briefings on Trade*. (2012).
- Dukhan, N., Patel, K. "Effect of Sample's Length on Flow Properties of Open-Cell Metal Foam and Pressure-Drop Correlations." *Journal of Porous Materials*. 18.6 (2011): 655-665.
- Engler, T. (2010). "PET524-5-fluidflow" *Flow Through Porous Media*. (2010): 6.1-6.3.
- "Flint Water Crisis Fast Facts." *CNN*. (2016).
- Harrison, J. (2004). Water Treatment Fundamentals. Lisle, IL, The Water Quality Association.
- Hassler, J. (1974). Purification with Activated Carbon. New York, NY, Chemical Publishing Co.
- Hoferer, J., Lehmann, M., Hardy, E., Meyer, J., Kasper, G. "Highly Resolved Determination of Structure and Particle Deposition in Fibrous Filters by MRI." *Chemical Engineering & Technology*. 29.7 (2006): 816-819.
- Jaganathan, S., Vahedi Tafreshi, H., Pourdeyhimi, B. "A realistic approach for modeling permeability of fibrous media: 3-D imaging coupled with CFD simulation." *Chemical Engineering Science*. 63.1 (2008): 244-252.
- Marcelino, V., Cnudde, V., Vansteelandt, S., Carò, F. "An evaluation of 2D-image analysis techniques for measuring soil porosity." *European Journal of Soil Science*. 58.1 (2007): 133-140.
- McGowan, W. (2000). Water Processing. Lisle, IL, The Water Quality Association.
- Nowicki, H., Nowicki, G., Schuliger, W., Sherman, B. "Monitoring Activated Carbon Drinking Water Filters." *Water Conditioning & Purification*. (2009).
- Pathapati, S., Sansalone, J. "CFD Modeling of Particulate Matter Fate and Pressure Drop in a Storm-Water Radial Filter." *Journal of Environmental Engineering*. 135.2 (2009): 77-85.
- Quick Facts - Flint city, Michigan*. U.S. Census Bureau. (2015).

- Reagor, Catherine. "Homebuyers, Beware: Lead Pipe Problems Not Always Required Disclosure." *The Arizona Republic*. (2016)
- Scheidegger, A. (1974). The Physics of Flow Through Porous Media. Toronto, Canada, University of Toronto Press.
- Sedghi-Asl, M., Rahimi, H., Salehi, R. "Non-Darcy Flow of Water Through a Packed Column Test." *Transport in Porous Media*. 101.2 (2014): 215-227.
- Small Drinking Water Systems Handbook*. Cincinnati, OH, U.S. Environmental Protection Agency, National Risk Management Research Laboratory. (2003)
- Strauß, F., Hoferer, J., Heuveline, V., Kasper, G., "Scalable Numerical Tools for Flow and Pressure Drop Computation in Fibrous Filter Media." *Chemical Engineering & Technology*. 32.5 (2009): 820-825.
- Sutherland, K. (2008). Filters and Filtration Handbook. Oxford, UK, Elsevier/Butterworth-Heinemann.
- Torquato, S. "Organizing Principles for Dense Packings of Nonspherical Hard Particles: Not All Shapes are Created Equal." *Physical Review E - Statistical, Nonlinear, and Soft Matter Physics*. 86.1 (2012).
- Wang, X., Kim, K., Lee, C., Kim, J. "Prediction of Air Filter Efficiency and Pressure Drop in Air Filtration Media Using a Stochastic Simulation." *Fibers and Polymers*. 9.1 (2008): 34-38.
- "WB5x 5x170FL WaterBetter® Filter Housings." *Harmsco Filtration Products*. 11 Aug 2016. <http://harmco.com/filter-housings/waterbetter-housings/wb-5x170fl-waterbetter-housings.html>
- White, H.E., Walton, S.F. "Particle Packing and Particle Shape." *Journal of the American Ceramic Society*. 20.1 (1937): 155-166
- Zeng, Z., Grigg, R. "A Criterion for Non-Darcy Flow in Porous Media." *Transport in Porous Media*. 63.1 (2006): 57-69
- Zhou, B., Tronville, P., Rivers, R. "Generation of 2-Dimensional Models for CFD Simulation of Fibrous Filter Media with Binder." *Fibers and Polymers*. 10.4 (2009): 526-538.

APPENDIX

```
1 function [ por ] = ImageAnalysis_Oct10()
2 %UNTITLED Summary of this function goes here
3 % Detailed explanation goes here
4 prompt = 'What is the file name you wish to analyze?';
5 pic = input(prompt,'s');
6 a = imread(pic);
7 a_gray2 = rgb2gray(a);
8 a_gray=a_gray2(1:1020, :);
9 d=imhist(a_gray);
10 peakright=zeros(1, 256);
11 peakleft=zeros(1,256);
12 peak=zeros(1,256);
13 valleyright=zeros(1,256);
14 valleyleft=zeros(1,256);
15 %Determine location of peaks and valleys in histogram
16 for x=1:256
17     x;
18     y=1;
19     z=1;
20     v=1;
21     w=1;
22     while x+y < 255 & d(x)>d(x+y)
23         y = y+1;
24         peakright(x) = (y-1);
25     end
26     while x-z > 0 & d(x)>d(x-z)
27         z = z + 1;
28         peakleft(x)=(z-1);
29     end
30     while x+v < 255 & d(x)<d(x+v)
31         v=v+1;
32         valleyright(x)=(v-1);
33     end
34     while x-w > 0 & d(x)<d(x-w)
35         w = w+1;
36         valleyleft(x)=(w-1);
37     end
38     peak(x)=min(peakright(x),peakleft(x));
39     valley(x)=min(valleyright(x),valleyleft(x));
40 end
41 %Determine location of 2nd peak in image histogram
42 u = 1;
43 while peak(u) < 20;
44     u = u+1;
45 end
46 %Set threshold at largest valley between start and 2nd peak in hist.
47 check=valley(1:u);
48 [M, thresh_level] = max(check);
49 thresh_level
```

```

50 thresh=thresh_level/256;
51 %Threshold gray image to BW
52 bw = im2bw(a_gray,thresh);
53 %Remove noise from threshold image
54 se=strel('disk',3);
55 bw_close=imclose(bw,se);
56 %Determine # of pixels in image
57 c = size(a_gray);
58 pix = c(1)*c(2);
59 %Determine # of black pixels (pores) in image
60 bpix = pix - sum(sum(bw_close));
61 %Calculate porosity
62 por = bpix/pix;
63 pic1=pic(1:(end-4));
64 savename=strcat(pic1,'-analyzed');
65 delete(findall(0,'Type','Figure'));
66 subplot(2,2,1),imshow(a), title(pic1);
67 subplot(2,2,2),imshow(a_gray), title('Grayscale Image');
68 subplot(2,2,3),imhist(a_gray), title('Grayscale Histogram');
69 subplot(2,2,4),imshow(bw_close), title('Thresholded Image');
70 print(savename,'-dpng');
71 figure
72 subplot(1,2,1),plot(valley),title('Valley');
73 subplot(1,2,2),plot(peak),title('Peak');

```

Figure 36 - MATLAB code “ImageAnalysis-Oct10” used to analyze digital microscope images for porosity.


```

1
2 #include <LiquidCrystal.h>
3
4 LiquidCrystal lcd(12, 11, 5, 4, 3, 2);
5
6 //initialize streaming output for succinct code when printing to serial monitor
7 template<class T> inline Print &operator <<(Print &obj, T arg) {
8     obj.print(arg);
9     return obj;
10 }
11
12 const int flowMeter = 7;        //digital pin 7 will be input for flow meter
13 const int transducer = A0;     //analog pin 0 will be input for pressure transducer
14 const int button = A1;        //analog pin 1 will be input for write to Excel button
15
16 const float betaFlow = 0.0;    //constants for flow rate low pass filter
17 const float betaPressure = 0.0; //constant for pressure low pass filter
18
19 int currFlowReading = 0;
20 int lastFlowReading = 0;
21
22 int currPulseTime = 0;
23 int lastPulseTime = 0;
24 double delTimeFilt = 0;
25
26 double flowRate = 0;
27
28 float currPressure = 0;
29 float currPressureFilt = 0;
30
31 long lastScreenTime = 0;
32
33 int buttonReading = 0;
34 long lastExcelTime = 0;
35
36
37
38 void setup() {
39     Serial.begin(9600);
40
41     pinMode(flowMeter, INPUT); //set digital pin 7 as INPUT
42     pinMode(transducer, INPUT); //set analog pin 0 as INPUT
43
44
45 }
46

```

```

47 void loop() {
48   currFlowReading = digitalRead(flowMeter);
49
50   //if the pulse just ended
51   if ( lastFlowReading - currFlowReading == 1) {
52     currPulseTime = millis();
53
54     //determine delta time (low pass filtered) between pulses
55     //delTimeFilt = delTimeFilt - (betaFlow * (delTimeFilt - (currPulseTime - lastPulseTime)));
56     delTimeFilt = currPulseTime - lastPulseTime;
57
58     //calculate the current flowrate in gallons / min
59     //0.00111937 is the volume of water in gallons associated with one pulse
60     //this based on 236 pulses / L
61     flowRate = 0.00111937 / ((delTimeFilt / 1000) / 60);
62
63   }
64
65   //update "last" pulse values
66   lastFlowReading = currFlowReading;
67   lastPulseTime = currPulseTime;
68
69   currPressure = analogRead(transducer);
70   currPressure = (currPressure*.1318)+.7812;
71
72   //determine current pressure (low pass filtered)
73   //currPressureFilt = currPressureFilt - (betaPressure * (currPressureFilt - currPressure));
74   currPressureFilt = currPressure;
75
76
77   //if it has been 1 second or longer before the last write to lcd screen command
78   if ( millis() - lastScreenTime >= 1000) {
79     //clear the screen and start in the first row
80     lcd.clear();
81
82     //the 2 means to use two decimal places
83     lcd.print(flowRate, 3);
84     lcd.print(" ");
85     //the 2 means to use two decimal places
86     lcd.print(currPressureFilt,2);
87     //update the time that the last write to lcd screen command occurred
88     lastScreenTime = millis();
89
90   }
91
92   buttonReading = analogRead(button);

```

```

93
94 //if the button is currently pressed and it has been longer than 1 second since the last write to Excel
95 if ( buttonReading > 300 && millis() - lastExcelTime > 1000) {
96   Serial.print("CELL,SET,C3,");
97   //the 4 means to include 4 decimal places
98   Serial.println(flowRate, 3);
99
100  Serial.print("CELL,SET,C4,");
101  //the 4 means to include 4 decimal places
102  Serial.println(currPressureFilt,2);
103  lastExcelTime = millis();
104 }
105
106 //Serial << "Transducer: " << currPressureFilt << ", " << "Flow Rate: " << flowRate << "\n";
107
108 }

```

Figure 37 - Arduino code “matt_arduino_rev_1” used to capture and record flow rate and pressure data in the water flow test.

Material Designation	1	2	3	
Carbon	MC20X50	MC40X200	MC80X325	
Size (µm)	Weight (g)			Mesh
<38	0	0	1.47	<400
38-45	0	0	3	325-400
45-53	0	0.46	7	270-325
53-75	0	0.54	27	200-270
75-106	0	3.7	50	140-200
106-150	0	24	47	100-140
150-180	0	19	11	80-100
180-250	0.15	38	2.29	60-80
250-425	4.7	59	0	40-60
425+	142	0.37	0	40+

Table 13 - Raw particle size data from sieve analysis for each material.

Batch	Block#	in OD	in ID	Measured with Calipers with .0005" res Length (in)	Measured with scale with res +/- 2 g Weight (g)
1	1	1.2	0.375	1.5605	22
1	2	1.2	0.375	2.31	32
1	3	1.2	0.375	3.0605	42
1	4	1.2	0.375	5.0665	70
1	5	1.2	0.375	1.558	22
1	6	1.2	0.375	2.3245	32
1	7	1.2	0.375	3.073	42
1	8	1.2	0.375	5.0565	70
1	9	1.2	0.375	1.56	22
1	10	1.2	0.375	2.328	32
1	11	1.2	0.375	3.081	42
1	12	1.2	0.375	5.0895	70

Batch	Block#	in OD	in ID	Measured with Calipers with .0005" res Length (in)	Measured with scale with res +/- 2 g Weight (g)
2	1	1.2	0.825	1.544	12
2	2	1.2	0.825	2.3115	20
2	3	1.2	0.825	3.0675	26
2	4	1.2	0.825	5.069	46
2	5	1.2	0.825	1.54	14
2	6	1.2	0.825	2.305	20
2	7	1.2	0.825	3.0475	28
2	8	1.2	0.825	5.0475	46
2	9	1.2	0.825	1.537	14
2	10	1.2	0.825	2.302	20
2	11	1.2	0.825	3.04	28
2	12	1.2	0.825	5.059	46

Batch	Block#	in OD	in ID	Measured with Calipers with .0005" res Length (in)	Measured with scale with res +/- 2 g Weight (g)
3	1	1.9	0.75	1.55	50
3	2	1.9	0.75	2.2795	74
3	3	1.9	0.75	3.0845	100
3	4	1.9	0.75	5.045	162
3	5	1.9	0.75	1.584	50
3	6	1.9	0.75	2.331	74
3	7	1.9	0.75	3.059	98
3	8	1.9	0.75	5.072	162
3	9	1.9	0.75	1.593	50
3	10	1.9	0.75	2.3185	74
3	11	1.9	0.75	3.072	98
3	12	1.9	0.75	5.053	162

Batch	Block#	in OD	in ID	Measured with Calipers with .0005" res Length (in)	Measured with scale with res +/- 2 g Weight (g)
4	1	1.9	0.75	1.5835	50
4	2	1.9	0.75	2.326	74
4	3	1.9	0.75	3.0475	98
4	4	1.9	0.75	5.04	162
4	5	1.9	0.75	1.5585	50
4	6	1.9	0.75	2.322	76
4	7	1.9	0.75	3.094	100
4	8	1.9	0.75	5.064	162
4	9	1.9	0.75	1.579	50
4	10	1.9	0.75	2.307	74
4	11	1.9	0.75	3.074	96
4	12	1.9	0.75	5.07	160

Batch	Block#	in OD	in ID	Measured with Calipers with .0005" res Length (in)	Measured with scale with res +/- 2 g Weight (g)
5	1	1.9	0.75	1.607	54
5	2	1.9	0.75	2.3535	78
5	3	1.9	0.75	3.0645	104
5	4	1.9	0.75	5.081	170
5	5	1.9	0.75	1.5885	52
5	6	1.9	0.75	2.339	76
5	7	1.9	0.75	3.069	100
5	8	1.9	0.75	5.0785	168
5	9	1.9	0.75	1.5825	52
5	10	1.9	0.75	2.345	78
5	11	1.9	0.75	3.0875	104
5	12	1.9	0.75	5.05	168

Batch	Block#	in OD	in ID	Measured with Calipers with .0005" res Length (in)	Measured with scale with res +/- 2 g Weight (g)
6	1	1.2	0.375	1.585	20
6	2	1.2	0.375	2.3215	30
6	3	1.2	0.375	3.081	40
6	4	1.2	0.375	5.061	66
6	5	1.2	0.375	1.5675	20
6	6	1.2	0.375	2.3265	30
6	7	1.2	0.375	3.0875	40
6	8	1.2	0.375	5.0865	68
6	9	1.2	0.375	1.559	20
6	10	1.2	0.375	2.298	30
6	11	1.2	0.375	3.0615	40
6	12	1.2	0.375	5.0815	66

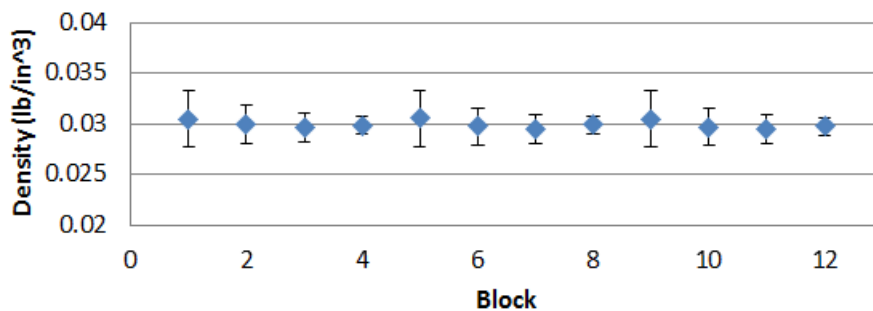
Batch	Block#	in OD	in ID	Measured with Calipers with .0005" res Length (in)	Measured with scale with res +/- 2 g Weight (g)
7	1	1.2	0.375	1.5725	22
7	2	1.2	0.375	2.3075	32
7	3	1.2	0.375	3.0725	42
7	4	1.2	0.375	5.0815	70
7	5	1.2	0.375	1.5655	22
7	6	1.2	0.375	2.2965	30
7	7	1.2	0.375	3.0945	42
7	8	1.2	0.375	5.0790	68
7	9	1.2	0.375	1.5885	22
7	10	1.2	0.375	2.324	32
7	11	1.2	0.375	3.0590	42
7	12	1.2	0.375	5.0630	68

Batch	Block#	in OD	in ID	Measured with Calipers with .0005" res Length (in)	Measured with scale with res +/- 2 g Weight (g)
8	1	1.2	0.825	1.5545	14
8	2	1.2	0.825	1.5705	14
8	3	1.2	0.825	1.5595	14
8	4	1.2	0.825	2.3205	22
8	5	1.2	0.825	2.32	22
8	6	1.2	0.825	2.32	22
8	7	1.2	0.825	3.076	28
8	8	1.2	0.825	3.0685	28
8	9	1.2	0.825	3.0715	26

Batch	Block#	in OD	in ID	Measured with Calipers with .0005" res Length (in)	Measured with scale with res +/- 2 g Weight (g)
9	1	1.2	0.825	1.5655	12
9	2	1.2	0.825	2.303	20
9	3	1.2	0.825	3.055	26
9	4	1.2	0.825	1.581	14
9	5	1.2	0.825	2.329	20
9	6	1.2	0.825	3.09	26
9	7	1.2	0.825	1.5615	12
9	8	1.2	0.825	2.3065	20
9	9	1.2	0.825	3.049	26

Table 14 - Raw height and weight data used to calculate density of each sample.

Density Batch 1



Density Batch 2

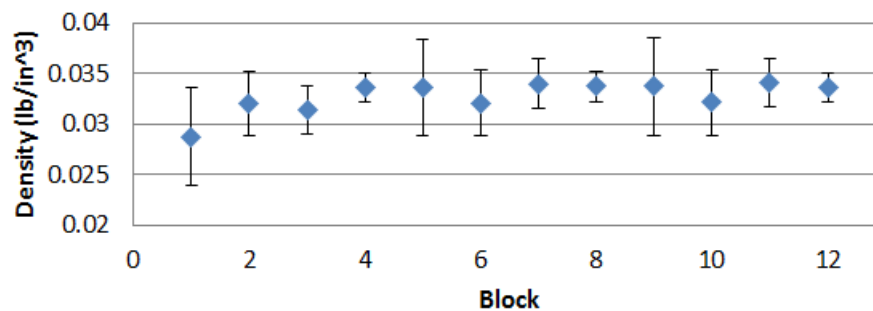
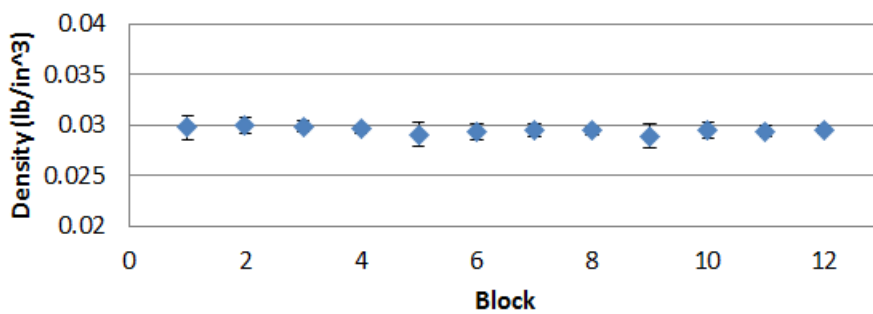
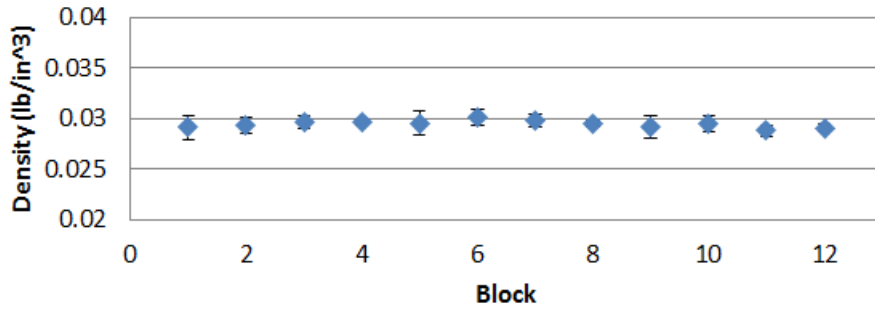


Chart Area

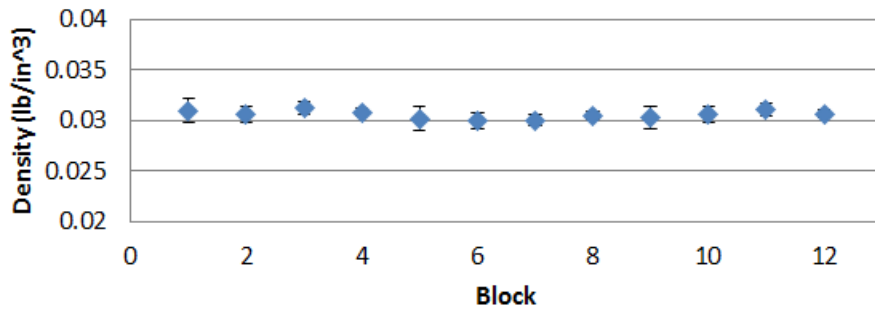
Density Batch 3



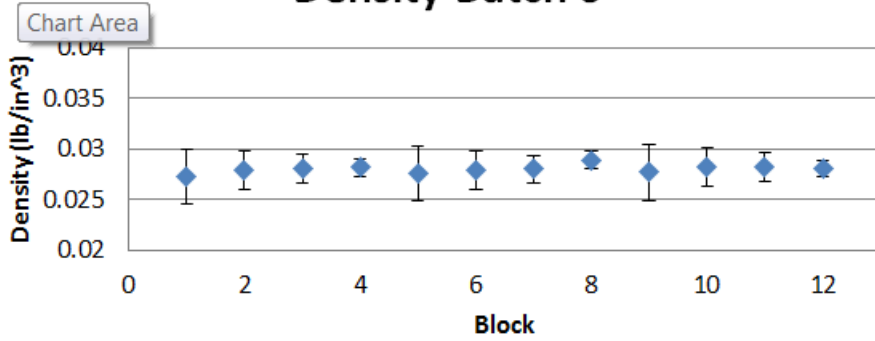
Density Batch 4



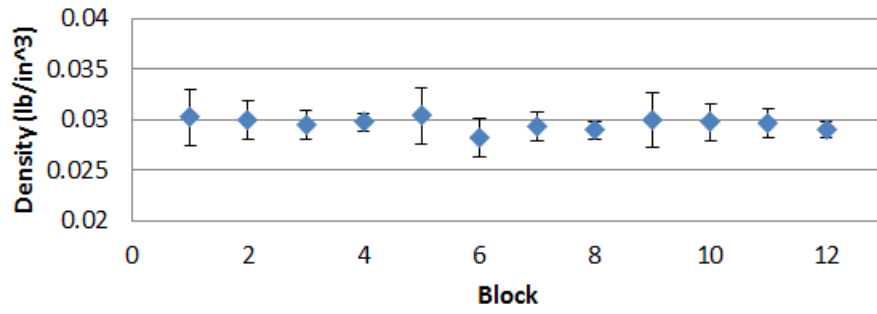
Density Batch 5



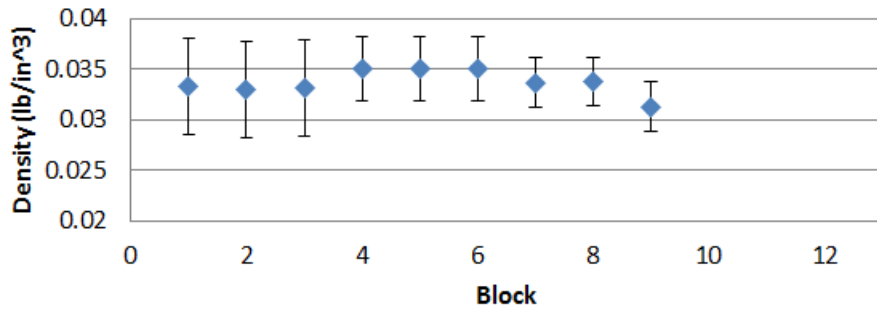
Density Batch 6



Density Batch 7



Density Batch 8



Density Batch 9

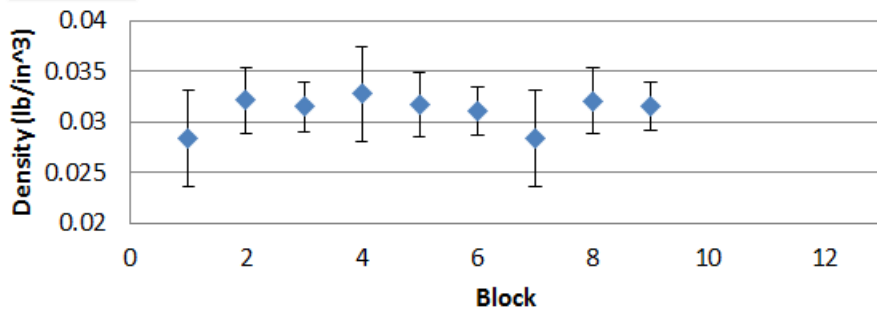


Figure 38 - Calculated density graphs for each batch of extruded samples.

Batch	Block#	Image 1 Porosity	Image 2 Porosity	Image 3 Porosity	Image 4 Porosity	Image 5 Porosity	Image 6 Porosity	Image 7 Porosity	Image 8 Porosity	Image 9 Porosity	Image 10 Porosity	Average Porosity
1	1	8.30%	16.07%		14.11%	13.34%	8.29%	10.07%	10.46%	9.26%	20.06%	12.22%
1	2	8.66%	6.11%		14.79%	20.98%	16.84%	18.05%	18.84%	9.24%	13.78%	14.14%
1	3	11.00%		10.78%	10.21%	6.82%	14.89%	6.57%	15.78%	7.51%	8.26%	10.20%
1	4	6.24%	12.28%	9.55%	7.23%	9.34%	5.03%	10.68%	5.20%	8.24%	7.53%	8.13%
1	5		8.23%	10.96%	14.57%	18.76%	6.51%	23.52%	11.04%	14.56%		13.52%
1	6	10.68%	9.75%	7.45%	11.14%	11.93%		18.67%	21.06%	12.78%	17.39%	13.43%
1	7	14.82%			7.40%	7.02%	22.23%		11.47%	12.67%		12.60%
1	8	9.90%	7.82%	9.73%	5.88%	23.58%	9.96%	6.60%	12.01%	25.73%	7.67%	11.89%
1	9		10.95%	16.27%	25.95%	13.51%	17.55%	11.94%	10.42%	11.70%	15.39%	14.85%
1	10	8.41%	14.25%	8.86%	8.55%	12.52%	12.95%	5.83%	8.68%	10.50%	8.78%	9.93%
1	11	9.74%	7.39%	6.84%	8.14%	6.29%	8.42%	10.11%	8.01%	10.97%	20.78%	9.67%
1	12	7.79%	12.05%	11.14%	10.51%	14.37%	10.95%	6.00%	9.47%	30.35%	10.47%	12.31%
1 Average												11.80%

Batch	Block#	Image 1 Porosity	Image 2 Porosity	Image 3 Porosity	Image 4 Porosity	Image 5 Porosity	Image 6 Porosity	Image 7 Porosity	Image 8 Porosity	Image 9 Porosity	Image 10 Porosity	Average Porosity
2	1	10.31%	8.79%	8.61%	10.29%	4.52%	14.39%	10.69%	11.02%	11.02%	14.13%	10.38%
2	2	8.59%	8.16%	8.45%	7.72%	12.15%	9.80%	11.50%	9.57%	7.73%	9.67%	9.33%
2	3	7.80%	8.82%	5.97%	8.33%	7.72%	6.51%	8.82%	5.11%	8.25%	7.18%	7.45%
2	4	8.74%	4.31%	5.76%			4.92%	6.34%	6.22%	8.05%	8.60%	6.62%
2	5			5.31%	4.59%		3.65%		4.64%	6.47%	7.73%	5.40%
2	6	3.89%		6.77%	5.07%	4.91%	4.08%	5.56%	6.50%	7.84%	6.94%	5.73%
2	7	6.17%	7.17%	5.80%	5.59%	6.83%	8.52%			4.31%	6.60%	6.37%
2	8	4.40%	4.36%		3.33%	7.72%	6.61%	4.83%	8.45%	6.57%	8.30%	6.06%
2	9	3.45%		3.92%				5.78%	5.91%	6.97%		5.21%
2	10		4.37%	7.32%	6.45%	4.95%	5.42%	5.74%	4.57%		5.34%	5.52%
2	11	5.26%	5.49%	6.66%	5.30%	2.76%	10.23%		3.93%	7.10%	4.81%	5.73%
2	12	4.41%	7.76%	4.51%	3.98%	5.72%	5.62%	5.45%		6.40%	4.18%	5.34%
2 Average												6.77%

Batch	Block#	Image 1 Porosity	Image 2 Porosity	Image 3 Porosity	Image 4 Porosity	Image 5 Porosity	Image 6 Porosity	Image 7 Porosity	Image 8 Porosity	Image 9 Porosity	Image 10 Porosity	Average Porosity
3	1	9.30%	8.01%	11.49%	10.30%	7.78%	9.71%					9.43%
3	2	19.31%	24.45%	3.09%		15.35%	12.52%	13.28%	16.42%			14.92%
3	3	12.39%	10.06%	15.74%	14.38%	17.19%	13.35%	12.02%				13.59%
3	4	23.10%	14.93%	16.86%	35.20%	14.03%	11.75%		14.13%	13.04%	15.08%	17.57%
3	5	22.72%	13.00%	11.11%	21.62%	21.64%	18.21%	14.32%				17.52%
3	6	14.89%	14.41%	15.27%	19.60%	19.23%	16.66%	27.29%	27.08%			19.30%
3	7	26.75%	16.20%	29.86%	8.83%	12.65%	25.56%	7.46%		18.50%		18.23%
3	8	22.24%	12.64%	24.70%	11.86%	13.45%	13.06%	17.80%	22.65%	24.31%		18.08%
3	9	20.67%	29.65%	21.10%	17.39%	37.58%	20.23%	37.59%				26.32%
3	10	24.92%	23.95%	24.95%	26.77%	33.25%	16.42%	6.26%	30.89%			23.43%
3	11	14.94%	8.06%	10.22%	25.92%	16.91%	17.23%					15.55%
3	12	31.17%	19.17%	21.35%	18.28%	34.61%	35.41%	27.21%	27.19%	16.00%	12.25%	24.26%
3 Average												18.56%

Batch	Block#	Image 1 Porosity	Image 2 Porosity	Image 3 Porosity	Image 4 Porosity	Image 5 Porosity	Image 6 Porosity	Image 7 Porosity	Image 8 Porosity	Image 9 Porosity	Image 10 Porosity	Average Porosity
4	1	12.41%	14.76%	16.20%	15.70%	24.10%	17.65%	18.79%		24.90%		18.06%
4	2	6.78%	22.48%	0.13%			15.41%	12.19%	20.92%	14.50%		13.20%
4	3	10.45%	13.33%	15.13%	16.03%	10.65%	10.00%		15.39%			13.00%
4	4	14.24%		11.48%			14.60%	11.05%	8.87%			12.05%
4	5		8.15%	11.47%	15.18%		14.59%	12.20%		12.21%		12.30%
4	6	13.67%	8.86%	21.77%	10.93%	28.61%	12.77%			15.16%		15.97%
4	7			8.15%	18.78%	6.49%	8.51%	15.34%	12.23%	7.84%	12.21%	11.19%
4	8	15.73%	11.10%	24.89%	12.96%	10.99%	8.14%	13.08%	15.18%	9.38%	13.24%	13.47%
4	9	11.82%	12.45%	16.41%	12.67%	17.31%	18.21%		15.62%	11.51%		14.50%
4	10			17.18%			11.76%			7.69%		12.21%
4	11		9.71%	8.18%	11.17%	19.28%	13.37%		11.99%			12.28%
4	12	20.04%		15.43%		9.05%		10.03%				13.64%
4 Average												13.66%

Batch	Block#	Image 1 Porosity	Image 2 Porosity	Image 3 Porosity	Image 4 Porosity	Image 5 Porosity	Image 6 Porosity	Image 7 Porosity	Image 8 Porosity	Image 9 Porosity	Image 10 Porosity	Average Porosity
5	1	13.56%	20.70%	15.51%	7.51%			10.67%	19.80%	10.27%	10.87%	13.61%
5	2		13.45%	15.42%		11.37%	13.68%		20.62%	16.46%	19.85%	15.84%
5	3					19.19%						19.19%
5	4						28.98%	11.65%				20.32%
5	5			7.91%			10.93%		11.03%			9.96%
5	6	8.88%	20.94%	17.33%		13.78%	16.51%	5.48%	10.02%			13.28%
5	7	15.60%		12.18%		19.61%	19.54%	15.82%	9.28%	14.53%	14.29%	15.11%
5	8	27.55%	17.13%	22.82%	10.54%	13.18%	15.72%	8.25%	20.32%	14.83%	7.21%	15.76%
5	9	29.37%	24.06%	18.78%	9.41%		12.68%	15.08%	21.48%			18.84%
5	10				22.04%		25.80%	26.79%	28.81%		23.54%	25.40%
5	11		12.14%			12.93%						12.54%
5	12		12.74%		19.05%			16.20%			10.01%	14.50%
5 Average												16.02%

Batch	Block#	Image 1 Porosity	Image 2 Porosity	Image 3 Porosity	Image 4 Porosity	Image 5 Porosity	Image 6 Porosity	Image 7 Porosity	Image 8 Porosity	Image 9 Porosity	Image 10 Porosity	Average Porosity
6	1	10.53%			8.41%	14.09%	8.60%	10.56%		7.45%	12.29%	10.28%
6	2	15.23%	6.54%	10.14%	17.13%	9.42%	16.18%	7.41%	10.76%	14.68%	16.73%	12.42%
6	3	11.73%	8.81%	14.53%	6.03%	7.56%	11.44%	8.23%	9.35%	9.48%	10.13%	9.73%
6	4		7.31%	12.09%	8.39%	8.63%	11.98%		7.20%	10.02%	12.77%	9.80%
6	5	10.44%	12.34%	10.85%	8.90%	13.40%	6.06%	6.97%	10.24%	12.36%	10.41%	10.20%
6	6	14.74%	10.66%	12.08%	7.96%	12.76%	22.09%	12.03%	9.15%	11.66%	10.95%	12.41%
6	7	11.02%	11.67%	9.79%	8.58%	12.24%	7.08%	8.77%	15.06%	9.35%	8.27%	10.18%
6	8	7.29%	9.35%		8.25%	9.37%	10.51%	9.40%	12.73%	8.93%	7.07%	9.21%
6	9	9.94%		10.05%	9.32%	7.02%	9.67%	25.87%	11.77%	8.91%	13.26%	11.76%
6	10	10.81%	10.08%	8.10%	13.56%	6.63%	7.26%	6.79%	6.73%	8.52%	11.50%	9.00%
6	11	10.80%	16.98%	8.60%	9.71%	12.31%	7.90%	7.68%	10.71%	7.70%	9.64%	10.20%
6	12	12.65%	9.31%		16.12%	10.95%	9.27%	7.60%	7.68%	7.83%	11.02%	10.27%
6 Average												10.47%

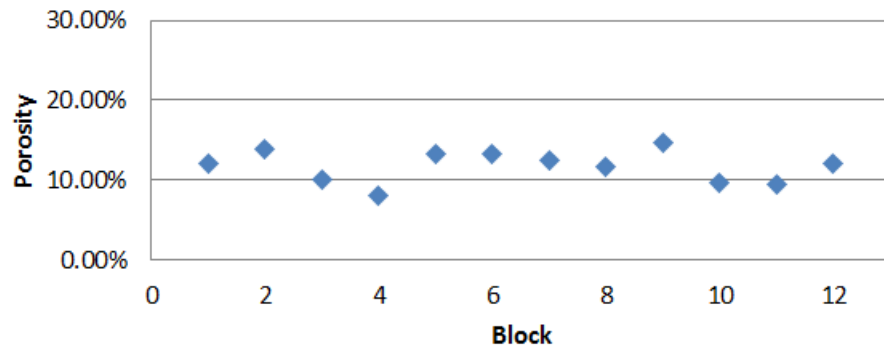
Batch	Block#	Image 1 Porosity	Image 2 Porosity	Image 3 Porosity	Image 4 Porosity	Image 5 Porosity	Image 6 Porosity	Image 7 Porosity	Image 8 Porosity	Image 9 Porosity	Image 10 Porosity	Average Porosity
7	1				8.03%			8.97%	8.17%			8.39%
7	2											
7	3						11.09%	6.38%				8.74%
7	4								8.45%	9.86%	6.97%	8.43%
7	5							11.07%	6.61%			8.84%
7	6				14.94%				12.00%			13.47%
7	7				6.45%				10.56%	9.02%	7.45%	8.37%
7	8				4.15%		4.54%					4.35%
7	9				8.34%	8.41%						8.38%
7	10					9.46%	11.10%	10.51%				10.36%
7	11										9.30%	9.30%
7	12					5.30%						5.30%
7 Average												0.0869

Batch	Block#	Image 1 Porosity	Image 2 Porosity	Image 3 Porosity	Image 4 Porosity	Image 5 Porosity	Image 6 Porosity	Image 7 Porosity	Image 8 Porosity	Image 9 Porosity	Image 10 Porosity	Average Porosity
8	1								5.89%			5.89%
8	2											
8	3											
8	4											
8	5											
8	6											
8	7											
8	8											
8	9	2.89%				1.98%					7.35%	4.07%
8												
8												
8 Average												0.0453

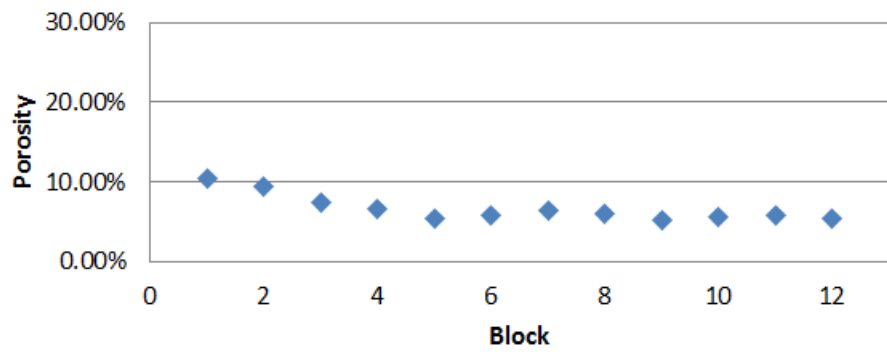
Batch	Block#	Image 1 Porosity	Image 2 Porosity	Image 3 Porosity	Image 4 Porosity	Image 5 Porosity	Image 6 Porosity	Image 7 Porosity	Image 8 Porosity	Image 9 Porosity	Image 10 Porosity	Average Porosity
9	1	6.97%	6.43%	2.21%	2.27%	6.23%	4.36%	5.55%	3.78%	5.10%	5.59%	4.85%
9	2	3.53%	4.25%	3.53%	4.91%	3.88%	5.04%	3.64%	3.57%	3.37%	5.57%	4.13%
9	3	2.49%	1.49%	2.72%	4.21%	3.51%	3.57%	2.80%	3.00%	2.86%	4.21%	3.09%
9	4	4.61%	6.90%	2.98%	4.51%	3.88%	1.20%	2.62%	4.30%	2.93%	2.99%	3.69%
9	5	2.35%	4.53%	3.79%	5.90%	2.75%	3.58%	5.03%	2.60%	4.93%	2.12%	3.76%
9	6		3.30%	5.32%	3.92%	5.78%	4.37%	4.16%	7.08%	4.01%	6.06%	4.89%
9	7	3.16%	4.14%	5.85%	6.28%	8.65%	3.39%	6.84%	4.64%	7.29%	5.75%	5.60%
9	8	5.20%	2.52%	6.52%	4.32%	5.35%	4.23%	5.28%	3.61%	3.92%	6.46%	4.74%
9	9	7.59%	5.84%	4.84%	6.92%	3.76%	5.21%	4.66%	5.09%	4.01%	5.10%	5.30%
9												
9												
9												
9 Average												4.44%

Table 15 - Raw height and weight data used to calculate density of each sample.

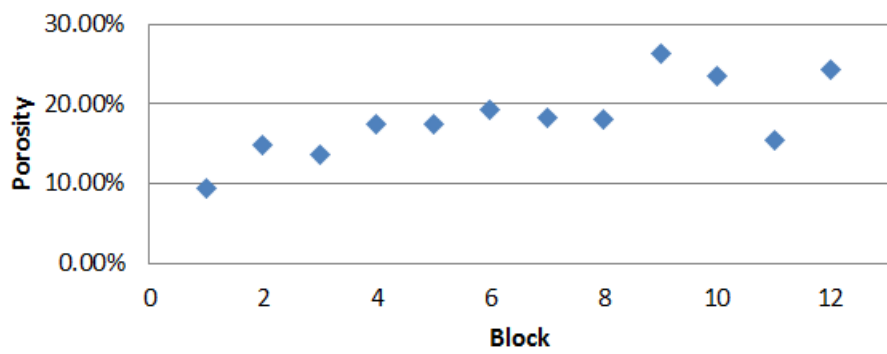
Batch 1



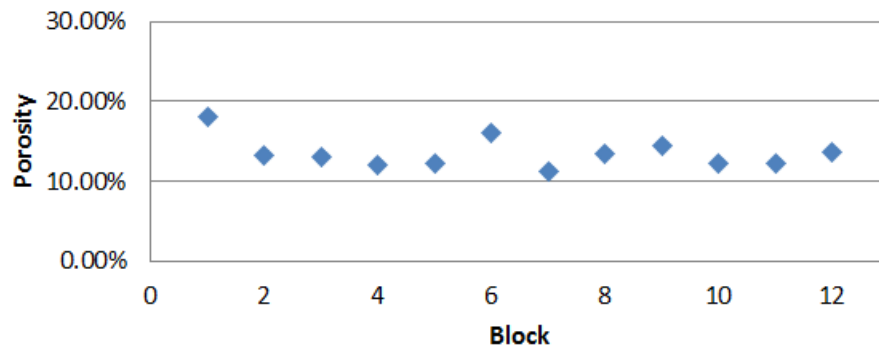
Batch 2



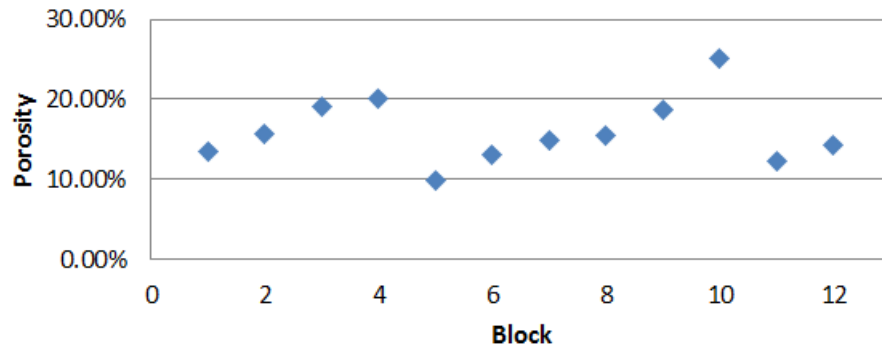
Batch 3



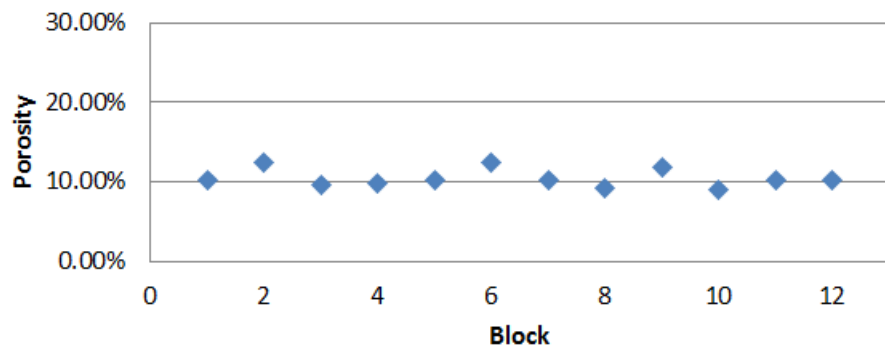
Batch 4



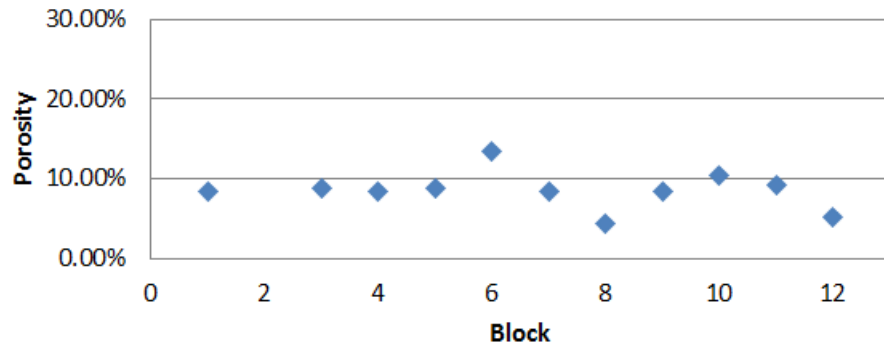
Batch 5



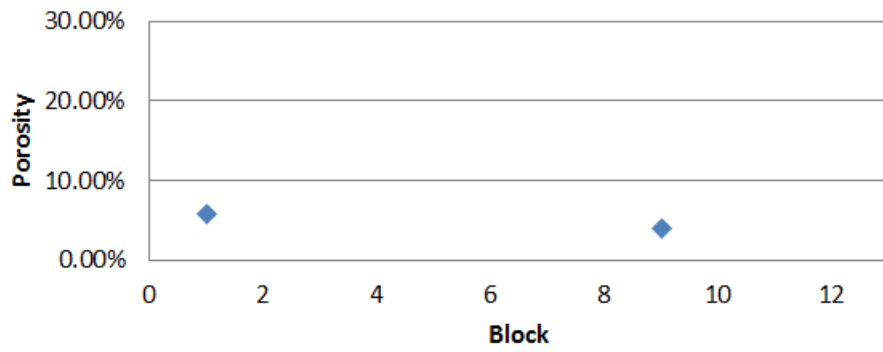
Batch 6



Batch 7



Batch 8



Batch 9

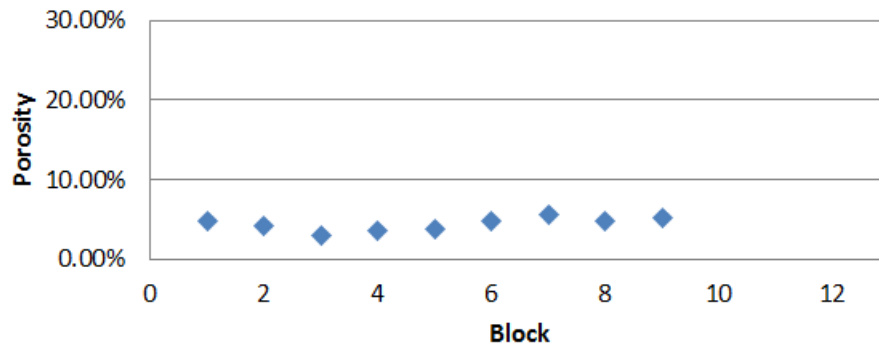


Figure 39 - Calculated porosity graphs for each batch of extruded samples.

Batch	Block#	Flow Rate			Pressure (Pa)				
		0.1	0.2	0.4	0.6	0.8	1		
1	1		106.55	262.20	460.99	631.64	817.30		
1	2		16.53	115.92	222.82	320.34	429.11		
1	3		1.53	89.67	181.56	267.83	348.47		
1	4			7.15	65.29	123.43	170.31		
1	5		55.91	204.07	365.35	519.12	637.27		
1	6		40.91	147.81	269.70	389.73	504.12		
1	7		3.40	89.67	181.56	260.33	348.47		
1	8			24.03	89.67	140.30	196.56		
1	9		104.67	288.46	453.49	622.27	779.80		
1	10		35.28	162.81	279.08	387.85	504.12		
1	11			59.66	134.68	209.69	286.58		
1	12	0.40	74.00		42.79	89.67	130.93		

Batch	Block#	Flow Rate			Pressure (Pa)				
		0.1	0.2	0.4	0.6	0.8	1		
2	1					57.79	95.30		
2	2					25.91	57.79		
2	3					14.66	44.66		
2	4					5.28	29.66		
2	5		33.41	157.18	288.46	410.35	515.37		
2	6			48.41	119.68	194.69	258.45		
2	7			3.40	52.16	89.67	142.18		
2	8					25.91	55.91		
2	9		20.28	129.05	230.32	337.22	445.99		
2	10			61.54	121.55	192.81	265.95		
2	11				46.54	95.30	140.30		
2	12					25.91	55.91		

Batch	Block#	Flow Rate			Pressure (Pa)				
		0.1	0.2	0.4	0.6	0.8	1		
3	1		241.57	513.50	768.55	1040.47	1293.64		
3	2		87.79	252.82	425.36	607.27	774.17		
3	3		22.16	136.55	249.07	348.47	449.74		
3	4			37.16	104.67	172.18	243.45		
3	5		130.93	324.09	522.87	719.79	931.70		
3	6		46.54	181.56	316.59	442.23	582.89		
3	7		20.28	119.68	226.57	333.46	440.36		
3	8			42.79	106.55	170.31	224.69		
3	9		134.68	350.34	541.63	732.91	909.20		
3	10		70.92	211.57	357.84	481.62	620.39		
3	11		27.78	132.80	243.45	354.09	440.36		
3	12			39.04	106.55	174.06	224.69		

Batch	Block#	Flow Rate			Pressure (Pa)			
		0.1	0.2	0.4	0.6	0.8	1	
4	1				31.53	100.92	166.56	230.32
4	2				18.41	63.41	119.68	168.43
4	3					39.04	78.42	123.43
4	4						27.78	55.91
4	5				57.79	134.68	202.19	271.58
4	6				29.66	87.79	145.93	200.32
4	7					33.41	76.54	115.92
4	8						14.66	39.04
4	9				21.97	82.17	138.43	204.07
4	10					24.03	61.54	100.92
4	11						22.16	46.54
4	12							25.91

Batch	Block#	Flow Rate			Pressure (Pa)			
		0.1	0.2	0.4	0.6	0.8	1	
5	1							
5	2		305.33	627.89	984.21	1323.65	1687.47	
5	3		110.30	312.84	504.12	671.03	841.68	
5	4		44.66	144.05	264.08	374.72	490.99	
5	5		271.58	609.14	922.32	1269.26	1563.69	
5	6		166.56	397.23	618.52	824.81	1059.22	
5	7		97.17	264.08	457.24	599.76	764.79	
5	8		37.16	144.05	247.20	350.34	459.11	
5	9		299.71	637.27	1012.34	1331.15	1649.96	
5	10		172.18	406.60	639.15	871.69	1092.98	
5	11		110.30	273.45	447.86	618.52	796.68	
5	12		25.91	132.80	247.20	340.97	444.11	

Batch	Block#	Flow Rate			Pressure (Pa)				
		0.1	0.2	0.4	0.6	0.8	1	1.2	
6	1				14.66	61.54	110.30	155.31	
6	2					9.03	39.04	72.79	
6	3						10.91	35.28	
6	4							1.53	20.28
6	5				12.78	59.66	108.42	155.31	
6	6					24.03	61.54	99.05	
6	7						39.04	69.04	
6	8							14.66	35.28
6	9				40.91	100.92	157.18	219.07	
6	10							18.41	42.79
6	11						24.03	55.91	
6	12							5.28	25.91

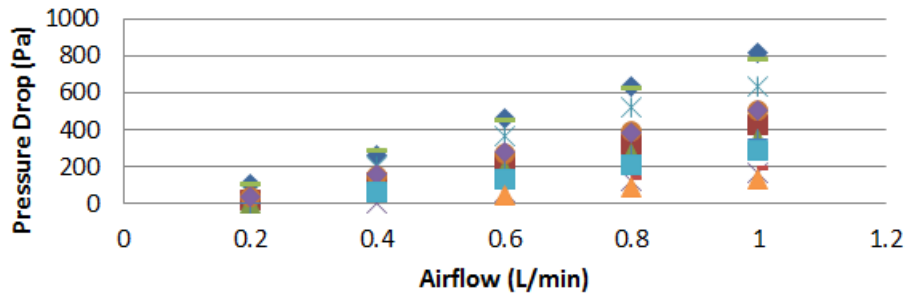
Batch	Block#	Flow Rate			Pressure (Pa)			
		0.1	0.2	0.4	0.6	0.8	1	
7	1		430.98	867.94	1293.64	1724.97		
7	2		222.82	487.24	753.54	1012.34	1280.52	
7	3		114.05	288.46	472.24	637.27	817.30	
7	4		40.91	155.31	258.45	365.35	475.99	
7	5		380.35	714.16	1151.12	1501.81		
7	6		70.92	235.95	387.85	573.51	787.30	
7	7			87.79	194.69	288.46	384.10	
7	8		22.16	125.30	230.32	324.09	415.98	
7	9		211.57	487.24	776.05	1040.47	1308.65	
7	10		149.68	352.22	566.01	776.05	974.83	
7	11		108.42	262.20	423.48	594.14	747.92	
7	12		25.91	117.80	217.19	314.71	414.10	

Batch	Block#	Flow Rate			Pressure (Pa)			
		0.1	0.2	0.4	0.6	0.8	1	
8	1		179.69	423.48	708.53	997.34	1246.76	
8	2		586.64	1124.86	1661.21			
8	3		545.38	1100.48	1623.70			
8	4		517.25	1038.60	1612.45			
8	5		757.29	1529.94				
8	6	453.49	909.20					
8	7		217.19	453.49	738.54	993.59	1263.64	
8	8		119.68	312.84	496.62	693.53	871.69	
8	9			72.79	149.68	226.57	297.83	

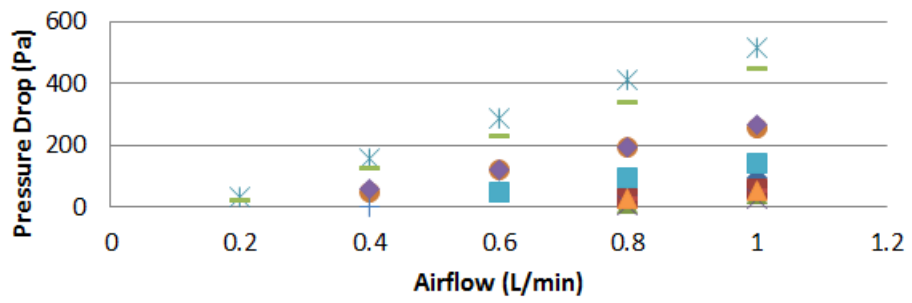
Batch	Block#	Flow Rate			Pressure (Pa)			
		0.1	0.2	0.4	0.6	0.8	1	1.2
9	1				48.41	100.92	147.81	198.44
9	2				46.54	97.17	147.81	194.69
9	3			7.15	55.91	99.05	142.18	196.56
9	4		37.16	149.68	277.20	389.73	498.50	
9	5			61.54	138.43	207.82	277.20	
9	6				29.66	67.17	110.30	147.81
9	7			20.28	70.92	121.55	177.81	230.32
9	8			20.28	76.54	132.80	187.19	243.45
9	9				42.79	85.92	130.93	172.18

Table 16 - Raw data collected from the air test for each batch of extruded samples.

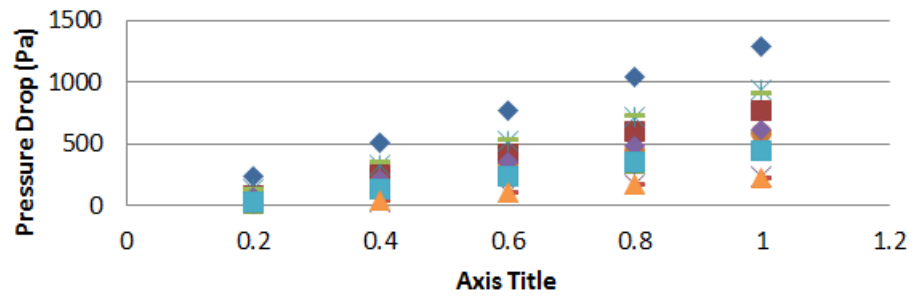
Batch 1 Air Data



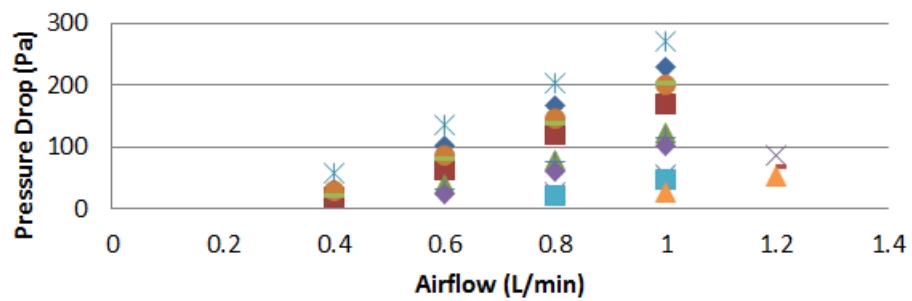
Batch 2 Air Data



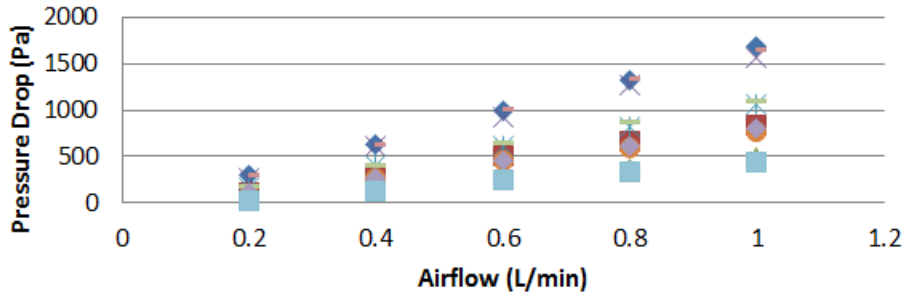
Batch 3 Air Data



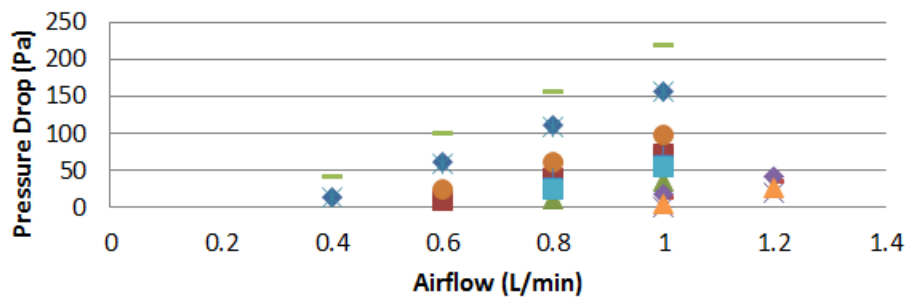
Batch 4 Air Data



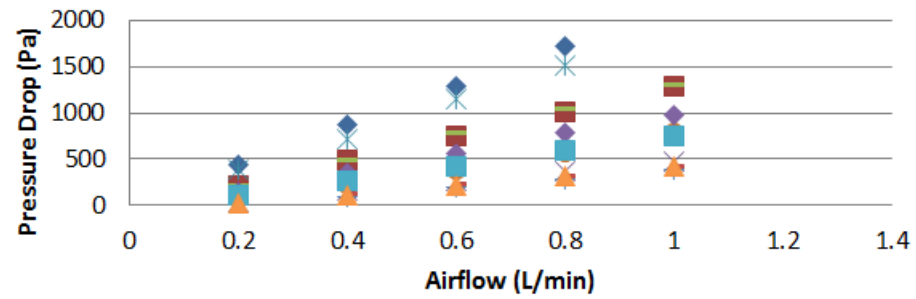
Batch 5 Air Data



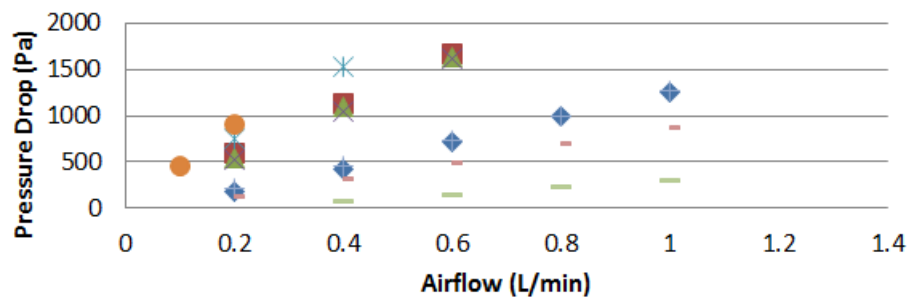
Batch 6 Air Data



Batch 7 Air Data



Batch 8 Air Data



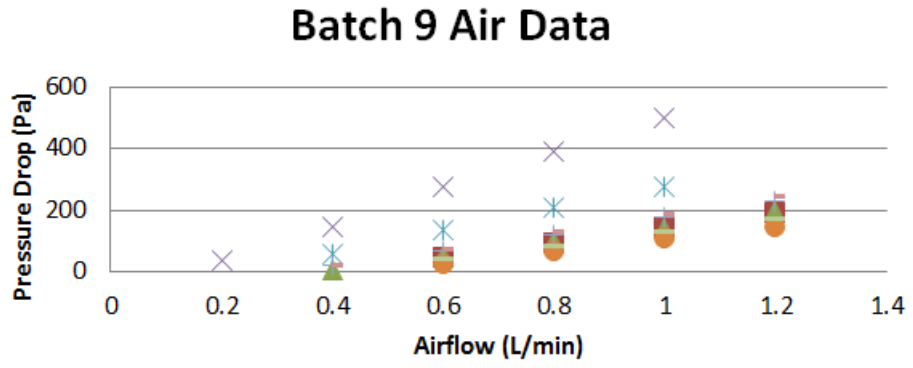


Figure 40 - Graphical summaries of air test data for each batch of extruded samples.

Batch	Block#	Flow Rate (L/min)		κ - Permeability (Darcy)					
		0.1	0.2	0.4	0.6	0.8	1	1.2	
1	1		2.646011	2.150457	1.83471	1.785349	1.724735		
1	2		11.52084	3.28581	2.564226	2.378156	2.219177		
1	3		94.05207	3.206209	2.375224	2.146902	2.062601		
1	4			24.27425	3.989929	2.814138	2.54931		
1	5		5.050287	2.767529	2.318728	2.175812	2.215534		
1	6		4.626298	2.561002	2.105261	1.942549	1.877177		
1	7		42.06096	3.193167	2.365562	2.199781	2.054211		
1	8			7.240686	2.910888	2.480502	2.213171		
1	9		2.694281	1.955353	1.865657	1.812833	1.808271		
1	10		5.355884	2.32151	2.031468	1.949007	1.874355		
1	11			4.786574	3.180774	2.723871	2.491327		
1	12				6.060996	3.856018	3.301144		

Batch	Block#	Flow Rate (L/min)		κ - Permeability (Darcy)					
		0.1	0.2	0.4	0.6	0.8	1	1.2	
2	1					6.35344	4.81603		
2	2					9.466156	5.304841		
2	3					12.6097	5.172414		
2	4					21.18448	4.713429		
2	5		2.754558	1.170971	0.957107	0.897058	0.892827		
2	6			2.540068	1.541296	1.263244	1.189491		
2	7			27.3255	2.674588	2.074486	1.635421		
2	8					4.335021	2.51083		
2	9		4.5463	1.428997	1.201032	1.093751	1.03375		
2	10			2.000832	1.519493	1.277193	1.157447		
2	11				3.005328	1.956829	1.661369		
2	12					4.325167	2.505122		

Batch	Block#	Flow Rate (L/min)		κ - Permeability (Darcy)					
		0.1	0.2	0.4	0.6	0.8	1	1.2	
3	1		0.938967	0.883465	0.885422	0.872024	0.876706		
3	2		1.756806	1.220115	1.087823	1.015949	0.996147		
3	3		5.144344	1.669448	1.372897	1.308407	1.267236		
3	4			3.750795	1.997366	1.618951	1.431306		
3	5		1.695292	1.369752	1.273499	1.233478	1.191156		
3	6		3.241097	1.661474	1.429277	1.364253	1.293821		
3	7		5.666861	1.920774	1.521842	1.378671	1.305008		
3	8			3.240252	1.951765	1.628065	1.54251		
3	9		1.638768	1.259943	1.222459	1.204541	1.213743		
3	10		2.138343	1.433523	1.271306	1.25945	1.222155		
3	11		4.119321	1.723582	1.41034	1.292858	1.299486		
3	12			3.564945	1.959104	1.598973	1.54831		

Batch	Block#	Flow Rate (L/min)		κ - Permeability (Darcy)					
		0.1	0.2	0.4	0.6	0.8	1	1.2	
4	1			14.08198	6.600067	5.332172	4.820022		
4	2			16.42398	7.150735	5.052148	4.48704		
4	3				8.866448	5.884814	4.673583		
4	4					10.0433	6.238112	4.871487	
4	5			7.807456	5.025136	4.462955	4.153347		
4	6			10.2105	5.173954	4.150333	3.779411		
4	7				10.20384	5.938386	4.901222		
4	8					18.94898	8.893003	6.033666	
4	9			20.27002	8.129519	6.434011	5.455664		
4	10				19.02408	9.905776	7.550359		
4	11					20.64766	12.28854		
4	12						13.38319	7.976507	

Batch	Block#	Flow Rate (L/min)		κ - Permeability (Darcy)					
		0.1	0.2	0.4	0.6	0.8	1	1.2	
5	1								
5	2		0.48926	0.475838	0.455354	0.451444	0.44264		
5	3		1.040162	0.733472	0.682742	0.683896	0.68154		
5	4		1.549347	0.96069	0.786089	0.738637	0.704652		
5	5		0.814982	0.7267	0.719914	0.697511	0.70772		
5	6		0.902468	0.756818	0.72907	0.728968	0.709549		
5	7		1.178952	0.867626	0.751644	0.764034	0.74896		
5	8		1.863026	0.961163	0.840174	0.790426	0.753954		
5	9		0.741289	0.697256	0.658387	0.667605	0.673261		
5	10		0.870747	0.737473	0.703734	0.687995	0.685875		
5	11		1.032413	0.832855	0.762783	0.736429	0.71468		
5	12		2.687239	1.048484	0.844916	0.816747	0.783823		

Batch	Block#	Flow Rate (L/min)		κ - Permeability (Darcy)					
		0.1	0.2	0.4	0.6	0.8	1	1.2	
6	1			37.87827	13.53125	10.06609	8.936143		
6	2				62.96144	19.41929	13.01728		
6	3					52.37656	20.2345		
6	4						284.377	25.7162	
6	5			43.92128	14.11238	10.35453	9.035908		
6	6				23.60576	12.29144	9.546145		
6	7					14.60142	10.31945		
6	8						29.50804	14.70775	
6	9			13.7958	8.388613	7.181423	6.440857		
6	10						52.00535	26.84721	
6	11					23.91803	12.85048		
6	12						82.00079	20.05057	

Batch	Block#	Flow Rate (L/min)		κ - Permeability (Darcy)					
		0.1	0.2	0.4	0.6	0.8	1	1.2	
7	1		0.649156	0.644689	0.648808	0.648765			
7	2		0.855668	0.782605	0.759052	0.753341	0.744464		
7	3		1.255497	0.992791	0.909633	0.89876	0.87598		
7	4		2.116271	1.11493	1.004966	0.947903	0.909451		
7	5		0.738865	0.787012	0.732401	0.748502			
7	6		2.701393	1.623863	1.481805	1.336144	1.216645		
7	7			3.238716	2.190731	1.971465	1.8507		
7	8		3.909367	1.382599	1.128262	1.069101	1.041164		
7	9		1.309074	1.136834	1.070647	1.064738	1.058183		
7	10		1.26473	1.074934	1.003374	0.975744	0.970965		
7	11		1.326473	1.097021	1.018843	0.968263	0.961474		
7	12		3.353973	1.475289	1.200237	1.104434	1.049185		

Batch	Block#	Flow Rate (L/min)		κ - Permeability (Darcy)					
		0.1	0.2	0.4	0.6	0.8	1	1.2	
8	1		0.507381	0.430571	0.38602	0.365651	0.365626		
8	2		0.153827	0.160448	0.162967				
8	3		0.166631	0.165159	0.167907				
8	4		0.118075	0.117609	0.11363				
8	5		0.080666	0.079856					
8	6	0.067353	0.067188						
8	7		0.212133	0.203198	0.187155	0.185485	0.182306		
8	8		0.385931	0.295275	0.279004	0.266384	0.264925		
8	9			1.267764	0.924793	0.814605	0.774616		

Batch	Block#	Flow Rate (L/min)				κ - Permeability (Darcy)			
		0.1	0.2	0.4	0.6	0.8	1	1.2	
9	1				5.609892	3.588079	3.062432	2.737218	
9	2				3.967085	2.533197	2.081736	1.896512	
9	3			12.96829	2.48905	1.873484	1.631406	1.416038	
9	4		2.412307	1.197766	0.970129	0.920046	0.899119		
9	5			1.977637	1.318759	1.171252	1.097591		
9	6				4.639295	2.731461	2.079131	1.86184	
9	7			8.949936	3.839491	2.986764	2.552169	2.364375	
9	8			6.059105	2.408277	1.850716	1.641267	1.514368	
9	9				3.259131	2.16398	1.775098	1.619715	

Table 17 - Calculated permeability values for each sample and air flow rate in each batch of extruded samples. Highlighted cells indicate values that were not considered in block average due to pressure gauge error.

Batch	Sample	GPM		psi		Linear			Quad C1 x^2 + C2x		
		Flow Rate	Pressure	R2	C1	R2	C1	C2			
1	1	1.244	40.45	0.981	31.501	0.998	6.5831	24.803			
1	1	1.083	35.18								
1	1	0.988	31.49								
1	1	0.79	23.32								
1	1	0.622	17.78								
1	1	0.415	11.33								
1	2	1.292	28.46	0.9822	20.968	0.9998	4.3418	16.407			
1	2	1.119	23.85								
1	2	0.988	20.42								
1	2	0.809	15.94								
1	2	0.616	11.85								
1	2	0.402	7.37								
1	3	1.221	21.61	0.968	16.335	0.9924	4.3205	11.962			
1	3	1.083	17.92								
1	3	1.002	15.41								
1	3	0.79	12.25								
1	3	0.589	8.82								
1	3	0.405	5.79								
1	4	1.292	17.26	0.9732	12.592	0.9905	2.5423	9.9017			
1	4	1.138	14.75								
1	4	1.002	11.98								
1	4	0.809	9.35								
1	4	0.616	6.98								
1	4	0.4	5.13								

Batch	Sample	GPM		psi		Linear			Quad C1 x^2 + C2x			Darcy
		Flow Rate	Pressure	R2	C1	R2	C1	C2	Permeal			
1	5	1.178	35.44	0.9748	28.417	0.9992	7.9068	20.475	2.3694			
1	5	1.101	31.75						2.3694			
1	5	1.018	29.12						2.3694			
1	5	0.809	21.47						2.3694			
1	5	0.611	15.54						2.3694			
1	5	0.402	9.74						2.3694			
1	6	1.244	27.4	0.9799	21.035	0.9994	4.835	16.019	2.121497			
1	6	1.119	24.24						2.121497			
1	6	1.033	21.47						2.121497			
1	6	0.79	15.54						2.121497			
1	6	0.6	11.33						2.121497			
1	6	0.412	7.63						2.121497			
1	7	1.244	20.02	0.9717	15.117	0.9993	4.2869	10.669	2.45318			
1	7	1.138	17.65						2.45318			
1	7	1.002	14.88						2.45318			
1	7	0.781	10.8						2.45318			
1	7	0.589	8.03						2.45318			
1	7	0.397	4.87						2.45318			
1	8	1.199	14.22	0.9543	10.8	0.9961	3.9794	6.819	2.534854			
1	8	1.083	11.85						2.534854			
1	8	0.988	10.4						2.534854			
1	8	0.8	7.9						2.534854			
1	8	0.622	5.79						2.534854			
1	8	0.4	3.68						2.534854			

Batch	Sample	GPM		psi	Linear			Quad C1 x^2 + C2x		
		Flow Rate	Pressure	R2	C1	R2	C1	C2		
1	9	1.199	39.66	0.983	31.876	0.999	6.8056	25.074		
1	9	1.083	35.31							
1	9	0.973	31.1							
1	9	0.819	25.03							
1	9	0.605	17.12							
1	9	0.397	11.46							
1	10	1.221	29.91	0.9757	22.92	0.9818	2.6911	20.172		
1	10	1.119	25.16							
1	10	1.002	22.13							
1	10	0.809	17.52							
1	10	0.605	13.17							
1	10	0.431	10.53							
1	11	1.244	20.55	0.9691	15.382	0.9993	4.6477	10.588		
1	11	1.101	17.12							
1	11	1.018	15.54							
1	11	0.809	11.46							
1	11	0.589	8.03							
1	11	0.397	5							
1	12	1.221	15.15	0.9609	11.44	0.9973	3.9253	7.4059		
1	12	1.049	11.98							
1	12	1.101	12.77							
1	12	0.8	8.16							
1	12	0.605	6.05							
1	12	0.397	3.81							

Batch	Sample	GPM		psi	Linear			Quad C1 x^2 + C2x		
		Flow Rate	Pressure	R2	C1	R2	C1	C2		
2	1	1.267	13.96	0.9407	10.112	0.9981	4.3478	5.6133		
2	1	1.101	11.59							
2	1	0.988	10.01							
2	1	0.819	7.24							
2	1	0.616	5.13							
2	1	0.407	3.02							
2	2	1.244	13.04	0.9256	9.2644	0.9968	4.5776	4.5774		
2	2	1.101	10.4							
2	2	0.988	8.82							
2	2	0.809	6.58							
2	2	0.628	4.74							
2	2	0.407	2.89							
2	3	1.221	12.38	0.9383	9.0801	0.996	4.0713	4.8928		
2	3	1.138	10.53							
2	3	1.002	8.82							
2	3	0.809	6.71							
2	3	0.622	4.6							
2	3	0.402	2.76							
2	4	1.199	11.06	0.9582	8.5443	0.9981	3.0894	5.4393		
2	4	1.101	9.74							
2	4	0.973	8.16							
2	4	0.829	6.45							
2	4	0.611	4.47							
2	4	0.4	2.89							

Batch	Sample	GPM		psi		Linear			Quad C1 x^2 + C2x		
		Flow Rate	Pressure	R2	C1	R2	C1	C2			
2	5	1.178	28.33	0.9777	22.879	0.9998	5.9916	16.902			
2	5	1.101	25.69								
2	5	0.988	22.66								
2	5	0.79	16.99								
2	5	0.594	12.25								
2	5	0.397	7.63								
2	6	1.267	20.16	0.9804	15.161	0.9988	3.279	11.753			
2	6	1.101	17.12								
2	6	1.018	15.15								
2	6	0.8	11.46								
2	6	0.605	8.16								
2	6	0.412	5.66								
2	7	1.267	15.41	0.968	11.635	0.9958	3.2051	8.3146			
2	7	1.101	13.57								
2	7	1.002	11.46								
2	7	0.79	8.43								
2	7	0.594	5.92								
2	7	0.412	4.08								
2	8	1.343	14.49	0.9803	10.114	0.9955	1.7976	8.1663			
2	8	1.158	11.59								
2	8	0.988	9.61								
2	8	0.79	7.63								
2	8	0.605	5.53								
2	8	0.417	4.08								

Batch	Sample	GPM		psi		Linear			Quad C1 x^2 + C2x		
		Flow Rate	Pressure	R2	C1	R2	C1	C2			
2	9	1.199	26.35	0.971	20.496	0.9983	5.9457	14.48			
2	9	1.119	23.19								
2	9	0.988	20.02								
2	9	0.8	15.41								
2	9	0.589	10.53								
2	9	0.4	6.98								
2	10	1.267	20.02	0.967	14.776	0.9997	4.5563	10.014			
2	10	1.119	16.86								
2	10	1.018	15.02								
2	10	0.8	10.8								
2	10	0.6	7.63								
2	10	0.402	4.87								
2	11	1.267	16.47	0.9691	12.066	0.996	3.2403	8.687			
2	11	1.138	13.7								
2	11	0.973	11.72								
2	11	0.8	8.82								
2	11	0.594	6.19								
2	11	0.4	4.34								
2	12	1.371	14.49	0.9464	9.5806	0.9985	3.4729	5.7936			
2	12	1.138	11.06								
2	12	0.973	9.08								
2	12	0.8	6.58								
2	12	0.6	4.74								
2	12	0.412	3.15								

Batch	Sample	GPM		psi		Linear		Quad C1 x^2 + C2x		
		Flow Rate	Pressure	R2	C1	R2	C1	C2		
3	1	1.083	47.97	0.9918	42.736	0.9992	5.971	37.414		
3	1	0.988	42.43							
3	1	0.84	35.31							
3	1	0.672	27.8							
3	1	0.542	22.13							
3	1	0.412	16.73							
3	2	1.178	34.92	0.9867	28.13	0.9959	4.5037	23.597		
3	2	1.119	31.36							
3	2	1.002	27.8							
3	2	0.809	21.74							
3	2	0.594	16.2							
3	2	0.405	10.27							
3	3	1.244	24.11	0.9841	18.82	0.998	3.5426	15.235		
3	3	1.066	20.81							
3	3	0.973	18.18							
3	3	0.8	14.36							
3	3	0.6	10.27							
3	3	0.405	6.71							
3	4	1.221	17.65	0.9684	13.691	0.9992	4.1533	9.4825		
3	4	1.101	15.67							
3	4	0.988	13.43							
3	4	0.772	9.74							
3	4	0.605	7.11							
3	4	0.4	4.6							

Batch	Sample	GPM		psi		Linear		Quad C1 x^2 + C2x		
		Flow Rate	Pressure	R2	C1	R2	C1	C2		
3	5	1.158	39.53	0.9886	32.638	0.9981	5.5043	27.141		
3	5	1.101	36.24							
3	5	1.018	32.81							
3	5	0.819	25.69							
3	5	0.6	18.44							
3	5	0.393	11.85							
3	6	1.221	30.3	0.98	23.481	0.9975	5.1466	18.175		
3	6	1.138	26.61							
3	6	1.018	24.11							
3	6	0.809	18.18							
3	6	0.634	13.43							
3	6	0.41	8.43							
3	7	1.221	25.56	0.979	19.688	0.9969	4.3999	15.222		
3	7	1.101	21.47							
3	7	0.988	19.5							
3	7	0.79	14.75							
3	7	0.6	10.53							
3	7	0.39	6.98							
3	8	1.221	18.18	0.9621	13.882	0.999	4.755	9.0774		
3	8	1.083	15.54							
3	8	0.988	13.57							
3	8	0.8	10.01							
3	8	0.589	7.11							
3	8	0.395	4.47							

Batch	Sample	GPM		psi		Linear			Quad C1 x^2 + C2x		
		Flow Rate	Pressure	R2	C1	R2	C1	C2			
3	9	1.199	38.61	0.9904	31.39	0.9997	5.0112	26.335			
3	9	1.101	35.05								
3	9	1.002	31.75								
3	9	0.8	24.24								
3	9	0.6	17.52								
3	9	0.402	11.33								
3	10	1.199	28.59	0.9893	22.993	0.9995	3.8297	19.132			
3	10	1.101	25.43								
3	10	1.002	23.19								
3	10	0.79	17.39								
3	10	0.589	12.64								
3	10	0.405	8.43								
3	11	1.267	25.03	0.9815	18.697	0.9994	4.0892	14.45			
3	11	1.101	20.55								
3	11	1.002	18.71								
3	11	0.809	14.36								
3	11	0.594	10.01								
3	11	0.388	6.32								
3	12	1.292	18.97	0.9737	13.751	0.9989	3.6117	9.9315			
3	12	1.119	15.67								
3	12	1.018	13.7								
3	12	0.8	10.01								
3	12	0.594	7.37								
3	12	0.382	4.47								

Batch	Sample	GPM		psi		Linear			Quad C1 x^2 + C2x		
		Flow Rate	Pressure	R2	C1	R2	C1	C2			
4	1	1.221	17.39	0.9779	13.247	0.9985	3.7166	9.5965			
4	1	1.002	13.17								
4	1	0.819	10.4								
4	1	0.611	6.98								
4	1	0.415	4.87								
4	1	0.196	2.23								
4	2	1.221	14.36	0.9753	10.981	0.9992	3.1916	7.8604			
4	2	1.002	11.19								
4	2	0.8	8.16								
4	2	0.6	5.79								
4	2	0.397	3.68								
4	2	0.252	2.36								
4	3	1.221	11.98	0.9816	9.2663	0.9995	2.4386	6.8593			
4	3	1.018	9.61								
4	3	0.8	6.98								
4	3	0.605	5								
4	3	0.39	3.02								
4	3	0.196	1.57								
4	4	1.317	11.59	0.962	8.006	0.9983	2.8215	5.0726			
4	4	1.002	7.9								
4	4	0.809	6.05								
4	4	0.616	3.94								
4	4	0.39	2.49								
4	4	0.197	1.31								

Batch	Sample	GPM		psi		Linear			Quad C1 x^2 + C2x		
		Flow Rate	Pressu	R2	C1	R2	C1	C2			
4	5	1.178	18.71	0.9726	14.665	0.9993	4.7608	10.14			
4	5	0.988	14.49								
4	5	0.8	11.06								
4	5	0.6	7.77								
4	5	0.407	5								
4	5	0.238	2.89								
4	6	1.244	16.07	0.973	11.984	0.9985	3.6061	8.4031			
4	6	1.002	11.98								
4	6	0.8	9.08								
4	6	0.589	6.19								
4	6	0.41	3.81								
4	6	0.216	2.36								
4	7	1.244	13.17	0.9688	9.7077	0.9988	3.2273	6.5088			
4	7	0.988	9.48								
4	7	0.819	7.5								
4	7	0.605	5								
4	7	0.4	3.15								
4	7	0.218	1.84								
4	8	1.292	10.53	0.9529	7.339	0.9987	2.9942	4.2776			
4	8	1.002	7.37								
4	8	0.8	5.26								
4	8	0.622	3.68								
4	8	0.379	2.1								
4	8	0.223	1.31								

Batch	Sample	GPM		psi		Linear			Quad C1 x^2 + C2x		
		Flow Rate	Pressu	R2	C1	R2	C1	C2			
4	9	1.244	16.6	0.9758	12.381	0.9993	3.6432	8.7411			
4	9	1.018	12.64								
4	9	0.809	9.22								
4	9	0.594	6.58								
4	9	0.405	4.21								
4	9	0.208	2.1								
4	10	1.221	12.25	0.9607	9.1188	0.9984	3.6412	5.5422			
4	10	1.002	9.22								
4	10	0.809	6.71								
4	10	0.594	4.47								
4	10	0.405	3.15								
4	10	0.198	1.18								
4	11	1.199	10.27	0.9472	7.6505	0.999	3.7733	3.9695			
4	11	1.018	7.9								
4	11	0.819	5.66								
4	11	0.594	3.68								
4	11	0.4	2.23								
4	11	0.209	1.18								
4	12	1.267	10.27	0.9322	7.1124	0.9993	3.7076	3.3522			
4	12	1.033	7.37								
4	12	0.85	5.39								
4	12	0.616	3.55								
4	12	0.405	1.97								
4	12	0.276	1.31								

Batch	Sample	GPM		psi		Linear		Quad C1 x^2 + C2x		
		Flow Rate	Pressure	R2	C1	R2	C1	C2		
5	1	1.018	56.93	0.9972	54.718	0.9993	4.2192	51.124		
5	1	0.946	51.66							
5	1	0.84	45.72							
5	1	0.64	34.52							
5	1	0.529	28.06							
5	1	0.395	21.21							
5	2	1.119	44.67	0.9953	38.886	0.9997	34.92	4.2414		
5	2	1.018	39.66							
5	2	0.908	35.05							
5	2	0.8	30.7							
5	2	0.6	22.53							
5	2	0.407	15.02							
5	3	1.158	40.58	0.9888	33.794	0.9902	1.9155	31.978		
5	3	1.018	33.86							
5	3	0.884	29.51							
5	3	0.809	26.09							
5	3	0.6	20.02							
5	3	0.402	14.49							
5	4	1.292	29.78	0.9943	22.451	0.9997	2.4039	19.955		
5	4	1.083	24.51							
5	4	0.973	21.74							
5	4	0.809	17.52							
5	4	0.605	12.91							
5	4	0.407	8.69							

Batch	Sample	GPM		psi		Linear		Quad C1 x^2 + C2x		
		Flow Rate	Pressure	R2	C1	R2	C1	C2		
5	5	1.049	52.31	0.9981	49.281	0.9989	2.2798	47.3347		
5	5	0.908	44.28							
5	5	0.79	39.4							
5	5	0.7	34.26							
5	5	0.589	28.72							
5	5	0.4	19.1							
5	6	1.138	43.09	0.9952	37.016	0.9984	3.3247	33.886		
5	6	1.002	37.16							
5	6	0.92	34.26							
5	6	0.819	29.25							
5	6	0.589	21.21							
5	6	0.425	15.41							
5	7	1.221	34.92	0.9939	28.098	0.9997	3.43	24.587		
5	7	1.119	32.02							
5	7	1.002	28.2							
5	7	0.819	22.4							
5	7	0.616	16.33							
5	7	0.4	10.4							
5	8	1.199	32.54	0.9901	26.142	0.9924	1.8848	24.252		
5	8	1.083	28.2							
5	8	1.002	25.69							
5	8	0.809	20.16							
5	8	0.6	15.28							
5	8	0.422	11.59							

Batch	Sample	GPM		psi		Linear		Quad C1 x^2 + C2x		
		Flow Rate	Pressure	R2	C1	R2	C1	C2		
5	9	0.988	50.21	0.9951	49.38	0.9974	4.0616	46.007		
5	9	0.92	45.07							
5	9	0.819	39.79							
5	9	0.685	33.73							
5	9	0.589	28.72							
5	9	0.405	19.36							
5	10	1.119	42.69	0.9957	37.64	0.9994	3.6115	34.281		
5	10	1.018	38.61							
5	10	0.884	33.47							
5	10	0.809	30.3							
5	10	0.611	22							
5	10	0.436	15.54							
5	11	1.199	35.58	0.9916	28.997	0.9992	4.0098	25.009		
5	11	1.066	31.62							
5	11	0.988	28.59							
5	11	0.8	22.26							
5	11	0.611	16.73							
5	11	0.417	11.33							
5	12	1.292	24.64	0.9911	18.814	0.998	2.446	16.215		
5	12	1.138	22							
5	12	1.018	19.23							
5	12	0.809	14.88							
5	12	0.611	10.53							
5	12	0.386	6.45							

Batch	Sample	GPM		psi		Linear: $\Delta P = C1*Q$		Quad: $\Delta P = C1*Q^2 + C2Q$		
		Flow Rate	Pressure	R2	C1	R2	C1	C2		
6	1	1.292	15.28	0.9656	11.188	0.9972	3.3387	7.7131		
6	1	1.066	12.38							
6	1	1.002	11.19							
6	1	0.809	8.43							
6	1	0.605	5.66							
6	1	0.388	3.42							
6	2	1.244	11.72	0.9296	8.5221	0.9975	4.1154	4.3094		
6	2	0.988	8.56							
6	2	0.809	6.05							
6	2	0.616	4.08							
6	2	0.415	2.63							
6	2	1.101	9.61							
6	3	1.221	9.74	0.9436	7.3605	0.9985	3.2877	4.0315		
6	3	1.083	8.43							
6	3	0.988	7.11							
6	3	0.829	5.53							
6	3	0.589	3.55							
6	3	0.395	2.1							
6	4	1.199	8.95	0.9267	6.6753	0.9955	3.53	3.0772		
6	4	1.119	7.9							
6	4	1.018	6.45							
6	4	0.8	4.74							
6	4	0.584	3.02							
6	4	0.382	1.84							

Batch	Sample	GPM		psi		Linear: $\Delta P = C1*Q$			Quad: $\Delta P = C1*Q^2 + C2Q$		
		Flow Rate	Pressure	R2	C1	R2	C1	C2			
6	5	1.221	15.41	0.9532	11.644	0.9995	4.7033	6.8629			
6	5	1.101	13.17								
6	5	0.988	11.46								
6	5	0.8	8.56								
6	5	0.611	5.79								
6	5	0.371	3.29								
6	6	1.267	13.3	0.9431	9.555	0.9993	4.1268	5.2713			
6	6	1.101	10.67								
6	6	1.002	9.61								
6	6	0.809	6.98								
6	6	0.589	4.47								
6	6	0.4	2.76								
6	7	1.221	11.46	0.9325	8.4348	0.9977	4.0498	4.3159			
6	7	1.101	9.61								
6	7	1.002	8.29								
6	7	0.809	5.92								
6	7	0.6	4.21								
6	7	0.417	2.63								
6	8	1.178	8.69	0.8952	6.5098	0.9972	4.4237	2.1338			
6	8	1.083	7.37								
6	8	0.973	6.45								
6	8	0.8	4.47								
6	8	0.622	2.89								
6	8	0.397	1.7								

Batch	Sample	GPM		psi		Linear: $\Delta P = C1*Q$			Quad: $\Delta P = C1*Q^2 + C2Q$		
		Flow Rate	Pressure	R2	C1	R2	C1	C2			
6	9	1.199	17.92	0.9524	13.797	0.9993	5.6381	8.0885			
6	9	1.101	15.81								
6	9	1.018	13.83								
6	9	0.79	9.88								
6	9	0.589	6.71								
6	9	0.393	4.21								
6	10	1.343	14.22	0.9314	9.5076	0.9992	4.4062	4.7054			
6	10	1.158	11.33								
6	10	1.002	9.35								
6	10	0.829	6.84								
6	10	0.579	4.08								
6	10	0.397	2.63								
6	11	1.292	11.46	0.9473	8.0687	0.9966	3.0599	4.8466			
6	11	1.138	9.22								
6	11	0.973	7.9								
6	11	0.8	5.66								
6	11	0.6	4.08								
6	11	0.41	2.49								
6	12	1.292	10.53	0.9163	7.1391	0.9984	3.898	3.0144			
6	12	1.119	8.16								
6	12	1.018	6.98								
6	12	0.819	5.13								
6	12	0.584	3.02								
6	12	0.393	1.97								

Batch	Sample	GPM		psi		Linear			Quad C1 x^2 + C2x		
		Flow Rate	Pressure	R2	C1	R2	C1	C2			
7	1	0.933	58.64	0.9967	62.636	0.9984	4.3209	59.417			
7	1	0.79	50.47								
7	1	0.7	44.01								
7	1	0.6	36.89								
7	1	0.49	30.04								
7	1	0.405	24.51								
7	2	1.101	47.7	0.992	41.957	0.9986	5.8961	36.487			
7	2	1.018	42.69								
7	2	0.895	37.82								
7	2	0.809	33.07								
7	2	0.605	23.98								
7	2	0.39	15.54								
7	3	1.221	37.03	0.9908	29.429	0.9999	4.4873	24.831			
7	3	1.119	33.47								
7	3	1.018	29.78								
7	3	0.781	22.26								
7	3	0.616	16.86								
7	3	0.402	10.8								
7	4	1.292	26.88	0.98116	19.729	0.9973	3.869	15.619			
7	4	1.158	22.79								
7	4	0.988	19.63								
7	4	0.809	14.75								
7	4	0.605	11.19								
7	4	0.402	6.84								

Batch	Sample	GPM		psi		Linear			Quad C1 x^2 + C2x		
		Flow Rate	Pressure	R2	C1	R2	C1	C2			
7	5	1.002	59.04	0.9967	59.394	0.997	1.5769	58.097			
7	5	0.895	53.9								
7	5	0.79	47.04								
7	5	0.678	40.98								
7	5	0.579	33.86								
7	5	0.42	23.85								
7	6	1.158	44.8	0.9958	37.928	0.9992	3.4532	34.643			
7	6	1.033	39.4								
7	6	0.895	33.73								
7	6	0.781	28.99								
7	6	0.605	22.79								
7	6	0.402	14.09								
7	7	1.244	34.39	0.9877	26.456	0.9992	4.5625	21.664			
7	7	1.158	30.96								
7	7	1.033	27.01								
7	7	0.819	20.68								
7	7	0.605	14.88								
7	7	0.41	9.88								
7	8	1.292	24.37	0.9873	18.147	0.9997	3.1238	14.834			
7	8	1.138	21.08								
7	8	1.018	18.18								
7	8	0.781	13.43								
7	8	0.584	9.74								
7	8	0.41	6.71								

Batch	Sample	GPM		psi		Linear		Quad C1 x^2 + C2x		
		Flow Rate	Pressure	R2	C1	R2	C1	C2		
7	9	1.049	56.66	0.9973	53.162	0.9999	4.478	49.353		
7	9	0.92	49.28							
7	9	0.809	42.83							
7	9	0.722	37.69							
7	9	0.546	28.46							
7	9	0.397	20.29							
7	10	1.138	39.53	0.9895	33.413	0.9992	5.6817	27.844		
7	10	1.083	36.5							
7	10	1.002	33.34							
7	10	0.79	25.43							
7	10	0.589	18.57							
7	10	0.4	12.12							
7	11	1.221	34.79	0.9917	27.776	0.9995	3.9393	23.765		
7	11	1.101	30.96							
7	11	1.002	28.06							
7	11	0.809	21.47							
7	11	0.594	15.67							
7	11	0.402	10.14							
7	12	1.244	23.71	0.9784	18.025	0.9993	4.2933	13.574		
7	12	1.138	20.81							
7	12	0.988	17.65							
7	12	0.829	14.09							
7	12	0.594	9.48							
7	12	0.412	6.58							

Batch	Sample	GPM		psi		Linear		Quad C1 x^2 + C2x		
		Flow Rate	Pressure	R2	C1	R2	C1	C2		
8	1	1.101	46.91	0.993	41.663	0.9992	5.5244	35.574		
8	1	1.002	42.69							
8	1	0.895	36.63							
8	1	0.8	32.68							
8	1	0.589	23.58							
8	1	0.407	15.94							
8	2									
8	2									
8	2									
8	2									
8	2									
8	2									
8	3	0.8	60.22	0.9982	76.575	0.9984	-2.7444	78.357		
8	3	0.685	53.5							
8	3	0.6	46.25							
8	3	0.501	38.21							
8	3	0.397	30.3							
8	3	0.205	15.94							
8	4	0.722	62.33	0.9785	88.21	0.9936	-19.991	99.759		
8	4	0.622	54.03							
8	4	0.529	46.25							
8	4	0.445	39.79							
8	4	0.41	37.42							
8	4	0.291	28.99							

Batch	Sample	GPM		psi		Linear			Quad C1 x^2 + C2x		
		Flow Rate	Pressure	R2	C1	R2	C1	C2			
8	5										
8	5										
8	5										
8	5										
8	5										
8	5										
8	6										
8	6										
8	6										
8	6										
8	6										
8	6										
8	7	1.033	49.55	0.9923	48.047	0.996	-4.2116	51.598			
8	7	0.908	42.83								
8	7	0.8	38.08								
8	7	0.707	33.99								
8	7	0.594	29.25								
8	7	0.405	21.08								
8	8	1.138	38.34	0.9981	33.653	0.9985	-0.8651	34.465			
8	8	1.018	34.13								
8	8	0.895	30.04								
8	8	0.8	26.75								
8	8	0.64	21.47								
8	8	0.431	15.28								

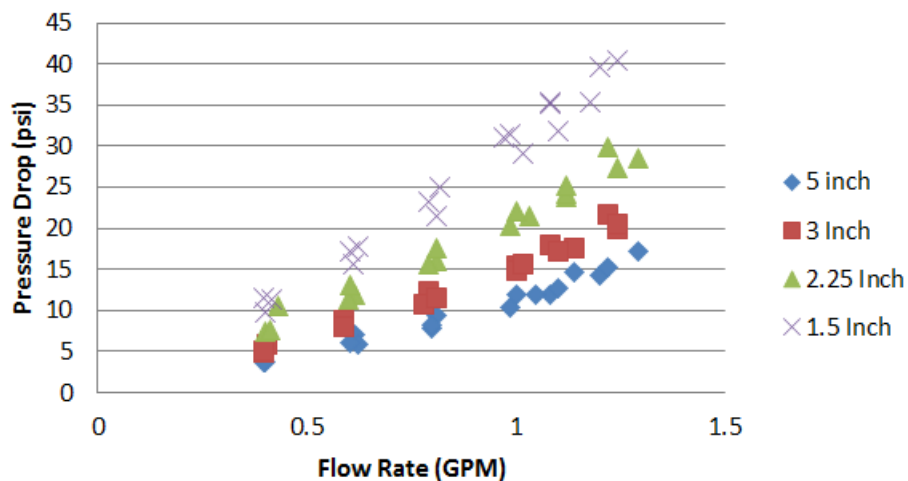
Batch	Sample	GPM		psi		Linear			Quad C1 x^2 + C2x		
		Flow Rate	Pressure	R2	C1	R2	C1	C2			
8	9	1.178	21.61	0.9937	17.859	0.996	1.2725	16.651			
8	9	0.988	17.65								
8	9	0.895	15.81								
8	9	0.8	13.7								
8	9	0.589	10.27								
8	9	0.407	7.5								

Batch	Sample	GPM		psi		Linear			Quad C1 x^2 + C2x		
		Flow Rate	Pressure	R2	C1	R2	C1	C2			
9	1	1.317	21.21	0.9651	14.795	0.9963	4.0769	10.495			
9	1	1.083	16.07								
9	1	1.002	14.09								
9	1	0.8	10.93								
9	1	0.611	8.03								
9	1	0.405	5.39								
9	2	1.244	18.71	0.9815	14.268	0.9946	2.6273	11.558			
9	2	1.101	15.94								
9	2	1.018	14.22								
9	2	0.8	10.53								
9	2	0.594	7.77								
9	2	0.39	5.53								
9	3	1.244	18.84	0.9816	14.324	0.9946	2.5745	11.654			
9	3	1.138	16.33								
9	3	1.002	14.22								
9	3	0.79	10.4								
9	3	0.616	8.16								
9	3	0.402	5.66								
9	4	1.199	39.27	0.9747	31.151	0.9981	8.3593	22.752			
9	4	1.101	35.05								
9	4	0.973	30.7								
9	4	0.809	23.32								
9	4	0.605	16.47								
9	4	0.384	10.53								

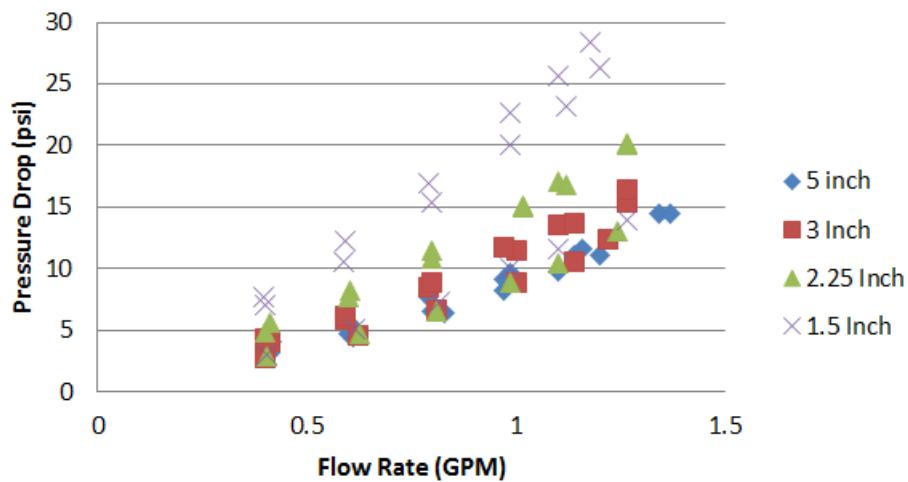
Batch	Sample	GPM		psi		Linear			Quad C1 x^2 + C2x		
		Flow Rate	Pressure	R2	C1	R2	C1	C2			
9	5	1.178	24.24	0.9802	19.352	0.9966	4.334	15.03			
9	5	1.083	21.08								
9	5	1.002	19.1								
9	5	0.809	14.75								
9	5	0.584	10.27								
9	5	0.388	6.98								
9	6	1.178	16.07	0.9844	12.917	0.9901	1.5767	11.338			
9	6	1.083	14.09								
9	6	1.033	12.77								
9	6	0.79	9.74								
9	6	0.589	7.37								
9	6	0.41	5.26								
9	7	1.221	22.13	0.9579	16.521	0.9924	5.3859	10.979			
9	7	1.119	18.71								
9	7	1.033	16.6								
9	7	0.8	11.72								
9	7	0.589	8.69								
9	7	0.41	5.92								
9	8	1.178	19.89	0.9741	15.713	0.9866	2.9518	12.763			
9	8	1.083	16.99								
9	8	1.018	15.54								
9	8	0.8	11.59								
9	8	0.594	8.69								
9	8	0.397	6.32								
9	9	1.221	16.73	0.9934	13.312	0.994	0.4705	12.83			
9	9	1.138	14.88								
9	9	0.973	12.77								
9	9	0.8	10.67								
9	9	0.594	7.5								
9	9	0.412	5.79								

Table 18 - Experimental pressure drop and flow rate data from water testing of all extruded samples.

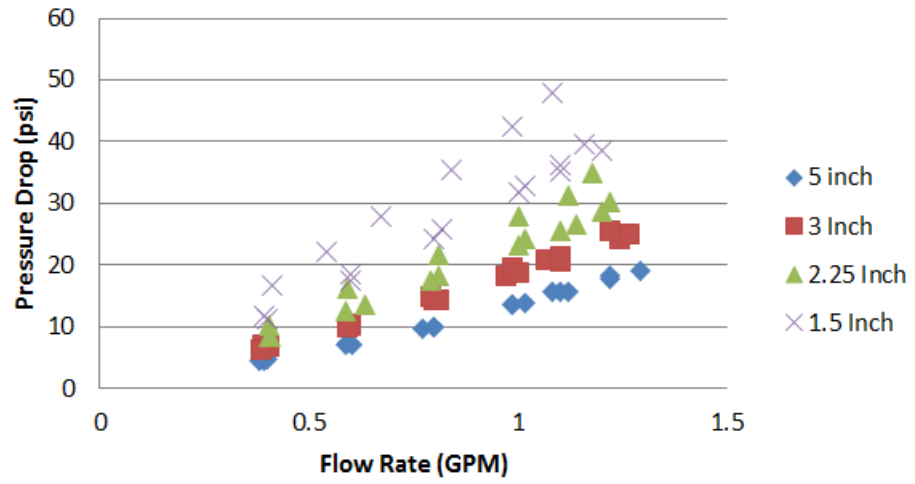
Batch 1 Water Test Data



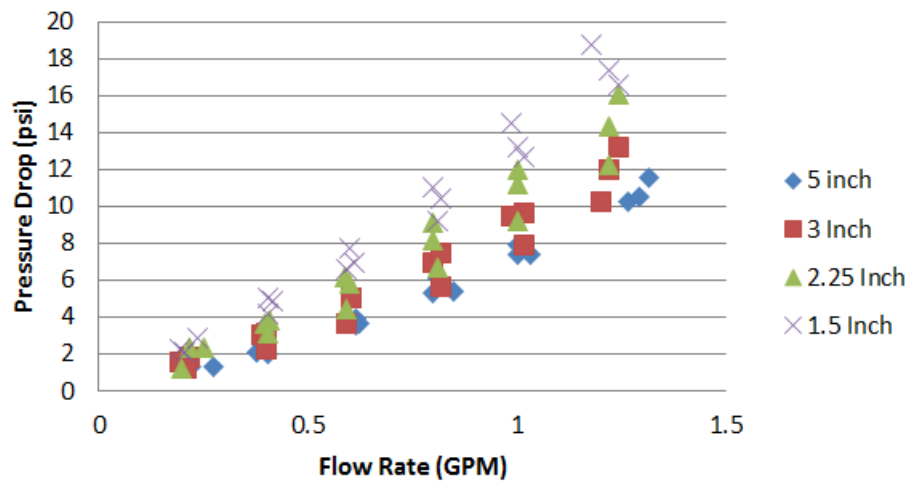
Batch 2 Water Test Data



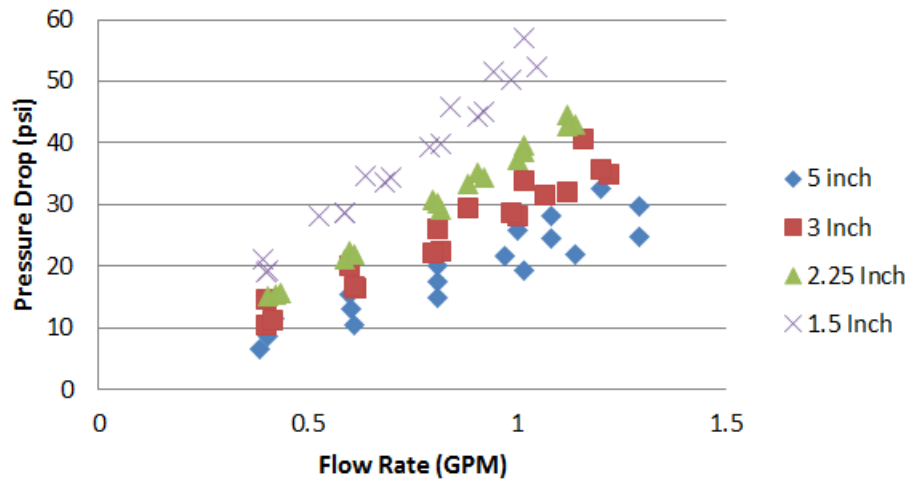
Batch 3 Water Test Data



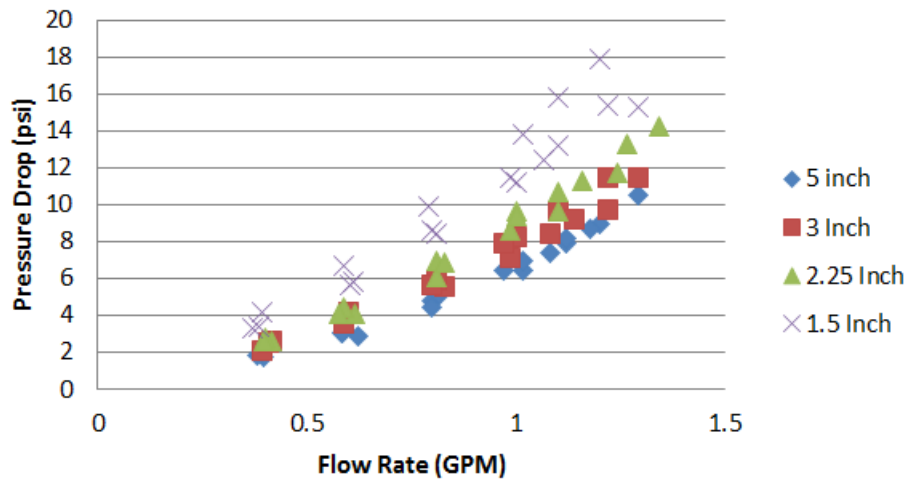
Batch 4 Water Test Data



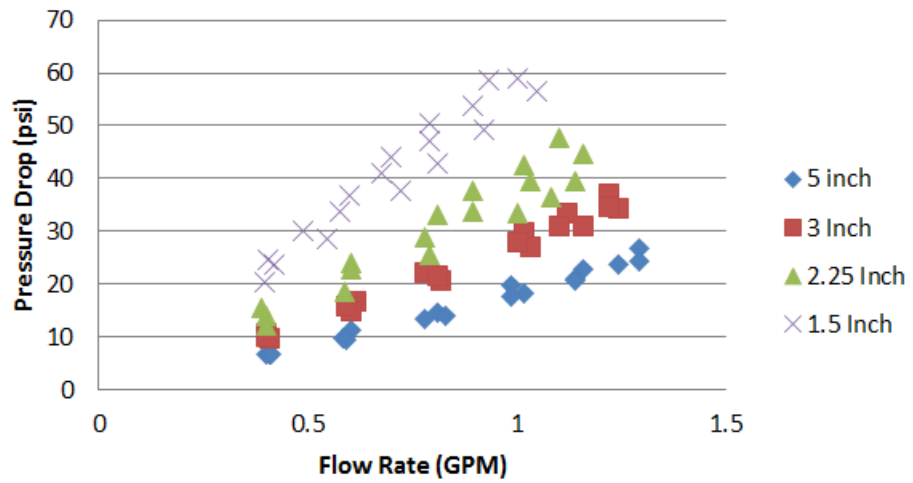
Batch 5 Water Test Data



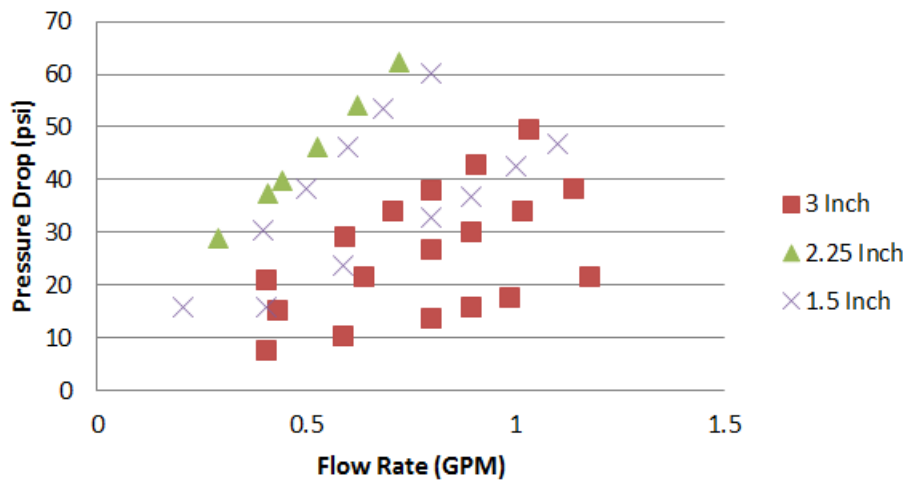
Batch 6 Water Test Data



Batch 7 Water Test Data



Batch 8 Water Test Data



Batch 9 Water Test Data

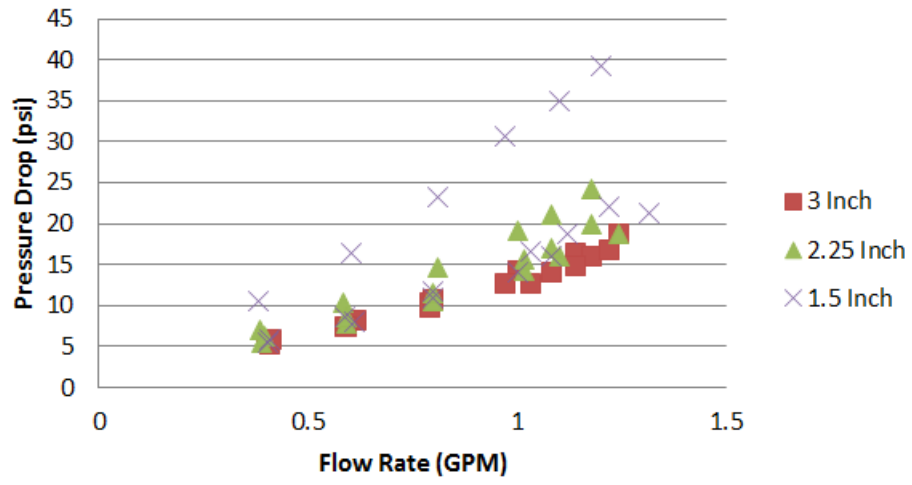


Figure 41 - Experimental pressure vs. flow curves from the water test for all Batches of samples.

LIST OF SYMBOLS AND ABBREVIATIONS

A – Cross-sectional area	Q – Volumetric flow rate
B – Non-Darcy coefficient	Re – Reynold’s number
C – Form drag coefficient	r_i – Inner radius
$C1$ & $C2$ – Trendline coefficients	r_o – Outer radius
AC – Activated carbon	SEM – Scanning electron microscope
D_p – Particle diameter	V – Superficial fluid velocity
Fo – Forchheimer number	VOC – Volatile organic compound
h – Height	U – Intrinsic fluid velocity
HOI – Heat of immersion	w – Weight
ID – Inner diameter	$X2$ – Modified Ergun coefficient
L – Length	ϵ – Porosity
OD – Outer diameter	κ – Permeability
ΔP – Pressure drop	μ – Viscosity
P_1 – High-side pressure	ρ – Fluid density
P_2 – Low-side pressure	

CURRICULUM VITA

NAME: Matthew William Okruch

ADDRESS: 9607 Ridgeside Dr.
Apt. 4
Louisville, KY 40291

DOB: Louisville, Kentucky – March 6, 1991

EDUCATION & TRAINING:

B.S., Mechanical Engineering, Summa Cum Laude
University of Kentucky
2009-2013

M.S., Mechanical Engineering
University of Louisville
2013-2016

PROFESSIONAL EXPERIENCE:

Edison Engineering Development Program
GE Appliances, Louisville, KY
2013-2016

Water Testing Technician
Bluegrass Kesco, Lexington, KY
2012-2013

Manufacturing Engineer Intern
Cummins, Inc., Charleston, SC
2012

Mechanical Engineer Intern
Gray Construction, Lexington, KY
2011-2012

Design Engineer Intern
Cummins, Inc., Columbus, IN
2011

HONORS & AWARDS:

Tau Beta Pi Engineering Honor Society
UK Presidential Scholarship
Kentucky Governor's Scholar